

1/81

CMCRCZ 10 (1), 1-124 (1981)

**ΧΗΜΙΚΑ ΧΡΟΝΙΚΑ**

ΝΕΑ ΣΕΙΡΑ

**CHIMIKA CHRONIKA**

NEW SERIES

**AN INTERNATIONAL EDITION  
OF THE GREEK CHEMISTS ASSOCIATION**

---

**SPECIAL ISSUE CONTAINING INVITED PAPERS PRESENTED  
AT THE FIRST BALKAN CHEMISTRY DAYS, ATHENS 1980**

---

**MANAGING COMMITTEE**

Elected members

MARIA BOTSIVALI

IRENE DILARIS-PAPADIMITRIOU

VASSILIOS M. KAPOULAS

GEORGIA

MARGOMENOU-

LEONIDOPOULOU

GEORGE SKALOS

Ex-officio members

PANAYOTIS PAPADOPOULOS

Assistant General Secretary of the G.C. Association

STELIOS CHATZIYANNAKOS

Treasurer of the G.C. Association

EDITOR - IN - CHIEF

M.I. KARAYANNIS

Analytical Chemistry, Univ. of Ioannina

**ASSISTANT EDITOR**

C.E. EFSTATHIOU

Analytical Chemistry, Univ. of Athens

**CONTRIBUTING EDITORS**

T.P. HADJIIOANNOU

Analytical Chemistry, University of Athens

C.N. POLYDOROPOULOS

Physical / Quantum Chemistry, Univ. of Ioannina

K. SANDRIS

Organic Chemistry, Tech. Univ. of Athens

**EDITORIAL ADVISORY BOARD**

N. ALEXANDROU

Organic Chemistry, University of Salonica

P. CATSOULACOS

Pharmaceutical Chemistry, Univ. of Patras

G.D. COMOULOS

Physical Chemistry, Athens

C.A. DEMOPOULOS

Biochemistry, Univ. of Athens

I. DILARIS - PAPADIMITRIOU

Organic Chemistry, University of Athens

A.E. EVANGELOPOULOS

Biochemistry, The National Hellenic Research Foundation, Athens

S. FILIANOS

Pharmacognosy, University of Athens

D.S. GALANOS

Food Chemistry, University of Athens

A.G. GALINOS

Inorganic Chemistry, University of Patras

P. GEORGACOPOULOS

Pharmaceutical Technology, Univ. of Salonica

I. GEORGATSOS

Biochemistry, Univ. of Salonica

M.P. GEORGIADIS

Organic Medicinal and Agricultural Chemistry.

Agricultural Univ. of Athens

N. HADJICHRISTIDIS

Polymer Chemistry, University of Athens

E. HADJIOUDIS

Photochemistry, C.N.R. "Democritos"

N.K. KALFOGLOU

Polymer Science/Applied Phys. Chem., Univ. of Patras

E. KAMPOURIS

Polymer Chemistry, Tech. Univ. of Athens

N. KATSANOS

Physical Chemistry, Univ. of Patras

V. KAPOULAS

Biochemistry, Univ. of Ioannina

D. KIOUSSIS

Petroleum/Petrochem. Technology, Univ. of Athens

A. KOSMATOS

Organic Chemistry, Univ. of Ioannina

P. KOUROUNAKIS

Pharmaceutical Chemistry, Univ. of Salonica

G.P. KYRIAKAKOU

Physical Organic Chemistry, Tech. Univ. of Athens

G. MANOUSSAKIS

Inorganic Chemistry, University of Salonica

I. MARANGOSIS

Chemical Mechanics, Tech. Univ. of Athens

I. NIKOKAVOURAS

Photochemistry, C.N.R. "Democritos"

D.N. NICOLAIDES

Organic Chemistry, University of Salonica

G. PAPAGEORGIOU

Biophysics, C.N.R. "Democritos"

V.P. PAPAGEORGIOU

Natural products, Tech. Univ. of Salonica

S. PARASKEVAS

Organic Chemistry, Univ. of Athens

G. PHOKAS

Pharmacognosy, Univ. of Salonica

M.J. SCULLOS

Environmental and Marine Chem. Univ. of Athens

G.A. STALIDIS

Physical Chemistry, Univ. of Salonica

A. STAVROPOULOS

Industrial Technology, G.S.I.S., Piraeus

I.M. TSANGARIS

Inorganic Chemistry, Univ. of Ioannina

G. TSATSARONIS

Food Chemistry/Technology, Univ. Salonica

G. VALCANAS

Organic Chemistry, Tech. Univ. of Athens.

A.G. VARVOGLIS

Organic Chemistry, University of Salonica

G.S. VASILIKIOTIS

Analytical Chemistry, Univ. of Salonica

E.K. VOUDOURIS

Food Chemistry, University of Ioannina

I. VOURVIDOU-FOTAKI

Organic Chemistry, University of Athens

I.V. YANNAS

Mechanical Engineering M.I.T., USA

D. YANNAKOUDAKIS

Physical Chemistry, Univ. of Salonica

Correspondence, submission of papers, subscriptions, renewals and changes of address should be sent to Chimika Chronika, New Series, 27 Kaningos street, Athens 147, Greece. Subscriptions are taken by volume at 500 drachmas for members and 1.000 drachmas for Corporations in Greece and 28U.S. dollars to all other countries except Cyprus, where subscriptions are made on request.

Printed in Greece by EPTALOFOS

Υπεύθυνος σύμφωνα με τον νόμο: Μ. Καραγιάννης, Παρμενίδου 15, Αθήνα.

# CHIMICA CHRONIKA, NEW SERIES

## CONTENTS

Vitamin B <sub>1</sub> (isolation, preparation, properties, mechanism of catalytic action) ( <i>in English</i> ) by N. Hadjiliadis, J. Markopoulos .....	1
Study of physical adsorption using the hole theory. I. Monolayer adsorption homogeneous surfaces ( <i>in English</i> ) by D.A. Jannakoudakis, P.J. Nikitas .....	23
Many-electron theory of discrete-discrete and discrete-continuum. Transition rates for systems with symmetry ( <i>in English</i> ) by C.A. Nicolaides, Y. Komninos, D.R. Beck .....	35
Structural analysis of chlorinated organic compounds by nuclear quadrupole resonance spectroscopy ( <i>in English</i> ) by D. Gegiou, F. Milia .....	59
The Kinetics of the deoxy ribonucleic acid - ribonucleic acid hybridization with simultaneous self-annealing of ribonucleic acid ( <i>in English</i> ) by N.A. Katsanos, H. Thomou .....	71
A modification of the A.O.A.C. drying oven method for total solid determination in milk and milk products ( <i>in English</i> ) by J.D. Efstathiou .....	87
The removal of organic entrainment in copper solvent extraction by flotation ( <i>in English</i> ) by K.A. Matis .....	93
Study of the catalysts Co/Al <sub>2</sub> O <sub>3</sub> and CoMo/Al <sub>2</sub> O <sub>3</sub> with photoelectron spectroscopy, diffused re- flection and analytical microscopy ( <i>in English</i> ) by P. Cajardo, A. Lycourghiotis, F. Delanay, P. Grange, B. Delmon .....	101
Synthesis of new N-Substituted Methoxy phenethylamines and their Pharmacological Action on C.N.S. ( <i>in English</i> ) by G. TSATSAS (Chemistry), Z. Papadopoulou-Daijoti, CH. Spuraki, D. Varonos ...	109
GLC-MS Computer analysis of the essential oil of mastic gum ( <i>in English</i> ) by V.P. Papageorgiou, A.N. Sagredos R. Moser .....	119

## **VITAMIN B<sub>1</sub> (Isolation, preparation, properties, mechanism of catalytic action)**

N. HADJILIADIS\* and J. MARKOPOULOS\*\*

\* University of Ioannina, Inorganic Chemistry Laboratory, Domboli 31, Ioannina, Greece. To whom correspondence should be addressed.

\*\* University of Athens, Inorganic Chemistry Laboratory, Navarinou 13a, Athens, Greece.

### **Isolation of thiamine**

In 1911 Funk<sup>1</sup> described in a series of papers the isolation from rice polishings of a substance capable to cure the disease beri-beri. This was called vitamin B and it is found in the rice polishings. In 1920 Emmet and Louros<sup>2</sup> proved that the substance, firstly called vitamin B, did not contain only one compound. Goldberger *et al*<sup>3</sup> found at least two different substances which belonged to the vitamin B complex: The antineuritic and the pellagra preventing factors, called vitamin B<sub>1</sub> and vitamin B<sub>2</sub> respectively. Later, other water soluble factors were discovered and took the names vitamin B<sub>3</sub>, vitamin B<sub>4</sub>... etc.

The first attempt to concentrate the antineuritic factor was made in 1912 by Suzuki *et al*<sup>4</sup>. They used an aqueous extract of rice polishings which they named «oryzanin». They tested «oryzanin» on pigeons maintained on a vitamin B-free diet and found the amount required to prevent «opisthotonus», a characteristic disease of these birds in the polyneuritic condition. The same year Edie *et al*<sup>5</sup> used a concentrate from yeast, called «tolurin» in tests to pigeons, while Funk<sup>6,7</sup> prepared concentrates from rice polishings and yeast. Several other investigators tried during the next years to prepare concentrated solutions of the vitamin, but only in 1926 Jansen and Donath<sup>8</sup> attained the greater concentration by treatment with acid clay. The acid clay was adsorbing vitamin B<sub>1</sub> from aqueous solution at pH=4.5. The vitamin was eluted afterwards, with baryta. Its activity was then detected by using rice birds (*Munia maja*) which, like pigeons, developed polyneuritis, when fed with vitamin B-free diets. With a series of experiments Jansen and Donath<sup>8</sup> succeeded finally in the isolation of vitamin B<sub>1</sub>, in the form of its crystalline hydrochloride. M.P. 250°C.

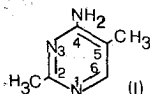
Vitamin B<sub>1</sub> was also isolated by Kinnorsley and Peters<sup>9,10</sup> from yeast, by Guha and Drummond<sup>11</sup> from wheat germ and by Williams<sup>12</sup> from rice polishings. The methods applied by different workers were not similar at all. Williams<sup>12,13</sup> produced sufficient amounts of the vitamin and succeed to find out its chemical structure.

### Chemical formula of Thiamine

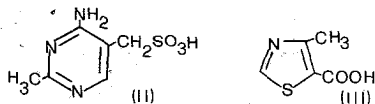
The structure of vitamin B<sub>1</sub> was elucidated by the excellent work of Williams and his collaborators<sup>14</sup>. Vitamin B<sub>1</sub> in neutral sulfite solution and room temperature was cleaved in to two halves, according to the following equation<sup>15</sup>:

$$\text{C}_{12}\text{H}_{18}\text{N}_4\text{SOCl}_2 + \text{Na}_2\text{SO}_3 \rightarrow \text{C}_6\text{H}_9\text{N}_3\text{SO}_3 + \text{C}_6\text{H}_9\text{NSO} + 2\text{NaCl} \quad (1)$$

The substance C<sub>6</sub>H<sub>9</sub>N<sub>3</sub>SO<sub>3</sub> upon acid hydrolysis gave ammonia<sup>15</sup> and the compound C<sub>6</sub>H<sub>8</sub>N<sub>2</sub>SO<sub>4</sub>. Both compounds with treatment with H<sub>2</sub>O at 200°C liberated sulfuric acid, whereas with alkalis they liberated sulfurous acid. Therefore, they both contain the sulfonic acid group. Both compounds gave also absorptions in the ultra-violet region, characteristic of the pyrimidine ring. The presence of this ring was confirmed also from the conversion of the compound C<sub>6</sub>H<sub>9</sub>N<sub>3</sub>SO<sub>3</sub> to the 4-amino-2,5-dimethyl-pyrimidine, with the action of sodium in aqueous ammonia. (Formula I).

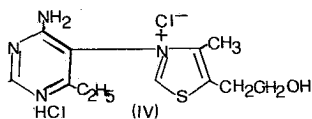


Formula I was confirmed synthetically<sup>16</sup>. With a similar procedure, 4-ethoxymethyl-4-hydroxy-2-methyl-pyrimidine was also synthesized<sup>15</sup>. This yielded 4-hydroxy-2-methyl-pyrimidyl-5-methane-sulfonic acid, on treatment with Na<sub>2</sub>SO<sub>3</sub>, identical with substance C<sub>6</sub>H<sub>8</sub>N<sub>2</sub>SO<sub>4</sub>. Therefore, the first half of the cleavage of thiamine of the empirical formula C<sub>6</sub>H<sub>9</sub>N<sub>3</sub>SO<sub>3</sub> should correspond to the 4-amino-2-methyl-pyrimidyl-5-methane-sulfonic acid (Formula II). The other half<sup>15</sup> of the formula C<sub>6</sub>H<sub>9</sub>NSO upon oxidation with HNO<sub>3</sub> gave 4-methyl-thiazole-5-carboxylic acid, identical with a substance prepared by Wohmann in 1890<sup>17</sup>. (Formula III)

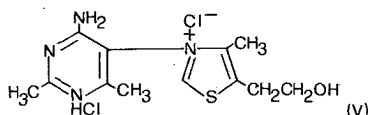


Since the compound C<sub>6</sub>H<sub>9</sub>NSO contained an alcoholic hydroxyl group which could easily be replaced by chlorine<sup>15</sup>, it was assumed to be the 5-β-hydroxyethyl-4-methyl thiazolium. The confirmation of this assumption was made by Clarke and Gurin<sup>18</sup> with synthesis.

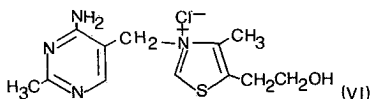
The first formula of thiamine which was proposed by Williams<sup>15</sup> before the structure of the pyrimidine part was elucidated, was:



Windaus et al<sup>19</sup> also proposed another erroneous formula.



The correct formula was finally proposed by Williams<sup>20</sup> and it is as follows:

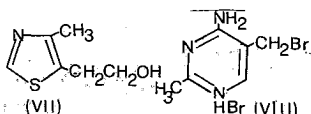


Structure (VI) has now been confirmed by an X-ray crystal structure determination<sup>21</sup>.

## Chemical synthesis of thiamine

### 1. Method of Williams and Cline<sup>22</sup>

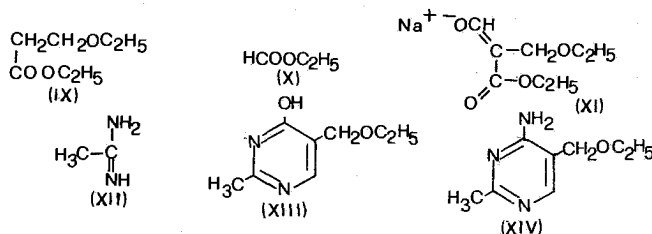
A total synthesis of vitamin B<sub>1</sub> was firstly achieved by Williams and Cline<sup>22</sup> by condensation of 5-β-hydroxyethyl-4-methyl-thiazole (Formula VII) with the hydrobromide salt of 4-amino-5-bromo-methyl-pyrimidine (Formula VIII).



The condensation product is the hydrobromide salt of vitamin B<sub>1</sub>, which is transferred to the hydrochloric salt by treatment with AgCl.

According to Williams<sup>16</sup> the pyrimidine derivative is made from the β-ethoxy-ethyl-propionic ester (Formula IX). This ester is condensed with formyl-

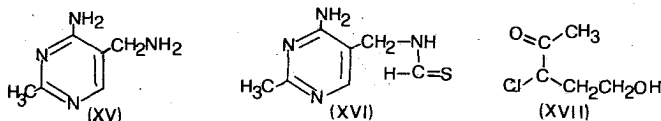
ethyl-ester (Formula X) in the presence of metallic sodium, to yield the compound (Formula XI), which then reacts with acetamidine (Formula XII) to produce the pyrimidine derivative (Formula XIII). The reaction of the latter with phosphorus oxychloride in alcoholic solution of ammonia, gives the product (Formula XIV), which is hydrolysed with HBr and gives the vitamin (Formula VI).



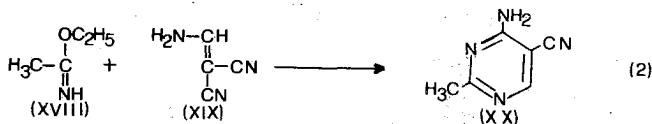
This synthetic method for vitamin B<sub>1</sub> is in extensive use today.

### 2. Method of Todd and Bergel<sup>23</sup>

Todd and Bergel<sup>23</sup> developed a different method. The pyrimidine derivative (Formula XV) is transformed to the 4-amino-2-methyl-5-thioformamido-methyl-pyrimidin (Formula XVI). This is then condensed with 3-chloro-5-hydroxy-2-pentanone (Formula XVII) resulting to the direct preparation of the hydrochloric acid salt of thiamine.



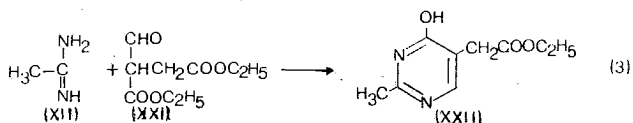
The pyrimidine derivative (XV) is synthesized from acetamido-ethyl-ether hydrochloride (XVIII) and amino-methylene-malodinitrile<sup>15,24</sup> (XIX) (Reaction 2).



The last product (XX) is reduced by the method of Todd<sup>15,24</sup> and finally is transformed to the thio-formamido-dimethyl derivative (Formula XVI).

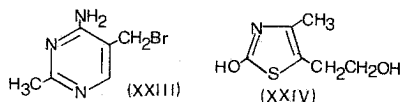
### 3. Method of Andersag and Westphal<sup>25</sup>

Andersag and Westphal<sup>24,25</sup> described the synthesis of a pyrimidine derivative (XXII) from acetamidine (XII) and formyl-succinic ester (XXI).



This finally yields 4-amino-5-bromomethyl-2-methyl-pyrimidine (Formula XXIII) with a series of reactions.

The same investigators synthesized also the thiazole derivative, 2-hydroxy-5-β-hydroxy-ethyl-4-methyl-thiazolium (Formula XXIV) by the interaction of 3-bromo-3-acetopropyl-acetate and barium isothiocyanide.



The two halves (Formula XXIII and XXIV) of thiamine react together and produce thiamine-bromide hydrobromide.

#### *Properties of thiamine chloride hydrochloride*

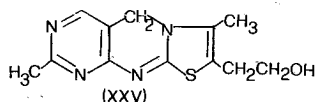
Thiamine chloride hydrochloride is the 3-(4'-amino-2'-methyl-pyrimidyl-5'-methyl)-5-β-hydroxyethyl-4-methyl thiazolium chloride hydrochloride and it is white and odourless in the solid state, when pure<sup>15</sup>. It is very soluble in water and less soluble in methanol and 95% ethanol. It is not stable in ether, acetone, chloroform and benzene. It is crystallized from aqueous ethanol solutions as hemihydrate and melts at 248-250°C with simultaneous decomposition<sup>15</sup>. Its stability in aqueous solutions depends primarily on the pH. Farrer<sup>26</sup> found that thiamine was completely destroyed, if boiled for 15 min at pH=9, while its proportions destroyed in an hour at pH=8, 7, 6, 5, 4 and 3 are 100, 67.8, 53.4, 40.0, 20.3 and 16%. The buffer used to attain the desired pH value also affects the stability of thiamine<sup>15</sup>. Thus, it is more stable in a buffer of phosphates than acetates or borates.

When thiamine hydrochloride is treated with NaHSO<sub>3</sub> for 2-3 days yields the slightly soluble product 4-amino-2-methyl-pyrimidyl-5-methano sulfonic acid. When a solution of thiamine hydrochloride in hydrochloric acid is treated with formaldehyde and diazotised sulfanilic acid, a pink color is formed; with the addition of isobutyl alcohol and shaking, the color is transferred to the alcoholic layer. This reaction is the basis for the quantitative estimation of thiamine and was discovered by Peters<sup>15</sup>.

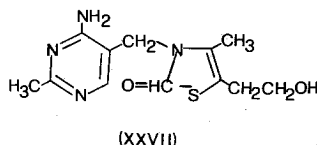
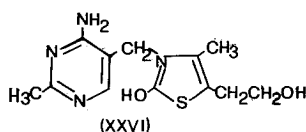
When a slightly alkaline solution of thiamine reacts with potassium ferricyanide, thiochrome is formed<sup>15,24</sup>.



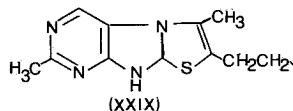
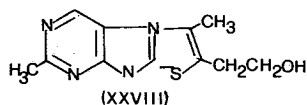
The reaction is also in use for the chemical estimation of the vitamin.



The action of alkali hydroxide solutions on thiamine has also been studied<sup>27</sup>. Upon addition of such a solution to thiamine, a pseudobase is produced (Formula XXVI) which is then transformed to colorless thiol (Formula XXVII).



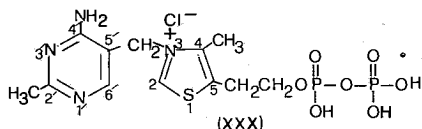
The thiol is oxidised to bisulfide. In strongly alkaline solution (pH > 11) thiamine is transformed to the corresponding yellow thiol (XXVIII) following the formation of the intermediate (XXIX).



Finally, from thiol (XXVIII) thiochrome is formed (XXV).

#### *Biological action of thiamine*

The biologically active form of thiamine is its pyrophosphate ester, thiamine pyrophosphate (TPP). (Formula XXX). This was first isolated from natural sources by Lohman and Schuster<sup>28</sup>.



TPP is prepared in low yields, with the action of  $\text{POCl}_3$  on thiamine<sup>29</sup>. Better yields are obtained by the reaction of the 5-bromo-ethyl-thiazol analog of thiamine hydrobromide with silver pyrophosphate in pyrophosphoric acid<sup>30,31</sup>.

TPP is the coenzyme of many enzymes and catalyzes different types of reactions. The enzymes using TPP are carboxylase, pyruvic dehydrogenase,

transketolase and phosphoketolase. For the catalytic action divalent metal ions, like  $Mg^{+2}$  are also required<sup>32</sup>.

The reactions that are catalysed by TPP are two main types; (a) the decarboxylation of  $\alpha$ -ketoacids and (b) the formation or degradation of  $\alpha$ -ketols<sup>32</sup>. According to the generally accepted view, these reactions proceed through an intermediate of the so-called «active aldehyde» which is formed between the C<sub>2</sub> of thiazole and the keto groups<sup>32</sup>. The «active aldehyde» is anionic and may give different kind of products<sup>32,33</sup>:

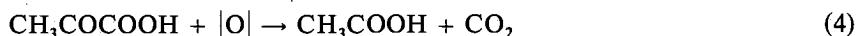
- (i) Its reaction with a proton yields aldehyde. For example, the non oxidative decarboxylation of pyruvic acid.
- (ii) By reacting with an oxidative agent like lipoic acid, yields acyl-dihydrolipoic acid (Oxidative decarboxylation of  $\alpha$ -ketoacids).
- (iii) The reaction with another aldehyde group (acetoin-reaction), and the transketolase reaction where the glycolaldehyde group of a ketose is transferred to an aldose.
- (iv) The reaction with inorganic phosphate (phosphorolysis) yields an acylphosphoric acid, a high energy compound.

#### *Mechanism of catalytic action*

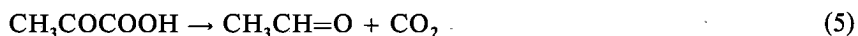
The catalytic action of TPP, as a coenzyme of different enzymes catalyzing many reactions, will be examined here. Emphasis will be given to the possible role of the bivalent metal ions during these reactions. All these reactions proceed through the formation of the «active aldehyde» of TPP<sup>32,33</sup>. The mechanism for the formation of the common for all the reactions «active aldehyde» may be the same, as far as TPP and metal ions are concerned. However, TPP was formerly thought as the coenzyme of only the enzyme carboxylase, and called «cocarboxylase» for that. The early investigations therefore, referred to the mechanism of decarboxylation of pyruvic acid, made by the enzyme carboxylase.

The enzyme carboxylase was isolated from the yeast<sup>28</sup> and it is constituted by a specific protein of molecular weight 150000 (apoenzyme), cocarboxylase or TPP (coenzyme) and metal ions like  $Mg^{+2}$  in the ratio (1:1:5) respectively. Pyruvic acid is transformed to acetaldehyde by the action of this enzyme and the many early investigators tried to establish this mechanism<sup>15</sup>.

The pyruvic acid can be metabolized in many ways. For example its oxidation to acetic acid and CO<sub>2</sub>, in the presence of air, was believed to be catalysed by TPP<sup>15</sup>.



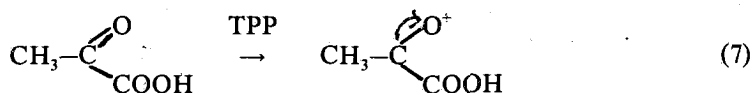
Lohman and Schuster proposed<sup>28,34</sup> that TPP catalysed the anaerobic decarboxylation of pyruvic acid to acetaldehyde and CO<sub>2</sub>.



Krebs *et al*<sup>35,36</sup> and Hill<sup>37</sup> believed that it could also dismutate as follows:



Barron *et al*<sup>38</sup> proposed that thiamine activates the pyruvic acid molecule as follows:

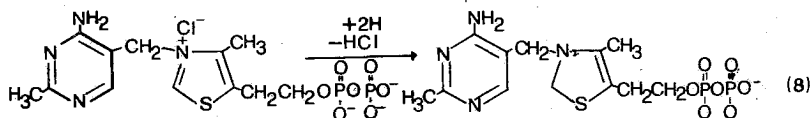


In this way, the activated pyruvic acid molecule is able to react in the proper way and be oxidized to acetic acid, reduced to lactic acid, decarboxylized to acetaldehyde, dismutate to lactic and acetic acid and carboxylized to oxaloacetic acid<sup>38</sup>.

Later, many experiments showed<sup>15</sup> that thiamine not only catalyzed the oxidation and dismutation of pyruvic acid, but as an integral part of the enzyme carboxylase and other enzymes, could take part in different reactions (See above).

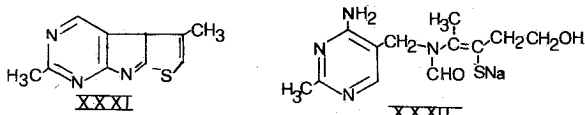
#### *Thiamine as a reversible oxidation-reduction system.*

Lipmann<sup>39,40</sup> proposed that in lactic acid bacteria as the *B. delbrücki*, thiamine acts as a dehydrogenating catalyst, producing reaction (1), while in the yeast it catalyses reaction (2). He finally<sup>41</sup> proposed reaction (3) for TPP in the pigeon brain tissue. Lipmann<sup>42</sup> also showed that thiamine pyrophosphate can be hydrogenated in the presence of Pt black or sodium dithionate to dihydrothiamine pyrophosphate.

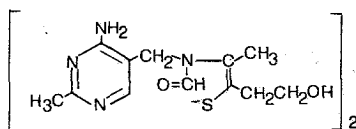


According to the reaction (8), Lipman proposed that cocarboxylase must act as a reversible oxidoreduction system as Warburg's yellow enzyme<sup>15</sup>.

Zima and Williams<sup>43</sup> also suggested that thiamine acts as an oxidation-reduction enzyme. They were based on the fact that thiamine decomposes to products XXXI and XXXII under the action of ethoxysodium or concentrated aqueous solutions of NaOH.



These products are converted to a disulfide XXXIII under the action of  $\text{I}_2$ , which is then reduced with tin and hydrochloric acid to thiamine again.

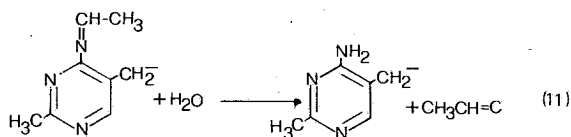
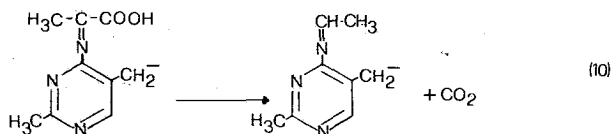
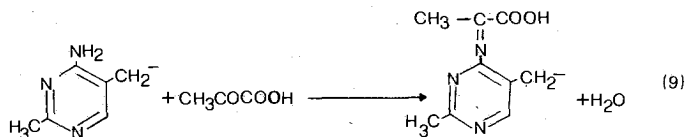


XXXIII

The disulfide has 60-70% the antineuritic action of thiamine. Since thiamine is stable only in acidic solutions, while its stability decreases as the pH rises, they concluded that in the cell at physiological pH, it must be found in the forms XXXI or XXXII. Therefore, Zima *et al*<sup>44</sup> proposed that thiamine's action as a biocatalyst must be due to an oxidation-reduction system with its disulfide, similar to the cysteine-cystine system. Thiamine is easily oxidized with dilute H<sub>2</sub>O<sub>2</sub> at pH~7.5 to its disulfide, while the disulfide, is reduced to thiamine or the corresponding thiol with cysteine or glutathione, but not with ascorbic acid. Later investigations<sup>45,46</sup> proved that neither the model of Lipmann<sup>15</sup> nor the one of Zima<sup>43,44</sup> were correct. It was proved that the cocarboxylase and its thiol form liberate CO<sub>2</sub> from pyruvic acid, while the disulfide pyrophosphate XXXIII was not active. Therefore, the idea of the thiamine action as an oxidation-reduction system was abandoned.

#### Formation of intermediate Schiff bases

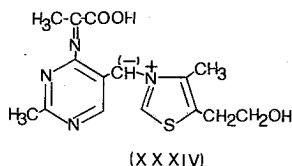
Langebeck<sup>47</sup> proposed a mechanism for the decarboxylation of pyruvic acid with the formation of acetaldehyde, through an intermediate of Schiff base, with the amino group of the pyrimidine moiety of thiamine (Scheme I).



Scheme I

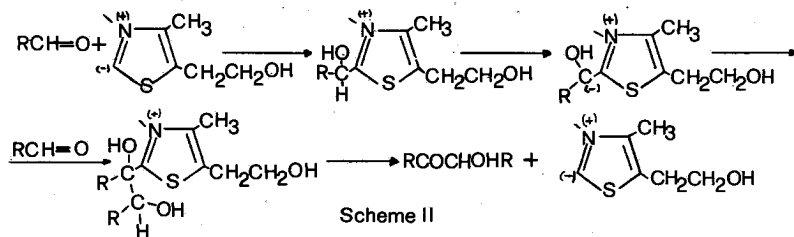
This mechanism was proposed based on the fact, that many primary amines are able to decarboxylize pyruvic acid through the formation of Schiff bases. Thiamine itself was not able to give the same reaction under the same conditions and this accounts against the proposed mechanism<sup>47</sup>. This inability of thiamine was attributed to the weak basic properties of the amino group, the lone pair of electrons of which, participate to the ring resonance. Langebeck<sup>47</sup> also did not give any role to the thiazole part of thiamine during the enzymatic action.

Wiesner and Valenta<sup>48</sup> also proposed an analogous to Langebeck's mechanism, where the intermediate Schiff base is stabilized through an «ylid» type structure (XXXIV).

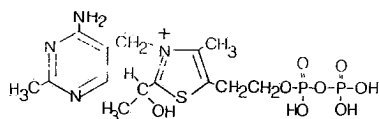


#### Thiamine as catalyst in non enzymatic models.

Mizuhara *et al*<sup>49,50</sup> in 1951, showed that thiamine at room temperature and at  $\text{pH} \approx 8.4$  can decarboxylate pyruvic acid, catalyze the formation of acetone and the reactions of diacetyl and acetaldehyde to acetic acid and acetone. Using this non enzymatic model, Breslow<sup>51</sup> proposed a mechanism for the formation of acetone from acetaldehyde and pyruvic acid. According to this mechanism, pyruvic acid is combined with the methylenic bridging group of the two rings of thiamine and forms an intermediate product, which loses  $\text{CO}_2$  and produces acetaldehyde, regenerating thiamine. However, Ingraham and Westheimer<sup>52,53</sup> in experiments with deuterated compounds, showed that the methylenic group is not ionized and this is contrary to the mechanism of Breslow<sup>51</sup>. Breslow<sup>54</sup> confirmed this result and proposed a similar mechanism, which implied the formation of a stable zwitterionic intermediate, with subsequent ionization of a hydrogen from  $\text{C}_2$  of the thiazole ring, as follows:



This mechanism is also supported from the works of Holzer *et al*<sup>55,58</sup>, who showed that the dismutation of pyruvic acid catalyzed by carboxylase is taking place through a condensation product of thiamine pyrophosphate, which was isolated (XXXV).



(X X X V)

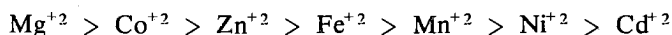
This active intermediate condensation product was called «active acetaldehyde». Breslow and McNelis<sup>59,60</sup> also prepared a series of model compounds, intermediate products of their mechanism, which were active catalyst. These were 2-( $\alpha$ -hydroxyethyl)-3-benzyl-4-methyl-thiazolium bromide and 3-benzyl-4-methyl thiazolium bromide. The mechanism of Breslow<sup>54,59,60</sup> is widely accepted today and has been confirmed from other works either<sup>15,61,62</sup>.

Haake *et al*<sup>63</sup> compared the H-D exchange rates of C<sub>2</sub> of thiazole, in the ions 3,4-dimethyloxazole, 3-4-dimethylthiazole and 1,3,4-trimethylimidazole. They found that the thiazole derivatives exchange this proton with deuterium, 3000 times faster than the imidazole derivatives and about 300 times slower than the oxazole ones. They concluded<sup>63</sup> that the thiazole derivatives possess the proper stability and rate in the formation of the «ylid» intermediate. They attributed this stability to the overlap of d orbitals of sulfur with  $\sigma$  orbitals of C<sub>2</sub>. Theoretical calculations performed by Pullman and Spanjard<sup>64</sup> had showed high  $\pi$  electron density on the C<sub>2</sub> of the thiazole ring of thiamine, in agreement with the greater kinetic acidity of this position. Sax *et al*<sup>65</sup> in their X-ray structure determination of hydroxyethylthiamine, find also a negative charge on C<sub>2</sub> of thiazole. However, the relative kinetic acidity order of oxazole and thiazole salts for the protons of C<sub>2</sub> were found inverse than predicted<sup>66</sup>. This led Pullman and Collin<sup>67</sup> to revised quantum mechanical calculations, which predicted a partial positive charge for this position. Gallo and Sable<sup>68</sup> agree with this conclusion from their <sup>13</sup>Cnmr studies of DL-2-( $\alpha$ -hydroxyethyl) thiamine and related compounds. According to these investigators<sup>68</sup> a partial positive charge on C<sub>2</sub> of thiazole explains the easy formation of carbanion at this position, either enzymatically or in model systems. The theoretical calculations of Jordan<sup>69</sup> also agree with this view.

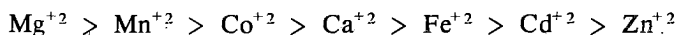
*Other mechanisms. Role of the different parts of TPP during the enzymatic reactions*

Despite the general acceptance of Breslow mechanism<sup>54,59,60</sup>, there are many questions unanswered in it<sup>70</sup>, as for example the role which the

pyrimidine moiety of thiamine may play during the enzymatic reactions. This mechanism does not take into account also the rôle which the bivalent metal ions may play in the enzymatic reactions, a fact which had been recognized since 1932<sup>71</sup>. Many investigations<sup>72,74</sup> performed on the rôle of bivalent metal ions, in the enzymatic action of thiamine pyrophosphate, showed that their activity varies and the most active were the  $Mg^{+2}$  ions. For the decarboxylation of pyruvic acid with carboxylase isolated from wheat germ<sup>72</sup>, the activity follows the order:



If the carboxylase is taken from the yeast<sup>73</sup>, the catalytic efficiency varies as follows:

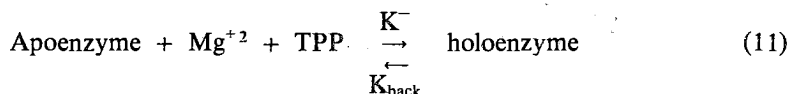


Finally, for transketolase taken from the yeast<sup>74</sup> the order is:

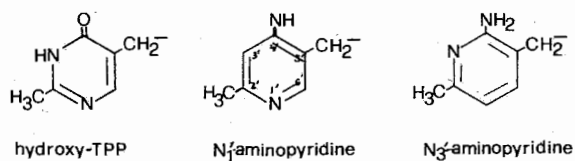


It was firstly supposed that the bivalent metal ions and particularly  $Mg^{+2}$ , act as bridges between the apoenzyme and coenzyme of thiamine pyrophosphate<sup>73,75,76</sup>. The presence of the pyrophosphate group is necessary, since pure thiamine and thiamine monophosphate do not show enzymatic action<sup>73</sup>. More recent investigations on the kinetics of coenzyme-apoenzyme binding, showed that the coenzyme is bound firmly to the apoenzyme only in the presence of  $Mg^{+2}$  ions<sup>77</sup>. The idea of  $Mg^{+2}$  ions bridging the apoenzyme and the coenzyme of thiamine pyrophosphate<sup>73,75,76</sup> is also supported from the fact that the antagonist of thiamine pyrophosphate, thiochrome can not combine with the apoenzyme in the absence of  $Mg^{+2,78}$ .

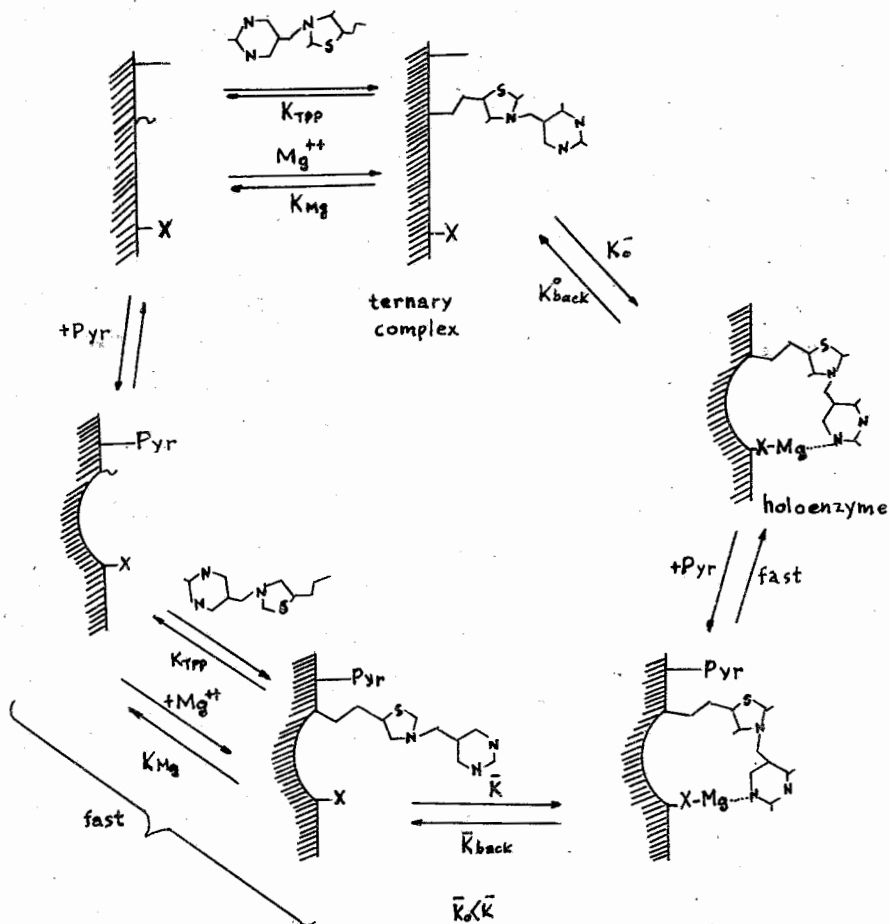
Schellenberger<sup>70</sup> studied with kinetic methods the recombination reaction of holoenzyme from its components, apoenzyme, metal ion and thiamine pyrophosphate, as follows:



He found that  $Mg^{+2}$  ions were necessary for the stable binding of the apoenzyme with TPP, as well as TPP for the stable binding of  $Mg^{+2}$ . In other words, all three components were indispensable for the formation of the thermodynamically stable holoenzyme, since it was not possible to detect stable bonds between TPP and  $Mg^{+2}$  ions only. Also the formation of the holoenzyme was not reversible. As far as the rôle of pyrimidine and thiazole parts of thiamine in the enzymatic reactions are concerned, he proposed a mechanism (Scheme III), using analogs of TPP, as for example hydroxy-TPP  $N_1'$ -aminopyridine and  $N_3'$ -aminopyridine.



The first two of these thiamine analogs show enzymatic activity and can bind to the apoenzyme, while the third does not. Therefore, he concluded that  $Mg^{+2}$  binds through the N<sub>1</sub> of the pyrimidine moiety with the apoenzyme and not through the amino group or the N<sub>3</sub>.

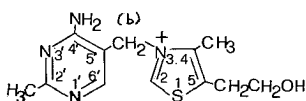


Scheme III



Witorf and Gubler<sup>79</sup> observed that the pyrimidine moiety of thiamine differs from the other naturally occurring pyrimidines in the 2'-methyl group and consequently it requires a different biosynthetic route from the others. These investigators<sup>79</sup> concluded with kinetic studies, that the 2'-methyl group of pyrimidine is rather used as the binding position of the coenzyme to the apoenzyme with hydrophobic interaction. Generally, there exist three possible binding regions of the coenzyme with the apoenzyme (a) region of ionic interaction of the pyrophosphate group, (b) region of hydrophobic interaction of the pyrimidine and thiazole parts and (c) region of charge transfer interaction between the positively charged part of thiamine and tryptophan residues of the enzyme<sup>80</sup>. The first region contains the pyrophosphate group of the coenzyme, which is bound through  $Mg^{+2}$  ions with different polar groups of amino-acids (possibly carboxylates) of the apoenzyme<sup>79</sup>. The second region contains the 2'-methyl group and the  $N_1'$  of pyrimidine together with the 4-methyl group of thiazole. As far as the last interaction is concerned, Shin *et al*<sup>80</sup> from the X-ray crystal structure determination of the complex thiamine-picrolinate dihydrate, concluded that this is of the dipole-induced dipole type interaction, through the pyrimidine ring, similar to the purine and pyrimidine interactions<sup>81</sup>. The  $N_1'$  position which had been proposed by Schellenberger<sup>70</sup> as the binding site with the apoenzyme through  $Mg^{+2}$  ions, is now proposed<sup>79</sup> as bound to a polar substrate with the aid of hydrogen bonding, because the coenzyme binding is greatly reduced at  $pH \sim 5$ , which corresponds to the  $pK$  of the protonation of this position<sup>21,82,83</sup>.

As to the role of the 4'-amino group of pyrimidine during the enzymatic reactions, it had been firstly proposed by Breslow and McNelis<sup>59</sup>, that it facilitates the removal of the  $C_2$  hydrogen of thiazole acting as a proton acceptor. However, it is known that this group is a weak base, because the lone electron pair on it participates to the ring resonance<sup>54,59,60</sup>. Schellenberger<sup>70,84</sup> had also proposed the same rôle for this group, but with increased basic properties due to the binding of the coenzyme to apoenzyme. The same thing had also been proposed by Biaglow *et al*<sup>85</sup>, and implies proper orientations of the two rings of pyrimidine and thiazole. These orientations are given from the two torsional angles<sup>86</sup>.  $\Phi_p = N_3 - C_b - C_5' - C_4'$  and  $\Phi_t = C_5 - C_b - N_3 - C_2$  (Formula XXXVI)



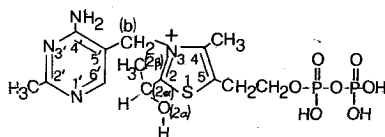
(XXXVI)

These angles are supposed to have positive values in the clockwise direction.

In order of the 4'-amino group to approach the C<sub>2</sub> position<sup>70,84,85</sup> the values of both these angles must be about  $\pm 90^\circ$  and thiamine has the so called structure V<sup>80</sup>. However, in non of the known structures of thiamine and its derivatives this structure has been found, except in oxythiamine very recently<sup>87</sup>. Oxythiamine possesses a 4'-keto oxygen and can form the intermediate active acetaldehyde as thiamine itself, but the reaction does not proceed further<sup>70</sup>. This had been attributed to its inability to act as a proton acceptor. When the thiamine derivatives are not substituted at the position C<sub>2</sub> they are in the F structure<sup>21,86,88</sup>, with  $\Phi_T = 0^\circ$  and  $\Phi_p = \pm 90^\circ$ , while in the C<sub>2</sub> substituted derivatives it is found in the S structure<sup>65</sup> with  $\Phi_T = \pm 100^\circ$  and  $\Phi_p = + 150^\circ$ .

Suchy *et al*<sup>89</sup> confirm the weak basic properties of the 4'-amino group with <sup>1</sup>Hnmr studies. However, these workers<sup>89</sup> do not exclude a similar rôle for this group or of another ring-nitrogen atom acting as proton acceptor, with the aid of an intra or inter molecular hydrogen bonding. This is because thiamine exchanges the C<sub>2</sub> hydrogen 10 times faster than oxythiamine, while the pK of the protonation of the former is about 5 and of the latter 2.3. However, the different inductive effect of thiamine and oxythiamine causing these differences can not be excluded<sup>82,89</sup>. For example N-benzylthiazole exchanges faster the protons of C<sub>2</sub> with deuterium than the N-methylthiazole<sup>59</sup>. This has been explained with the greater electron donor properties of the benzyl group as compared to the methyl<sup>59</sup>. Gallo and Sable<sup>68</sup> also consider the inductive effect as responsible for the different kinetic acidity of thiamine from its analogs, from <sup>13</sup>Cnmr studies of N-substituted thiazole derivatives.

The rôle that had been given to the 4'-amino group of the pyrimidine moiety was not only limited to aid the release of the C<sub>2</sub> protons, but also to the creation of carbanion with proton acceptance from the C(2 $\alpha$ ) of the intermediate condensation product of active acetyldehyde (Formula XXXVII) and also release of the 2'-hydroxyethyl group with hydroxyl detachment<sup>59</sup>.

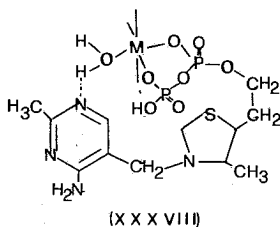


(XXXVII)

Sax *et al*<sup>65</sup> determined the crystal structures of 2-( $\alpha$ -hydroxyethyl)-3,4-dimethylthiazolebromide and DL-2-( $\alpha$ -hydroxyethyl) thiamine chloride hydrochloride and found that the 4'-amino group of pyrimidine was far from the C<sub>2</sub> substituent of thiazole (Structure S). The values of the torsional angles were  $\Phi_p = -145.6^\circ$  and  $\Phi_T = -100.3^\circ$  for 2-( $\alpha$ -hydroxyethyl) thiamine<sup>65</sup>. Therefore, the 4'-amino group can not act as a proton acceptor from O (2 $\alpha$ ). The O (2 $\alpha$ ) atom is near the sulfur S<sub>1</sub> atom, due to intermolecular S<sup>+</sup> ...O<sup>-</sup> interaction between them<sup>65</sup>. The structure S is stabilized in this way. The same conformation exists also in solution as it is revealed by the <sup>1</sup>Hnmr studies of 2-( $\alpha$ -hydroxyethyl)thiamine<sup>90-92</sup>. Therefore, it is rather improbable that the conformation will change during the enzymatic actions<sup>65</sup>. Jordan<sup>69</sup> concludes with quantum mechanical calculations that 2-( $\alpha$ -hydroxyethyl) thiamine is much less flexible than the non substituted at C<sub>2</sub> thiamine and thiamine pyrophosphate in respect to the relative positions which can take the pyrimidine and thiazole rings relative to each other.

#### *Rôle of the bivalent metal ions*

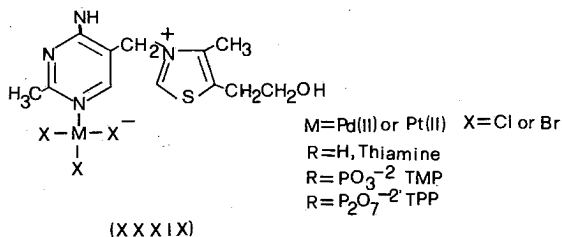
As to the rôle of the bivalent metal ions in the enzymatic action of thiamine, besides Schellenberger<sup>70</sup> who proposed that Mg<sup>+2</sup> binds to N<sub>1</sub>' of pyrimidine, White and Drago<sup>93</sup>, based on <sup>1</sup>Hnmr studies, also proposed that Co<sup>+2</sup> and Ni<sup>+2</sup> ions bind to N<sub>1</sub>' of thiamine pyrophosphate. On the other hand, Gallo *et al*<sup>94</sup> also with <sup>1</sup>Hnmr, proposed that Co<sup>+2</sup> and Ni<sup>+2</sup> are not directly bound to N<sub>1</sub>', but they approach this position with hydrogen bonding through a water molecule (Formula XXXVIII).



Grande *et al*<sup>95</sup> with <sup>1</sup>Hnmr and <sup>31</sup>Pnmr studies, found that Mn<sup>+2</sup> binds to the pyrophosphate group of TPP.

Despite the many indications for the metallic ions approaching the N<sub>1</sub>' position of pyrimidine in aqueous solutions<sup>70,93,94</sup>, all the isolated solid adducts of metal ions with thiamine are ionic salts of the type [MX<sub>4</sub>]<sup>-2</sup> [Th]<sup>+2</sup> or [MX<sub>4</sub>]<sup>+2</sup> [Th]<sup>+1</sup><sub>2</sub><sup>96-99</sup>,

where  $M = \text{Co}^{+2}$ ,  $\text{Ni}^{+2}$ ,  $\text{Cu}^{+2}$ ,  $\text{Zn}^{+2}$ ,  $\text{U}^{+4}$  and  $X = \text{Cl}^-$ ,  $\text{Br}^-$ . Marzotto *et al*<sup>100</sup> suggested that  $\text{Cu}^{+2}$  binds to  $\text{N}_1'$  of pyrimidine in aqueous solutions. However, the X-ray crystal structure determination of the complex isolated in the solid state<sup>98</sup>, proved it to be an ionic salt. The same thing was also proven in the crystal structure of the  $\text{U}^{+4}$ -thiamine complex<sup>96</sup>. Richardson *et al*<sup>101</sup> concluded from the X-ray crystal structure determination of the complex thiaminium tetrachlorocadmate monohydrate, that the existence of a direct metal-ligand bond would lead to a large loss of resonance energy of thiamine. This is why the direct metal thiamine bond is very difficult to be formed. Only in the case where the metal-ligand bond energy is greater than the loss in resonance energy plus the solvation energy of the metallic ions, such a bond could exist<sup>101</sup>. Perhaps the only examples of metal thiamine derivative complexes which present a direct metal- $\text{N}_1'$  of pyrimidine bond are the ones of Pd (II) and Pt (II)<sup>102</sup> which correspond to the general formula XXXIX. These molecules are zwitterionic, with a positive charge on the thiazole nitrogen and a negative charge due to the excess of chlorine atoms. It should be noted that the protonation of thiamine takes also place at the same  $\text{N}_1'$  position<sup>21,82,84</sup>.



The reason for the relatively easy formation of these complexes is possibly the great bond strength of the Pd-N and Pt-N bonds. A comparison of M-N force constants is given in Table 1<sup>103</sup>.

TABLE 1: Force constants of different N-M bonds.  $K$  in  $\text{mdynes}/\text{\AA}$ .

Complex	$K$
$\text{Cr}(\text{NH}_3)_6 \text{Cl}_2$	0.94
$\text{Co}(\text{NH}_3)_6 \text{Cl}_3$	1.05
$\text{Cu}(\text{NH}_3)_4 \text{Cl}_2$	1.24
$\text{Pd}(\text{NH}_3)_4 \text{Cl}_2$	1.71
$\text{Pt}(\text{NH}_3)_4 \text{Cl}_2$	2.22

In conclusion, the proposal of other workers also<sup>70,93,94</sup> that the metallic ions bind through  $\text{N}_1'$  of the pyrimidine moiety of thiamine, directly or through hydrogen bonding in the enzymatic reactions is rationalized, since the positive



Since the methylated thiamine presents greater enzymatic activity than thiamine, as well as accelerates the «ylid» formation, decarboxylation and acetoin formation, it is concluded<sup>104</sup> that the presence of the positive charge on N<sub>1</sub><sup>+</sup> and consequently of the positive metal ions, is of great importance for the charge transfer through inductive effects from the one ring in to the other. Nevertheless, the electrostatic field created from the presence of the positive charge on N<sub>1</sub><sup>104</sup> may be responsible for this behavior.

The thiamine molecule is a stable combination of pyrimidine and thiazole with a positive charge on it. In spite of the many efforts made to elucidate the mechanism of the catalytic action of thiamine enzymes and its derivatives and the many mechanisms that have been proposed, none of them can be considered as complete. At present, the experimental evidence available, only to suggestions can lead relative to the rôle that the different parts of the molecule may play in the enzymatic reactions. Perhaps, its complete elucidation must take into account the rôle of the metal ions, a fact that had been ignored in most cases until now. Doubtless, there remains a lot of effort and work to be done before it is completely elucidated.

## References

1. Funk C., *J. Physiol.*, **43**, 395 (1911).
2. Emmett A.D. and Louros G.O., *J. Biol. Chem.*, **43**, 265 (1920).
3. Goldberger J., Wheeler G.A., Lillie R.D. and Rogers L.M., *U.S. Publ. Health Rep.* **41**, 297 (1926).
4. Suzuki U., Shamimura T. and Okade S., *Biochem. J.* **43**, 89 (1912).
5. Edie E.S., Evans W.H., Moore B., Simpson G.C.E. and Webster A., *Biochem. J.*, **6**, 234 (1912).
6. Funk C., *J. Physiol.*, **46**, 487 (1913).
7. Funk C., *Brit. Med. J.*, **1**, 814 (1913).
8. Jansen B.C.P. and Donath W.F., *Proc. K. Acad. Wetensch. Amsterdam*, **29**, 1390 (1926).
9. Kinnerley H.W. and Peters R.A., *Biochem. J.*, **22**, 419 (1928).
10. Ibió., **27**, 225, 232 (1933).
11. Guha B.C. and Drummond J.C., *Biochem. J.* **23**, 880 (1929).
12. Williams R.R., Waterman R.E. and Keresztesy J.C., *J. Amer. Chem. Soc.*, **56**, 1187 (1934).
13. Williams R.R., *J. Amer. Chem. Soc.*, **57**, 229 (1935).
14. Williams R.R., «Vitamin B<sub>1</sub> and its use in Medicine», Macmillan (1938).
15. Robinson F.A., «The Vitamin Co-Factors of Enzyme Systems», Pergamon Press, London (1966).
16. Williams R.R., Ruehle A.E. and Finkelstein J., *J. Amer. Chem. Soc.*, **59**, 526 (1937).
17. Wöhmann M., *Annalen*, **259**, 299 (1890).
18. Charke H.T. and Gurin S., *J. Amer. Chem. Soc.*, **57**, 1876 (1935).
19. Windaus A., Tschesche R. and Grewe R., *Z. Physiol. Chem.*, **237**, 98 (1935).
20. Williams R.R., *J. Amer. Chem. Soc.*, **58**, 1063 (1936).
21. Kraut J. and Reed H.J., *Acta Cryst.*, **15**, 747 (1962).
22. Williams R.R. and Cline J.K., *J. Amer. Chem. Soc.*, **58**, 1504 (1936).
23. Todd A.R. and Bergel F., *J. Chem. Soc.*, 364 (1937).
24. Dyke S.F., «The Chemistry of Vitamins» Interscience Publishers, London, New York, Sydney... Chapt. 2 (1965).
25. Andersag H. and Westphal K., *Ber.*, **70**, 2035 (1937).
26. Farrer K.T.H., *J. Proc. Austral. Chem. Inst.*, **8**, 113 (1941).

27. Maier G.D. and Metzler D.E., *J. Amer. Chem. Soc.*, **79**, 4386 (1957).
28. Lohmann K. and Schuster P., *Biochem. Z.*, **294**, 188 (1937).
29. Tauber H., *J. Amer. Chem. Soc.*, **60**, 730 (1938).
30. Weil-Malberber H., *J. Soc. Chem. Ind.*, **58**, 1021 (1939).
31. Weil-Malberber H., *Biochem. Z.*, **34**, 980 (1940).
32. Lehninger A.L., «*Biochemistry*», Worth Publishers, Inc., New York, page 337 (1975).
33. Kapoulas V., «*Aspects of Biochemistry*», Athens, page 66 (1972).
34. Lohmann K. and Schuster P., *Naturwiss.*, **25**, 26 (1937).
35. Krebs H.A., *Nature*, **138**, 288 (1936).
36. Krebs H.A. and Johnson W.A., *Biochem. J.*, **31**, 645 (1937).
37. Hills G.M., *Biochem. J.*, **32**, 383 (1938).
38. Barron E.S.G., Lyman C.M., Lipton M.A. and Goldinger J.M., *J. Biol. Chem.*, **140**, 11 (1941).
39. Lipmann F., *Nature* **140**, 25 (1937).
40. Lipmann F., *Enzymologia*, **4**, 65 (1937).
41. Lipmann F., *Skand. Arch. Physiol.*, **76**, 225 (1937).
42. Lipmann F., *Nature*, **138**, 1097 (1936).
43. Zima O. and Williams R.R., *Ber.*, **73**, 941 (1940).
44. Zima O., Ritsert K. and Moll T., *Z. Physiol. Chem.*, **267**, 210 (1941).
45. Karrer P. and Krishna H., *Helv. Chim. Acta.*, **33**, 555 (1950).
46. Karrer P. and Viscontini M., *Helv. Chim. Acta*, **29**, 711 (1946).
47. Langebeck W., «*Die Organischen Katalysatoren*» Julius Springer, Berlin, page 55 (1935).
48. Wiesner K. and Valenta Z., *Experientia*, **12**, 192 (1956).
49. Mizuhara S., Tamura R. and Arata H., *Proc. Japan Acad.*, **27**, 302 (1951).
50. Mizuhara S. and Handler P., *J. Amer. Chem. Soc.*, **76**, 571 (1954).
51. Breslow R., *Chem. and Ind.*, R. 28 (1956).
52. Ingraham L. and Westheimer F., *Chem. and Ind.*, 846 (1956).
53. Fry K., Ingraham L. and Westheimer F., *J. Amer. Chem. Soc.*, **79**, 5225 (1957).
54. Breslow R., *J. Amer. Chem. Soc.*, **80**, 3719 (1958).
55. Holzer H. and Beauchamp K., *Angew. Chem.*, **71**, 776 (1959).
56. Holzer H. and Beauchamp K., *Biochim. Biophys. Acta.*, **46**, 225 (1961).
57. Holzer H., *Angew. Chem.*, **73**, 721 (1961).
58. Goedde H.W., Ulrich B., Stahlmann C. and Holzer H., *Biochem. Z.*, **343**, 204 (1965).
59. Breslow R. and McNelis E., *J. Amer. Chem. Soc.*, **81**, 3080 (1959).
60. Breslow R. and McNelis E., *J. Amer. Chem. Soc.*, **82**, 2394 (1962).
61. Krampitz L.O., Greull G., Miller C.S., Bicking J.B., Skeggs H.R. and Sprague J.M., *J. Amer. Chem. Soc.*, **79**, 5525 (1957).
62. White F.G. and Ingraham L.L., *J. Amer. Chem. Soc.*, **82**, 4114 (1960).
63. Haake P., Bausher L.P. and Miller W.B., *J. Amer. Chem. Soc.*, **91**, 1113 (1969).
64. Pullman B. and Spanjaard C., *Bioch. Biophys. Acta*, **46**, 576 (1961).
65. Sax M., Pulsinelli P. and Pletcher J., *J. Amer. Chem. Soc.*, **96**, 155 (1974).
66. Bruice T.C. and Benkovic S., *Bioorganic Mechanisms*, W.A. Benjamin Inc., New York, page 219 (1966).
67. Collin R.L. and Pullman B., *Arch. Biochem. Biophys.*, **108**, 535 (1964).
68. Gallo A.A. and Sable H.Z., *J. Biol. Chem.*, **251**, 2564 (1976).
69. Jordan F., *J. Amer. Chem. Soc.*, **98**, 808 (1976).
70. Schellenberger A., *Angew. Chem., Inter. Ed.*, **6**, 1024 (1967).
71. Anhagen E., *Z. Physiol. Chem.*, **204**, 149 (1932).
72. Singer T.P. and Pensky J., *J. Biol. Chem.*, **196**, 375 (1952).
73. Green D.E., Herbert D. and Subrahmanyam V., *J. Biol. Chem.*, **138**, 327 (1941).
74. Kochetov G.A., Fillipov P.P. and Usmanov R.A., *Biokhimiya*, **34**, 810 (1969).
75. Green D.E., Herbert D. and Subrahmanyam V., *J. Biol. Chem.*, **135**, 795 (1940).
76. Williams R.J.P., *Biol. Rev., Cambridge Phil. Soc.*, **28**, 381 (1953).

77. Schellenberger A. and Hübner G., Hoppe-Seylers, Z. Pysiol. Chem., **348**, 491 (1967).
78. Wittorf J.H. and Gubler C.J., Eur. J. Biochem., **14**, 53 (1970).
79. Wittorf J.H. and Gubler C.J., Eur. J. Biochem., **22**, 544 (1971).
80. Shin W., Pletcher J., Blank G. and Sax M., J. Amer. Chem. Soc., **99**, 3491 (1991).
81. Bugg C.E., Thomas J.M., Sundaralingam M. and Rao S.T., Biopolymers, **10**, 175 (1971).
82. Hopmann R.F.W. and Brugnoli G.P., Nature New Biology, **246**, 157 (1973).
83. Cain A.H., Sullivan G.R. and Roberts J.D., J. Amer. Chem. Soc., **99**, 6423 (1977).
84. Schellenberger A., Müller V., Winter K. and Hübner G., Hoppe-Seylers, Z. Physiol. Chem. **344**, 244 (1966).
85. Biaglow J.E., Miezal J.H., Suchy J. and Sable H.Z., J. Biol. Chem., **244**, 4054 (1969).
86. Pletcher J. and Sax M., J. Amer. Chem. Soc., **94**, 3998 (1972).
87. Shin W., Pletcher J., Sax M. and Blank G., J. Amer. Chem. Soc., **101**, 2462 (1979).
88. Karle I. and Britts K., Acta Cryst., **20**, 118 (1966).
89. Suchy J., Miezal J.J., Bantle G. and Sable H., J. Biol. Chem. **247**, 5905 (1972).
90. Ullrich J. and Manuschreck A., Eur. J. Biochem., **1**, 110 (1967).
91. Miezal J.J., Votaw R.G., Krampitz L.O. and Sable H.Z., Bioch. Biophys. Acta, **141**, 205 (1967).
92. Miezal J.J., Bantle G., Votaw R.G., Rosmer I.A. and Sable H.Z. J. Biol. Chem., **246**, 5213 (1971).
93. White W.D. and Drago R.S., Inorg. Chem., **10**, 2727 (1971).
94. Gallo A.A., Hansen I.L., Sable H.Z. and Swift T.J., J. Biol. Chem., **247**, 5913 (1972).
95. Grande H.J., Houghton R.L. and Veeger C., Eur. J. Biochem., **37**, 563 (1973).
96. Marzotto A., Bandoli G., Clemente D.A., Benetello F. and Galzigna L., J. Inorg. Nucl. Chem., **35**, 2769 (1973).
97. Talbert P.T., Weaver J.A. and Hambright P., J. Inorg. Nucl. Chem., **32**, 1024 (1970).
98. Caira M.R., Fazakerley G.V., Linder P.W. and Nassinibeni L.R., Acta Cryst., **B30**, 1660 (1974).
99. Fazakerley G.V. and Russell J.C., J. Inorg. Nucl. Chem., **37**, 2377 (1975).
100. Marzotto A., Nicolini M., Signor A. and Galzigna L., Atti Acad. Peloritana Pericolanti, Classe Sci. Fis. Mat. Nat., **50**, 79 (1970).
101. Richardson M.F., Franklin K. and Thompson D.M., J. Amer. Chem. Soc., **97**, 3204 (1975).
102. Hadjiliadis N., Markopoulos J., Pneumatikakis G., Katakis D. and Theophanides T., Inorg. Chim. Acta., **25**, 21 (1977).
103. Ferraro J.R., «Low-Frequency Vibrations of Inorganic and Coordination Compounds», Plenum Press, New York (1971), page 199.
104. Jordan F. and Mariam Y.H., J. Amer. Chem. Soc., **100**, 2534 (1978).



## STUDY OF PHYSICAL ADSORPTION USING THE HOLE THEORY

### I. MONOLAYER ADSORPTION ON HOMOGENEOUS SURFACES

D.A. JANNAKOUDAKIS, P.J. NIKITAS

*Laboratory of Physical Chemistry Fac. of Physics & Mathematics, University of Thessaloniki, Greece*

#### Summary

The hole theory of the liquid state is applied to describe the physical adsorption of gases on homogeneous solids. Equations are derived for the equation of state, the adsorption isotherm and the critical properties.

The equation of state is tested with Monte Carlo data and a good agreement is obtained. The adsorption isotherm is used to fit the adsorption data for the systems Argon-graphite and Argon-boron nitride at two different temperatures. The agreement with experiment is also found to be quite good. Deviations appearing at the critical region are due to the assumption of the random distribution of holes and molecules.

All molecular parameters except the gas-solid interaction are taken from outside sources. The gas-solid interaction parameters obtained by the present theory agree well with previously used values.

**Key words:** Argon, Hole theory, Physical adsorption.

#### Introduction

A large number of studies on the lattice theories of the liquid state have been carried out and various properties of liquids as well as phenomena which can be correlated with them, have been analysed by means of these theories<sup>1</sup>.

The hole theories<sup>2</sup> are an interesting part of the lattice or better of the quasilattice models. They are based on the simple L-JD theory<sup>3</sup> and they have received a satisfactory interpretation concerning the liquid state's phenomena, when a linear relation of the free volume on the number of neighbouring holes is supposed<sup>4,5,6,7</sup>.

The idea of holes in the liquid state has been first established by Eyring and it has led to the growth of the significant structures theory<sup>8</sup>. Even if this idea seems to be of a rather inventive character in what it concerns the liquid state, the presence of holes in the adsorption phase is one of the most steady assumptions. This shows that the hole theory, as well as every other theory

bearing on the assumption of holes in the liquid state, can be successfully extended to and also describe the phenomenon of physical adsorption<sup>9</sup>.

In this paper a model of physical adsorption of monatomic molecules on an energetically uniform surface based on the hole theory of liquids is developed. The two-dimensional adsorbed phase is regarded as a two-dimensional fluid, the number of holes of which is related to the experimentally measurable surface coverage. The proposed model is tested against Monte Carlo data and with the experimental results of Argon adsorption on highly graphitized carbon blacks (p-33) and on hexagonal boron nitride (BN).

## Theory

### a. The model

The adsorbed phase is considered to be a two-dimensional liquid-like layer adsorbed on a structureless, energetically uniform surface. The surface therefore imposes no structure on the adsorbed layer which is assumed to be in hexagonal close-packed configuration. The particles of the adsorbed phase interact 1. with the surface and 2. between themselves. The interaction with the surface is assumed to fall off rapidly enough with distance so we should regard that only a monomolecular layer is formed at low temperatures. The potential energy between the adsorbed molecules is assumed to be given by the additive contributions of an intermolecular potential which is satisfactorily represented by a Lennard-Jones «6-12» potential.

The molecules vibrate normal to the adsorbing surface and each of them is free to move in the cell which is formed by the presence of neighbouring molecules. The number  $L$  of cells is supposed to be greater than the number  $N$  of the adsorbed molecules so that finally some of the cells remain vacant.

### b. Partition function

If it is assumed that each adsorbed molecule is free to move in a singly occupied cell formed by its  $c$  nearest neighbors and that within its cell the molecule is under the influence of a field  $\Psi(r)$ , where  $r=0$  is located at the minimum in  $\Psi(r)$ , then the partition function of this molecule is

$$q_i = (\lambda \cdot a_f(0)) \cdot q_{\text{vib.}} \cdot \exp\left(\frac{U_0^*}{kT}\right) \cdot \exp\left(\frac{-\Psi(0)}{2kT}\right) \quad (1)$$

The first factor in Eq. (1) is the partition function for a «Devonshire» two-dimensional fluid<sup>10</sup>, where  $\lambda$  is  $2\pi mkT/h^2$  and  $a_f(0)$  is the free area for the  $i$  molecule which is given by<sup>11</sup>

$$a_f(0) = \pi a^2 \int_0^{0.2757} \exp\{-[\psi(r) - \psi(0)]/kT\} dy \quad (2)$$

where  $a$  is the radius of the cell containing the  $i$  adsorbed molecule and  $y = (r/a)^2$ , where  $r$  is the distance from the cell center to the molecule.

The second term  $q_{\text{vib}}$  is the harmonic oscillator partition function for vibrations normal to the adsorbing surface and it is represented by

$$q_{\text{vib}} = \exp\left(-\frac{x}{2}\right) / 1 - \exp(-x), \quad (3)$$

where  $x = \frac{h\nu}{kT}$

Finally, in Eq. (1) the two last factors are a correction for the energy zero.  $U_0$  is the adsorbate-adsorbent interaction energy.

Equation (1) is true when each cell is formed by  $c$  «uniformly smeared» nearest neighbouring molecules. According to the proposed model  $L$  is greater than  $N$  and therefore the nearest neighbouring molecules are not uniformly smeared. The presence of holes in the system has the following consequences<sup>4</sup>:

1. The change of the coordination number  $c$  of every molecule  $i$ , that is

$$c_i = y_i c$$

where  $y_i$  is some number between zero and unity.

2. The change of the energy term  $-\Psi(0)/2kT$ , (which becomes  $-y_i \Psi(0)/2kT$  if it is assumed that the potential energy of a molecule depends only on the number of neighbouring holes and not on their arrangement).

The canonical partition function can be found if we multiply  $q_i$  and add over all permissible arrangements of the  $N$  molecules:

$$Z_{\text{ads}} = \lambda^N q_{\text{vib}}^N \exp\left(\frac{NU_0}{kT}\right) \sum_{\langle y_i \rangle} \prod_{i=1}^N a_f(y_i) \cdot \exp[-y_i \Psi(0)/2kT] \quad (4)$$

where  $a_f(y_i)$  is given by the linear relation<sup>4,6</sup>

$$a_f(y_i) = y_i \cdot a_f(0) + (1 - y_i) \omega \quad (5)$$

in which  $\omega$  is the free area of a molecule having empty all its nearest neighbouring sites.  $\omega$  is equal to  $A/L$ , where  $A$  is the total surface of the system.

The sum in Eq. (4) is easily evaluated by means of the Bragg-Williams approximation<sup>12</sup>:

$$Z_{\text{ads}} = \lambda^N \cdot q_{\text{vib}}^N \cdot \exp\left(\frac{NU_0}{kT}\right) \cdot \frac{L!}{N! (L-N)!} \cdot [a_f(\bar{y}_i)]^N \cdot \exp[-\bar{y}_i N \Psi(0)/2kT] \quad (6)$$

where

$$\bar{y}_i = \frac{N}{L} = \frac{\omega}{v} \quad \text{and} \quad v = \frac{A}{N}$$

If we assume that the intermolecular potential is given by a Lennard-Jones «6-12» potential

$$u(r_{ij}) = 4\varepsilon \cdot \left\{ \left( \frac{\sigma}{r_{ij}} \right)^{12} - \left( \frac{\sigma}{r_{ij}} \right)^6 \right\} \quad (7)$$

we take the relations

$$\Psi(0) = \frac{3\sqrt{3} \cdot c \cdot \varepsilon}{16} \left( \frac{3\sqrt{3}}{\omega^{*6}} - \frac{8}{\omega^{*3}} \right) \quad (8)$$

$$a_f(0) = \frac{2\sqrt{3}\pi}{3} \omega \int_0^{0.2757} \exp \left\{ -1 \frac{3\sqrt{3}c\varepsilon}{16kT} \left( \frac{3\sqrt{3}}{\omega^{*6}} l(y) - \frac{8}{\omega^{*3}} m(y) \right) \right\} dy \quad (9)$$

where  $l(y)$  and  $m(y)$  are the well known functions<sup>10</sup>

$$l(y) = (1+y)(1+24y+76y^2+24y^3+y^4)(1-y)^{-11} - 1 \quad (10)$$

$$m(y) = (1+4y+y^2)(1-y)^{-5} - 1 \quad (11)$$

In Eq. (8) and (9)  $\omega^*$  is given by

$$\omega^* = \frac{\sqrt{3}}{2} \cdot \frac{a^2}{\sigma^2} = \frac{\omega}{\sigma^2} \quad (12)$$

because  $a$  and  $\omega$  are related, for a hexagonal close packed configuration, by the expression  $\omega = \sqrt{3} \cdot a^2/2$

### c. Thermodynamic properties

The Helmholtz free energy for the adsorbed phase is given by

$$A_{\text{ads}} = -kT \ln Z_{\text{ads}}$$

or

$$\begin{aligned} A_{\text{ads}} = & -NkT \ln \lambda - NkT \ln q_{\text{vib}} - NU_0 - NkT \ln a_f(\bar{y}_i) \\ & + \frac{1}{2} \frac{\omega}{v} N \Psi(0) - NkT \frac{v}{\omega} \ln \frac{v}{\omega} + NkT \left( \frac{v}{\omega} - 1 \right) \ln \left( \frac{v}{\omega} - 1 \right) \end{aligned} \quad (13)$$

The volume per cell is determined by minimizing  $A_{\text{ads}}$

$$\left( \frac{\partial A_{\text{ads}}}{\partial \omega} \right)_{\mu, T} = 0 \quad (14)$$

and the equation of state is calculated from

$$PA = -v \left( \frac{\partial A_{\text{ads}}}{\partial v} \right)_{\omega, T}$$

which gives

$$\frac{PA}{NkT} = \frac{\omega - a_f(0)}{a_f(0) + v - \omega} + \frac{\omega}{v} \frac{\Psi(0)}{2kT} - \frac{v}{\omega} \ln \left( 1 - \frac{\omega}{v} \right) \quad (15)$$

This is of the same form with that of the three-dimensional fluid<sup>(4)</sup>. The chemical potential for the adsorbed phase is given by

$$\mu_{\text{ads}} = \left( \frac{\partial A_{\text{ads}}}{\partial N} \right)$$

and it is

$$-\frac{\mu_{\text{ads}}}{kT} = \ln [\lambda \cdot q_{\text{vib}} \cdot a_f(\bar{y}_i)] \cdot \left( \frac{v}{\omega} - 1 \right) + \frac{U_0}{kT} - \frac{\omega}{v} \frac{\Psi(0)}{kT} + \frac{a_f(0) - \omega}{a_f(0) + v - \omega} \quad (16)$$

The adsorption isotherm can be obtained by equating  $\mu_{\text{ads}}$  and  $\mu_{\text{gas}}$ , where  $\mu_{\text{gas}}$  is the chemical potential of the gas phase in equilibrium with the adsorbed phase. For a monatomic gas  $\mu_{\text{gas}}$  is given by

$$\mu_{\text{gas}}/kT = \mu_{\text{gas}}^0/kT + \ln P \quad (17)$$

where

$$\mu_{\text{gas}}^0/kT = - \ln (\lambda^{3/2} kT)$$

and  $P$  is the gas pressure.

The resulting adsorption isotherm is

$$\ln P = -\frac{\mu_{\text{gas}}^0}{kT} - \ln [\lambda \cdot q_{\text{vib}} \cdot a_f(\bar{y}_i)] \cdot \left( \frac{v}{\omega} - 1 \right) - \frac{U_0}{kT} + \frac{\omega}{v} \frac{\Psi(0)}{kT} - \frac{a_f(0) - \omega}{a_f(0) + v - \omega} \quad (18)$$

If  $\theta$  is the surface coverage, then

$$\theta = \frac{N}{N_{\text{max}}} = \frac{N}{L} = \frac{\omega}{v}$$

Introducing this to Eq. (18) and assuming that  $a_f(0) \approx 0$ , which is a good approximation, we obtain

$$\ln P = \ln \frac{\lambda^{1/2} kT}{q_{\text{vib}} \cdot \omega} - \frac{U_0}{kT} - \ln \frac{(1-\theta)^2}{\theta} + \frac{\theta}{1-\theta} + \theta \cdot \frac{\Psi(0)}{kT} \quad (19)$$

$$\text{or} \quad \frac{\theta}{(1-\theta)^2} \exp\left(\frac{\theta}{1-\theta}\right) \exp\left(\frac{\theta\Psi(0)}{kT}\right) = \beta \cdot P \quad (20)$$

$$\text{where} \quad \beta = \frac{q_{\text{vib}} \cdot \omega}{\lambda^{1/2} kT} \exp\left(\frac{U_0}{kT}\right) \quad (21)$$

#### d. Critical properties

The critical properties of the adsorbed phase can be evaluated by equating to zero the first and the second derivatives of the pressure with respect to surface coverage. The critical properties are

$$\theta_c = 0.31 \quad (22)$$

$$T_c = -\Psi(0)/k \cdot 8.22 \quad (23)$$

### Results and discussion

#### a. Equation of state

The values of  $\omega^*$ , obtained from Eq. (14) are given in Table I and they are very close to those given by Henderson<sup>4</sup> for the three-dimensional problem. The reduced parameters  $T^*$  and  $v^*$  are  $kT/e$  and  $v/\sigma^3$  respectively. It must be noted that the influence of  $a_f(0)$  is generally insignificant.

Once values of  $\omega^*$  have been obtained, the compressibility factor  $PA/NkT$ , is easily calculated from Eq. (15) as a function of  $v^*$ . In Fig. 1 calculations based on Eq. (15) are compared with low-temperature Monte-Carlo experiments of Tsien and Valleau<sup>13</sup>. Although in Monte Carlo experiments the specific details of the computation can have pronounced effects on the results, the agreement of the results of the two methods is considered to be satisfactory.

#### b. Adsorption isotherm

Theoretical adsorption isotherms for Argon adsorbed on graphite and on boron nitride have been calculated using Eq. (19). Table II contains the molecular parameters used in this theory and Table III shows the values of  $\Psi(0)$  and its dependence on the surface coverage.

TABLE I: Equilibrium values of  $\omega^*$

$v^* \backslash T^*$	0.7	0.8	0.9	1.0	1.2	1.4
1.0	0.96	0.96	0.95	0.94	0.94	0.94
1.2	1.04	1.04	1.03	1.03	1.01	1.00
1.4	1.08	1.08	1.07	1.06	1.05	1.04
1.6	1.10	1.10	1.09	1.08	1.07	1.06
1.8	1.11	1.11	1.10	1.09	1.08	1.07
2.0	1.12	1.11	1.11	1.10	1.09	1.08
2.2	1.12	1.11	1.11	1.10	1.09	1.08
2.4	1.12	1.12	1.11	1.11	1.10	1.09
2.6	1.12	1.12	1.12	1.11	1.10	1.09
2.8	1.13	1.13	1.12	1.11	1.10	1.09
3.0	1.13	1.13	1.12	1.11	1.11	1.10
3.5	1.13	1.13	1.12	1.12	1.11	1.10
4.0	1.13	1.13	1.13	1.12	1.11	1.10
100.0	1.14	1.14	1.14	1.13	1.12	1.12

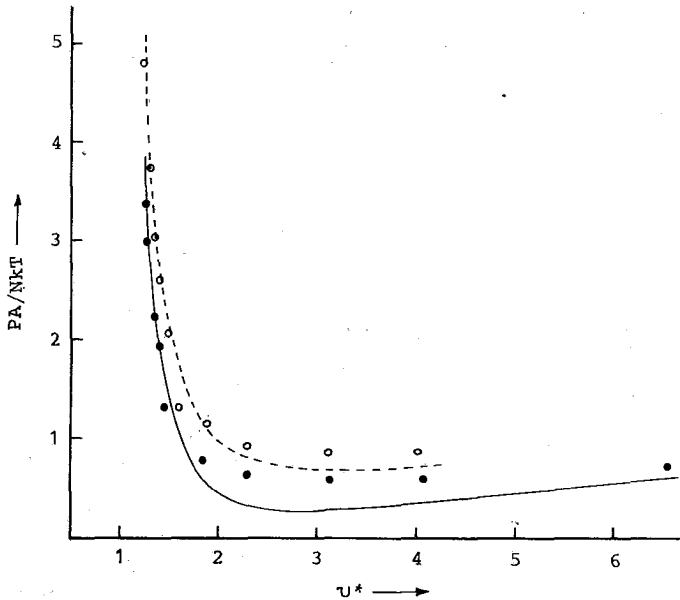


FIG. 1: Calculated and Monte Carlo values of compressibility factor. Monte Carlo data at  $T^* = 0.95$  (●●●) and at  $T^* = 0.70$  (ooo). Theoretical calculations at  $T^* = 0.95$  (—) and at  $T^* = 0.70$  (---).

TABLE II: *Molecular properties and parameters for Ar adsorption on graphite and BN.*

Property	Ar-P33	Ar-BN
$U_0$ cal/mole	2150 <sup>a</sup>	1894 <sup>a</sup>
$\nu$ sec <sup>-1</sup>	1.4.10 <sup>12b</sup>	1.1·10 <sup>12b</sup>
$\epsilon/k$ °K	96 <sup>c</sup>	96 <sup>c</sup>
$\sigma$ Å	3.405 <sup>d</sup>	3.405 <sup>d</sup>
$V_m$ cc (STP)/gm	3.66 <sup>e</sup>	5.06 (78°K) <sup>f</sup> 4.26 (90°K) <sup>f</sup>

a. Determined for the best fit of data.

b. See Ref. 9 in text.

c. Sams, J.R., Constabaris, G., and Halsey, G.P., J. Chem. Phys. **36**, 1334 (1962).

d. Hirshfelder, J.C., Curtiss, C.F., and Bird, R.B., *Molecular Theory of Gases and Liquids* (John Wiley & Sons, Inc. New York, 1954).

e. See Ref. 14 in text.

f. See Ref. 15 in text.

TABLE III: *Values of  $\Psi(0)/kT$  as calculated from Eq. (8).*

$\theta$	0.1	0.2	0.3	0.4	0.5	0.6	0.7	0.8
$T^*$	0.8	0.8	0.8	0.8	0.8	0.8	0.8	0.8
$-\Psi(0)/kT$	7.35	7.35	7.39	7.39	7.40	7.42	7.42	7.40
$T^*$	0.95	0.95	0.95	0.95	0.95	0.95	0.95	0.95
$-\Psi(0)/kT$	6.36	6.36	6.37	6.37	6.39	6.39	6.38	6.34

Figures 2. and 3. compare the theoretical isotherms with the experimental results of Ross and Oliver<sup>14</sup> for the system Ar-C and of Ross and Pultz<sup>15</sup> for the system Ar-BN at two different temperatures. The agreement is quite good at low and intermediate coverages.

The isotherm temperature dependence is also predicted quite well by this theory. The agreement is better for the isotherms at 90.1 °K than that at 77.6 °K.

It should be pointed out that all molecular parameters except the gas-solid interaction parameter, are taken from the bibliography. The gas-solid interaction energy  $U_0$  is adjusted to fit the experimental data. For the Ar-BN system  $U_0$  has been found to be equal to 1894 cal/mole, a value which is very close to 1900 cal/mole which has been obtained by Newsome<sup>16</sup> using the significant structure theory and to 1950 cal/mole which has been obtained by McAlpin and Pierotti<sup>9</sup> using the Frenkel, Halsey-Hill equation. Also the value  $U_0 = 2150$  cal/mole for the system Ar-C is in agreement with the value 2200 cal/mole obtained by McAlpin and Pierotti<sup>9</sup>.

### c. Critical properties

The critical properties have been calculated from Eq. (22) and (23) and these are:



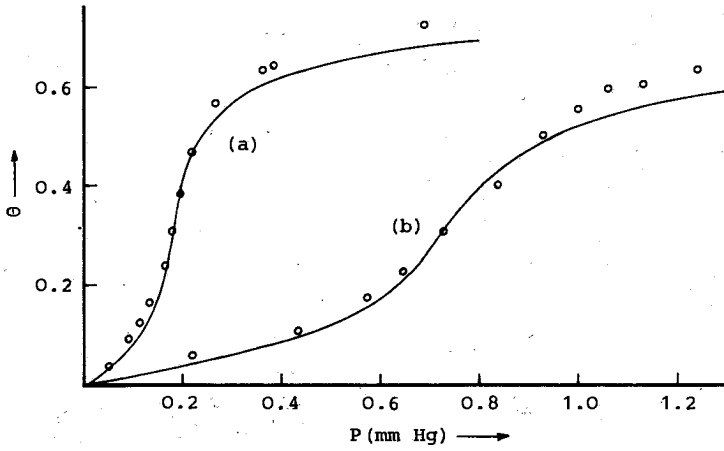


FIG. 2: Isotherms of Argon on graphite (a) and boron nitride (b) at 77.6°K. Points data from Ref. 14,15. Solid lines theoretical calculations.

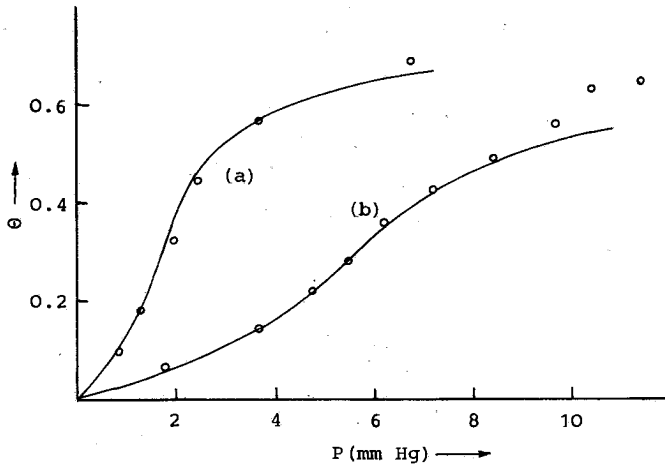


FIG. 3: Isotherms of Argon on graphite (a) and boron nitride (b) at 90.1°K. Points data from Ref. 14,15. Solid lines theoretical calculations.

$$\begin{aligned}\theta_c &= 0.31 \\ T_c^* &= 0.726 \\ v_c^* &= 3.645\end{aligned}$$

$$\left(\frac{PA}{NkT}\right)_c = 0.378$$

On the basis of their Monte Carlo study, Tsien and Valleau<sup>15</sup> found that the values of  $T_c^*$  range from 0.625 to 0.70. They estimated  $v_c^*$  at 2.63 and  $(PA/NkT)_c$  at 0.45.

There are very few data to make a reliable experimental estimate of the critical temperature for a number of systems. The critical temperature for Argon has been experimentally found to be around 68°K<sup>17</sup>.

The present model gives a theoretical value of 69.7 °K which is very close to the experimental one.

The critical coverage for the present model is 0.31 close to the value of 0.33 which is the critical coverage for a two-dimensional van der Waals fluid. The experimental data don't lead to a proper value of the critical coverage which must be close to 0.4 for a number of systems.

As a concluding remark, we may say that the present model works quite well at low and intermediate coverages and it generally gives a good picture of the adsorbed phase properties.

The deviations appearing at the critical region and at high coverages were within our expectations. This is due to the fact that the validity of two fundamental assumptions is limited to relatively high temperatures and low densities. These assumptions concern: 1) the linear dependence between the free area  $a_f(0)$  and the number of neighboring holes which according to Blomgren<sup>6</sup> doesn't hold for large densities and 2) the random distribution of holes and molecules which at the critical region doesn't give satisfactory results.

## Περίληψη

*Μελέτη τής φυσικής προσροφήσεως με τη θεωρία τών όπών  
I. Μονομοριακή προσρόφηση πάνω σε όμογενείς επιφάνειες*

Στήν έργασία αύτή γίνεται έφαρμογή τής θεωρίας τών όπών τής ύγρης καταστάσεως στή θεωρητική μελέτη του φαινομένου τής φυσικής προσροφήσεως άδρανών άερίων πάνω σε όμογενείς επιφάνειες.

Γιά τόν καθορισμό τής συναρτήσεως κατανομής γίνονται δύο κυρίως ύποθέσεις. Δεχόμαστε α) ότι ή έλεύθερη επιφάνεια κινήσεως ενός προσροφημένου μορίου έξαρτάται γραμμικά από τόν αριθμό τών γειτονικών όπών και β) ότι ύπάρχει μιá τυχαία κατανομή μορίων και όπών στο όλο σύστημα.

Βάσει τῶν ὑποθέσεων αὐτῶν βρίσκονται οἱ θεωρητικὲς σχέσεις γιὰ τὴν καταστατικὴ ἐξίσωση, γιὰ τὴν ἰσόθερμη προσροφήσεως καὶ γιὰ τὰ κρίσιμα δεδομένα τῆς προσροφημένης στιβάδας.

Ἡ καταστατικὴ ἐξίσωση ἐλέγχθηκε μὲ δεδομένα Monte-Carlo καὶ ἡ ἰσόθερμη προσροφήσεως χρησιμοποιήθηκε γιὰ τὴν προσαρμογὴ τῶν πειραματικῶν δεδομένων τῆς προσροφήσεως τοῦ Ag πάνω σὲ C καὶ πάνω σὲ BN γιὰ δύο διαφορετικὲς θερμοκρασίες. Ἡ συμφωνία μεταξὺ θεωρητικῶν καὶ πειραματικῶν δεδομένων ὡς καὶ τῶν ἀποτελεσμάτων Monte-Carlo θεωρεῖται πολὺ ἱκανοποιητικὴ. Μικρὲς ἀποκλίσεις παρατηροῦνται μόνο στὴν κρίσιμη περιοχὴ.

Ὅλες οἱ μοριακὲς παράμετροι, ἐκτὸς ἀπὸ τὴν ἐνέργεια ἀλληλεπιδράσεως μεταξὺ προσροφημένου ἀερίου καὶ στερεοῦ ὑποβάθρου, ἐλήφθησαν ἀπὸ τὴ βιβλιογραφία. Ἡ ἐνέργεια ἀλληλεπιδράσεως μεταξὺ προσροφημένου ἀερίου καὶ στερεοῦ ὑποβάθρου προσδιορίστηκε βάσει τοῦ προτεινόμενου μοντέλλου καὶ βρέθηκε σὲ πολὺ ἱκανοποιητικὴ συμφωνία μὲ τὶς τιμὲς ποὺ δίνονται στὴ βιβλιογραφία.

---

## References and Notes

1. Barker, J.A.: Lattice Theories of the Liquid State, Pergamon, Oxford 1963.
2. Hill, T.L.: Statistical Mechanics, McGraw-Hill Book company, New York 1956.
3. Lennard-Jones, J.E. and Devonshire, A.F.: Proc. Roy. Soc. (London) A 163, 53 (1937); A 165,1 (1938).
4. Henderson, D.: J. Chem. Phys. 37, 631 (1962).
5. Henderson, D.: J. Chem. Phys. 39, 54 (1963).
6. Blomgren, G.E.: J. Chem. Phys. 34, 1307 (1961); 38, 1714 (1963).
7. McLellan, A.G.: J. Chem. Phys. 40, 567 (1964).
8. Eyring, H., Ree, T., and Hirai, N.; Proc. Natl. Acad. Sci. U.S. 44, 683 (1958).
9. McAlpin, J.J. and Pierotti, R.A.: J. Chem. Phys. 41, 68 (1964); 42, 1842 (1965).
10. Devonshire, A.F.: Proc. Roy. Soc. (London) A163, 132 (1937).
11. The upper limit in the integral of Eq. (2) has been determined by the refined procedure suggested by Hill in Ref. 2 p. 378.
12. Guggenheim, E.A.: Mixtures, Oxford University Press, London 1951.
13. Tsien, F. and Valleau, J.P.: Mol. Phys. 27, 177 (1974).
14. Ross, S. and Olivier, J.P.: J. Phys. Chem. 65, 608 (1961).
15. Ross, S. and Pultz, W.W.: J. Colloid Sci. 13, 397 (1958).
16. Newsome, D.S.: J. Phys. Chem. 78, 2600 (1974).
17. Prenzlow, C.F. and Halsey, G.D.: J. Phys. Chem. 61, 1158 (1957).

## **MANY – ELECTRON THEORY OF DISCRETE – DISCRETE AND DISCRETE – CONTINUUM TRANSITION RATES FOR SYSTEMS WITH SYMMETRY**

CLEANTHES A. NICOLAIDES, YANNIS KOMNINOS

*Theoretical and Physical Chemistry Institute, National Hellenic Research Foundation, 48, Vassileos Constantinou Avenue, Athens 501/1 - Greece*

DONALD R. BECK

*Physics Department, University of Illinois, Urbana, Illinois 61820 U.S.A.*

### **Summary**

We present the essentials of a flexible and efficient theory of photoabsorption rates. By taking advantage of the system and transition operator symmetry, this theory predicts simply and consistently the important single and pair subshell correlation clusters which affect the photoabsorption cross-section the most. Thus, we show that the old and seemingly very complicated, conceptually as well as computationally, transition probability problem can be reduced to small computational proportions for closed as well as open shells. Furthermore, a general subshell cluster expansion and the application of simple rules allow the a priori identification of the major correlation effects in the discrete as well as in the continuous spectrum which influence conspicuously various experimental measurements of electronic structure and dynamics such as hyperfine structure and photoabsorption cross-sections. There have been many applications of this theory with results which agree with accurate experimental values. Here, two new applications are included: 1) The very accurate calculation of the Li, Be<sup>+</sup> 1s<sup>2</sup>2s<sup>2</sup>S – 1s<sup>2</sup>2p <sup>2</sup>P<sup>o</sup> oscillator strengths treated as a three electron problem and 2) The photoionization of the F <sup>2</sup>P<sup>o</sup> ground state to the <sup>3</sup>S channel including the effects of the 2s2p<sup>6</sup> <sup>3</sup>S autoionizing state.

### **I. Introduction**

In the past 10 years or so, the process of photoabsorption in atoms and molecules has been under increased experimental and theoretical examination. Experimental advances in photoelectron spectroscopy, lifetime measurements, UV and Synchrotron radiation photoabsorption and laser spectroscopy have been producing accurate and complementary information about the electronic structure and dynamics of atoms, molecules and solids. In particular, *absolute* transition probabilities can now be measured for a number of atomic and molecular transitions with accuracies of 1%-20% [e.g. 1]. In view of this

challenge, theoreticians have responded with advanced many-body approaches aiming at explaining or predicting qualitatively and, more important, quantitatively the relative or even the absolute transition probabilities of a variety of processes which involve valence and core electrons, discrete-discrete and discrete-continuum transitions. This goal has sometimes been met and sometimes has not, depending on the type of theory and transition. Generally however, the theoretical progress has been such that it allows for a more optimistic view than that of Brown [2] who, in reviewing the field of transition probabilities in 1973 concluded [ref. 2, p. 12]. «There seems little immediate hope that the wavefunctions obtainable from the traditional means of quantum chemistry will consistently yield highly accurate transition moments».

Due to the large number of possible types of transitions and of atomic and molecular systems, it is desirable to have a *photoabsorption* theory rather than a theory of electronic structure such as «singles and doubles configuration-interaction», which can analyze, systematize and compute accurately and efficiently the electron correlation effects which affect the transition probabilities the most. Such a theory must be able to deal with the *excited* state of the discrete or continuous spectrum and satisfy the following requirements:

- 1) It should be applicable with ease to open shell, multideterminantal states.
- 2) It should be able to predict cross sections for single as well as multi-electron excitations from the valence or the core shells.
- 3) It should be consistent, efficient and computationally manageable, accurate and simple to apply as well as to interpret.

This paper has two aims: 1) To review briefly a theory of photoabsorption called FOTOS, for First Order Theory of Oscillator Strengths, which started in 1973 with the above objectives [3-6]. By now FOTOS has yielded a plethora of accurate results for a variety of atomic and molecular discrete-discrete and discrete-continuum transitions with considerable consistency and economy of money and time.

2) To present a few characteristic old and new FOTOS results which refer to its capabilities for accuracy, to excitations to regions of valence-Rydberg interactions and to transitions to the continuum in the presence of resonances.

## II. FOTOS (First Order Theory of Oscillator Strengths)

Seven to ten years ago, some of the first reasonably accurate and efficient many-electron calculations of transition probabilities of a number of atomic transitions were carried out at Yale, [5-9], using wave-functions which included the «non-dynamical» spin-orbital correlation effects of the Sinanoglu NCMET [10-12]. These calculations established for the first time for electronic transitions in equivalent shells of atomic ions what had been known since the time of the Coulomb approximation for many Rydberg transitions of single electrons: That the photoabsorption process, although a many-electron affair, can in many cases be described quantitatively in terms of small wave-functions with specific correlation effects.

These facts were interpreted by us not in terms of the static concept of electronic structure (e.g. «charge distribution» etc.) but in terms of the dynamic transition process. Thus, we suggested that they simply implied the following relation [10,11]:

$$|\langle \Psi_i | T | \Psi_f \rangle|_{\text{exact}}^2 \simeq |\langle \tilde{\Psi}_i | T | \tilde{\Psi}_f \rangle|_{\text{approx}}^2 \quad (1)$$

where  $\Psi$ ,  $T$  and  $\tilde{\Psi}$  are the exact wavefunction, the transition operator and the approximate wavefunction respectively. This led us naturally to the question: «Is there a general and efficient photoabsorption many-body theory which is capable of producing transition matrix elements such that equ. 1 is satisfied?»

The answer to this question has thus far turned out to be positive. In the past few years we have developed, programmed and applied a theory (FOTOS) which computationally is based on subshell configuration-interaction methods. Its first results, published in 1975 [3], concerned one and two electron transitions to mixed valence- (Rydberg, continuum) discrete and autoionizing states and resolved the then existing discrepancy between theory and experiment.

#### A. The Zeroth Order Vector

In FOTOS, the zeroth order wave-function  $\Psi_0$  is based on the Fermi-Sea (F-S) of the states involved in the transition. This choice is derived from considerations of the electronic structure as revealed by the shell model. The Fermi-Sea concept [15, 16] goes beyond the single-configuration zeroth-order model and refers to many essential configurations as describing the fundamental shells where, from a pictorial point of view, electrons spend the overwhelming part of their time. The choice of these configurations is based on spectroscopic, energy near-degeneracy and magnitude of off-diagonal matrix elements criteria.

Thus, the zeroth order fundtions for the states participating in the transition are taken to be a linear combination of all FS configurations:

$$\begin{aligned} \Psi_0 &= \Psi_{\text{FS}} = \sum_K C_K \Phi_K \\ \Phi_K &= \sum_L d_L \Delta_L^K (\alpha^K_1, \alpha^K_2, \alpha^K_3, \dots, \alpha^K_N) \end{aligned} \quad (2)$$

$\Phi_K$  corresponds to a configuration, built in terms of SCF Hartree-Fock orbitals, with index  $K$ .  $\Delta_L^K$  are Slater determinants built in terms of the corresponding spin-orbitals,  $\alpha^K$ . The coefficients  $d_L$  are obtained by direct diagonalization of the symmetry operators. The  $c_K$  are obtained by direct diagonalization of the total Hamiltonian. Obviously, the optimum choice of the orbitals  $\alpha^K$  and the  $c_K$  coefficients comes from the Multi-Configurational Hartree-Fock method. However, for reasons of computer economy, the orbitals from one or two separate SCF calculations can be used without significant loss of accuracy.

### B. The Form of the Transition Matrix Element

We start by reminding the reader that, in nonrelativistic theory, what is observed in photoabsorption (emission) processes is proportional to the square of the amplitude

$$\langle \Psi_i | e^{i\vec{k}\cdot\vec{r}} \vec{p} \cdot \vec{\varepsilon} | \Psi_f \rangle,$$

where  $\vec{K}$  is the wave-vector and  $\vec{\varepsilon}$  the polarization vector of the photon,  $\vec{r}$  the position and  $\vec{p}$  the momentum of the electron.

The expansion of  $e^{i\vec{k}\cdot\vec{r}}$  ( $= 1 + i\vec{k}\cdot\vec{r} + \dots$ ) yields the various tensor components (an ad hoc introduction of spin is required for M1, etc.) and the resulting symmetry selection rules for electric and magnetic dipole, quadrupole etc. radiation. These selection rules do not only refer to quantum numbers of the exact wave-functions. They also apply to the electronic coordinates of the individual electrons treated as occupying atomic or molecular orbitals of a particular symmetry.

Thus, it seems desirable to develop a photoabsorption theory which looks at the form of the transition matrix elements (i.e. the form of the wave-functions for initial  $|i\rangle$ , and final  $|f\rangle$ , states) using as basis these selection rules and the radial form of the corresponding transition operators rather than emphasizing the accurate solution of the time independent Schrödinger equation for initial and final states which, as it turns out, is unnecessary.

Let us consider the most common type of transition, the electric dipole process. We write for the exact wave-functions of the initial and final states:

$$\Psi_i = \Psi_i^0 + X_i \quad \Psi_f = \Psi_f^0 + X_f \quad (3)$$

so that the exact transition matrix element is:

$$\begin{aligned} \langle D \rangle = \langle \Psi_i | D | \Psi_f \rangle = & \langle \Psi_i^0 | D | \Psi_f^0 \rangle + \langle \Psi_i^0 | D | X_f \rangle \\ & + \langle X_i | D | \Psi_f^0 \rangle + \langle X_i | D | X_f \rangle \end{aligned} \quad (4)$$

The principal contribution to  $|\langle D \rangle|^2$  comes from the first term. For example, consider the  $^1S \rightarrow ^1P^o$  transitions in alkaline earth type configurations with two ns electrons outside the closed shell. The Fermi-Sea vector for the ground state will have the configurations (core)  $(s^2+p^3+d^2) ^1S$  while the excited state F-S vector will have the (core)  $(sp+pd+df) ^1P^o$  configurations. These configurations suffice to explain semi-quantitatively the photoelectron spectra [ref. 3, (p. 84), 17] and form the basis for a quantitative treatment of the transition probabilities [18]. Since  $\Psi_i^0$  and  $\Psi_f^0$  have, in general, the largest coefficients in the wave-function expansion, the next two terms dictate the part of the function space of  $X_i$  and  $X_f$  which is connected directly with the zeroth order Fermi-Sea vectors and therefore contributes to  $|\langle D \rangle|^2$  the most.

Let  $X^{IN}$  depict the correlation function space of  $|i\rangle$  and  $|f\rangle$  which interacts directly via  $D$  with  $\Psi_f^0$ ,  $\Psi_i^0$  respectively. Let  $\chi^{NON}$  be its noninteracting orthogonal complement. Eq. 4 is then equivalent to:

$$\begin{aligned} \langle \Psi_i | D | \Psi_f \rangle = & \langle \Psi_i^0 | D | \Psi_f^0 \rangle + \langle \Psi_i^0 | D | X_f^{IN} \rangle + \langle X_i^{IN} | D | \Psi_f^0 \rangle + \\ & \langle X_i^{IN} | D | X_f^{IN} \rangle + \langle X_i^{NON} | D | X_f^{IN} \rangle + \langle X_i^{IN} | D | X_f^{NON} \rangle + \langle X_i^{NON} | D | X_f^{NON} \rangle \end{aligned} \quad (5)$$

Analysis of a few atomic systems has revealed that  $\chi^{NON}$  corresponds to correlation vectors with small coefficients which are reasonably well decoupled from  $\Psi^0$  and  $\chi^{IN}$ . This implies the following:

a) Their direct contribution to  $|\langle D \rangle|^2$  is very small. That is, the last three terms of eq. 5 are negligible because of the small coefficients and because not all correlation vectors in  $\chi_i$  and  $\chi_f$  are connected via D.

b) Their neglect does not affect the coefficients of  $\Psi^0$  and  $\chi^{IN}$  significantly.

The above observations together with an analysis of previous results on transition probabilities [8, 10], has led us to the following theory:

The *form* of the parts of  $\chi_i$  and  $\chi_f$  which contribute the most to  $\langle \Psi_i | D | \Psi_f \rangle$  can be obtained from the first order terms  $\langle \Psi_i^0 | D | X_f \rangle$  and  $\langle X_i | D | \Psi_f^0 \rangle$ , by applying the one electron dipole selection rules to the molecular or atomic orbitals of the Fermi-Sea configurations. The derived new  $X_i^{IN}$  and  $X_f^{IN}$  constitute a projected Hilbert space which, as predicted by electronic structure theory [15] and confirmed by computation, contains all vectors of spectroscopic significance together with others which contribute to the character of the wave-function. These have the largest coefficients in the correlation vector space and therefore contribute the most to  $\langle X_i | D | X_f \rangle$  as well. Since off-diagonal properties, i.e. transition probabilities, involve the *square* of the corresponding matrix element (in contrast to diagonal properties), the remaining vectors with small coefficients have only a small contribution either through the last three terms of eq. 5 or through normalization. Thus eq. 5 is approximated well by:

$$\begin{aligned} \langle \Psi_i | D | \Psi_f \rangle \simeq & \langle \Psi_i^0 | D | \Psi_f^0 \rangle + \langle \Psi_i^0 | D | X_f^{IN} \rangle \\ & + \langle X_i^{IN} | D | \Psi_f^0 \rangle + \langle X_i^{IN} | D | X_f^{IN} \rangle \end{aligned} \quad (6)$$

The analysis and computation of eq. 5 is based on the subshell cluster expansion of the wave-function (since the selection rules apply to subshells) and their subsequent development in terms of one electron F-S or virtual functions. The terms which are kept must also survive certain perturbation theory and nonorthonormality (NON) criteria [19]. Since the F-S orbitals are computed separately for initial and final states, there can be significant NON between the two sets in which case, in spite of the fact that D is a monoelectronic operator, subshell *pair* excitations survive in the correlation functions of eq. (6). Thus, the form of the FOTOS wave-functions for initial and final states is:

$$\Psi^{FOTOS} = \Phi_{HF} + \Phi_{HF}^{-1} \sigma(r_1) + \Phi_{HF}^{-2} \pi(r_1, r_2) \quad (7)$$



where only *specific* single ( $\sigma$ ) and pair ( $\pi$ ) correlation functions enter. Thus, eq. (7) represents a *projected* subshell cluster expansion which is predicted for each type of system under examination.

### c. Implementation of FOTOS

According to the above, the photoabsorption process is described quantitatively by the FOTOS amplitude,  $\langle \psi_i^{\text{FOTOS}} | D | \psi_F^{\text{FOTOS}} \rangle$ . The calculation of this matrix element accounting for nonorthonormality is described in [6]. Here we outline the calculation of the wave-functions of eq. 7.

Depending on whether the one-electron expansion of  $\sigma$  and  $\pi$  contains F-S or virtual orbitals, these functions can be separated into orthogonal parts:

$$\sigma = \sigma_{\text{FS}} + \sigma_{\text{virtual}} \quad (8a)$$

$$\pi = \pi_{\text{FS}} + \pi_{\text{FS-virtual}} + \pi_{\text{bi-virtual}} \quad (8b)$$

The computational techniques for the calculation of these functions differ, depending on whether the state of interest is a) the lowest of its symmetry b) embedded in a Rydberg series c) embedded in the continuum (i.e. it is autoionizing).

#### A) Bound State Lowest of its Symmetry

We will analyze this case in reasonable detail taking as example the  $^1S - ^1P^o$  resonance line of the  $KL3s^2 \ ^1S \rightarrow KL3s3p \ ^1P^o$  isoelectronic series.

We keep the K-L shells frozen since nonorthonormality (NON) indicates that their contribution to the oscillator strength is of higher order (i.e. it is small).

For the ground state, the F-S vector is:

$$\Psi_0 (^1S) = a|KL3s^2\rangle + b|KL3p^2\rangle + c|KL3d^2\rangle$$

where the coefficients a, b and c depend (but not very much in this case) on the types of radial functions used for the 3s, 3p and 3d orbitals.

For the excited state, the F-S vector is:

$$\Psi_0 (^1P^o) = a'|KL\bar{3}s\bar{3}p\rangle + b'|KL\bar{3}p\bar{3}d\rangle$$

In Mg, due to the significantly different SCF fields of the  $^1S$  and  $^1P^o$  states, the NON between initial and final 3s, 3p and 3p orbitals is nonnegligible. On the other hand, NON is unimportant in the ions. These facts have implications as to the types of correlation effects which enter the calculation (For example, see ref. 18 for a calculation on the ions).

Having defined the Fermi-Seas, we proceed to obtain  $X^{\text{IN}}$  of eq 5. This is done by employing first «angular» and then «radial» (energy) quantization.

#### a) Angular quantization

Application of the dipole selection rules to the one electron symmetries of the F-S vectors, yields the following «first order symmetry configurations»:

$$\begin{aligned} (s^2, p^2, d^2) \ ^1S \otimes \underline{D} &\rightarrow (sp, pd, df) \ ^1P^0 \\ (sp, pd) \ ^1P^0 \otimes \underline{D} &\rightarrow (s_1s_2, p_1p_2, d_1d_2) \ ^1S \end{aligned} \quad (9)$$

b) *Radial (energy) quantization*

With each one electron symmetry we associate a radial expansion:

$$|k_i\rangle = \sum_{n=3} \alpha_i^{(n)} |nk_i\rangle \quad (10a)$$

$$= \alpha_i^{(3)} |3k_i\rangle + b|V_{k_i}\rangle \quad (10b)$$

The second term of eq. 10b is a parametrized one electron function orthogonal to the F-S orbital. It is a *virtual* orbital. In practice, it is approximated by one or two Slater type orbitals (STO) whose exponents are optimized variationally as described below.

When expansions of the type 10b are put back into eqs. 9, we obtain correlation vectors which, with respect to the single configuration description of the states (i.e.  $3s^2 \ ^1S$  and  $3s3p \ ^1P^0$ ), contain single ( $\sigma$ ) and pair ( $\pi$ ) subshell correlation functions of specific angular symmetries only. When NON is significant, some of the pair functions for each state survive the mono-electronic dipole selection rules. Thus, in the case of Mg we obtain the following terms in the FOTOS wave-functions:

- $|^1s\rangle_{\text{FOTOS}}$ : 1)  $KL3s^2 = \Phi_{\text{HF}}$   
 2)  $KL3p^2, 3d^2 = \Phi^{-2} \pi_{\text{FS}}$ ; the 3p, 3d orbitals of the  $\pi_{\text{FS}}$  are obtained from separate HF or MCHF computations.  
 3)  $KL3sv_s = \Phi^{-1} \sigma_{\text{virtual}}$   
 4)  $KL3pv_p, 3dv_d = \Phi^{-2} \pi_{\text{FS-v}}$   
 5)  $KLv_s v'_s, v_p v'_p, v_d v'_d = \Phi^{-2} \pi_{\text{si-virtual}}$   
 $|^1p^0\rangle_{\text{FOTOS}}$ :  
 1)  $KL\bar{3}s\bar{3}p = \Phi_{\text{HF}}$   
 2)  $KL\bar{3}p\bar{3}d = \Phi^{-1} \sigma_{\text{FS}}$   
 3)  $KL \bar{3}s v_p, \bar{3}p v_s, \bar{3}p v_d = \Phi^{-1} \sigma_v$   
 4)  $KL \bar{3}d v_p, \bar{3}d v_f = \Phi^{-2} \pi_{\text{FS-v}}$   
 5)  $KL v_s v_p, v'_p v'_d, v'_d v_f = \Phi^{-2} \pi_{\text{bi-virtual}}$

The optimization of the correlation functions is done in the following way: Firstly, the  $\pi_{\text{bi-virtual}}$  are computed by minimizing the energy of

$$\frac{\langle \Phi + \Phi^{-2}\pi | H | \Phi + \Phi^{-2}\pi \rangle}{\langle \Phi + \Phi^{-2}\pi | \Phi + \Phi^{-2}\pi \rangle}$$

as a function of the nonlinear parameters, for each symmetrized pair. This type of computation fixes the radial characteristics of the bi-virtual pair functions well. Secondly, the  $\sigma_{\text{virtual}}$  and  $\pi_{\text{FS-virtual}}$  are computed by minimizing the energy of

$$\frac{\langle \Phi + \sigma_{FS} + \sigma_v + \pi_{FS} + \pi_{FS-v} | H | \Phi + \sigma_{FS} + \sigma_v + \pi_{FS} + \pi_{FS-v} \rangle}{\langle \Phi + \sigma_{FS} + \sigma_v + \pi_{FS} + \pi_{FS-v} | \Phi + \sigma_{FS} + \sigma_{FS} + \pi_{FS-v} \rangle}$$

Thirdly, all five parts of eqs. 8 are put together and the FOTOS function is computed from a single diagonalization of a small matrix without any further optimization of the STO exponents.

### B) Bound State, not lowest of its symmetry

In this case, care must be taken to give additional flexibility to the virtual orbitals of eq. 10.

The lower states can be Rydberg or valence states. If the state of interest is a Rydberg, one, the lower states are «created» by the orbital expansion of both  $\sigma$  and  $\pi$  functions excluding  $\pi_{bi-virtual}$ . If the state is valence configuration, then the lower valence and Rydberg functions correspond to  $\pi_{FS}$  and  $\pi_{FS-virtual}$ . One may then proceed as in the first case provided the exact number of lower zeroth order states are included explicitly so that the separation theorem of the eigenvalues allows the identification of the root of interest. If the number of the lower states is large or unknown (as is usually the case with molecules), one or two configurations with the orbital symmetry characteristics of the Rydberg series lying below the state of interest seem to allow the application of similar variational procedures [5, 14]. We have reported calculations using both approaches [3, 5, 28].

### C) Valence Autoionizing State

In this case, it is the «hole-filling» correlations corresponding to the  $\pi_{FS-virtual}$  term that cause difficulty due to their degeneracy with the main configuration. According to our theory of autoionization [29, 30], first we compute all correlation effects which contribute to the localization of the state using the procedures of (a). This yields the correlated square-integrable function  $\Psi_0$ . The interaction with the continuum is then computed at the end, as a principal value integral, using an expansion of  $\pi_{FS-virtual}$  in terms of scattering orbitals. If the interaction with the continuum is weak, then a square integrable representation of the continuum correlation vectors seems to work well with respect to the overall character of the wave-function [29, 30]. For example, for the He  $1s^2 \ ^1S \rightarrow 2s2p \ ^1p^o$  transition, the FOTOS oscillator strengths, using square-integrable functions only, agree with experiment [29].

## III. Heuristic Applications of FOTOS

As a many-body theory concerned with the photoabsorption process directly, FOTOS reduces dramatically the magnitude of computation while keeping the accuracy high and making physical effects transparent (e.g. see table 2). Furthermore, it allows systematic analysis and prediction of the influence of correlation effects without performing calculations [e.g. p. 84 of ref. 3].

Here we give three examples of these characteristics:

1) *A priori analysis of the approximate magnitude of a transition probability computation. The  $H_2O$   ${}^1A_1 \rightarrow {}^1B_1$  Transition:*

This line has been studied accurately by Buenker and Peyerimhoff [20] who used wave-functions of about 2000 configurations. FOTOS cannot surpass the reliability of this computation. On the other hand, as shown below, the required computation is at least an order of magnitude smaller and, most important, this can be predicted simply via the FOTOS analysis. Furthermore, should an improvement in the computation is desired, this can be done easily and judiciously without increasing the magnitude of computation significantly.

We assume a single configuration Fermi-Sea vector. This means that

$$\Psi_0 ({}^1A_1) = \Phi_{HF} = A (K2\alpha_1^2 1b_2^2 3\alpha_1^2 1b_1^2)$$

$$\Psi_0 ({}^1B_1) = \Phi_{HF} = A (K2\alpha_1^2 1b_2^2 3\alpha_1^2 1b_1 4\alpha_1)$$

Furthermore, we assume that initial and final state HF orbital are orthogonal between them. Then, the FOTOS analysis predicts 12 ground and 7 excited state configurations:

$$|{}^1A_1\rangle: 2\alpha_1^2 1b_2^2 3\alpha_1^2 1b_1^2, 2\alpha_1 1b_2^2 3\alpha_1^2 1b_1^2 4a_1, 2\alpha_1 1b_2^2 3\alpha_1^2 1b_1 4a_1 2b_1,$$

$$2\alpha_1 1b_2^2 3\alpha_1^2 1b_1 4a_1 v_{b_1}, 2\alpha_1^2 1b_2^2 3\alpha_1 1b_1^2 4a_1, 2\alpha_1^2 1b_2^2 3\alpha_1 1b_1 4a_1 2b_1,$$

$$2\alpha_1^2 1b_2^2 3\alpha_1 1b_1 4a_1 v_{b_1}, 2\alpha_1^2 1b_2^2 3\alpha_1^2 4a_1^2, 2\alpha_1^2 1b_2^2 3\alpha_1^2 4a_1 5a_1, 2\alpha_1^2 1b_2^2 3\alpha_1^2 4a_1 v_{a_1},$$

$$2\alpha_1^2 1b_2^2 3\alpha_1^2 1b_1 2b_1, 2\alpha_1^2 1b_2^2 3\alpha_1^2 1b_1 v_{b_1}$$

$$|{}^1B_1\rangle: 2\alpha_1^2 1b_2^2 3\alpha_1^2 1b_1 4a_1, 2\alpha_1^2 1b_2^2 3\alpha_1^2 1b_1 5a_1, 2\alpha_1^2 1b_2^2 3\alpha_1^2 1b_1 v_{a_1},$$

$$2\alpha_1^2 1b_2^2 3\alpha_1 1b_1^2 2b_1, 2\alpha_1^2 1b_2^2 3\alpha_1 1b_1^2 v_{b_1}, 2\alpha_1 1b_2^2 3\alpha_1^2 1b_1^2 2b_1, 2\alpha_1 1b_2 3\alpha_1^2 1b_1^2 v_{b_1}$$

where the  $v$ , are the non spectroscopic virtual one electron functions.

The small number of correlation vectors are in accord with the fact that  $H_2O$  has proven an «easy» test for the various many-body which have been applied for the interpretation of its spectrum [This computation has now been performed — see ref. 6].

## 2) *General Electronic Structure Rules Derived from FOTOS*

Three are of course many types of correlation vectors which influence the transition process. However, applications of FOTOS have singled out three types of correlation effects which are systematically the most dominant ones. For a number of photoabsorption experiments in the UV and higher energy region, these effects are presented in terms of simple rules readily applicable to atoms in the free or the solid state and, in some cases, to molecules. These rules refer both to the discrete and to the continuous spectrum. They reduce the essential information contained in the many-body description of the electronic structure to a few notions based mainly on orbital symmetry and the proximity of energy quantum numbers.

### a) «Fermi-Sea» Correlations for Ground and Excited States

We have already referred to these in our discussion on the choice of the

proper zeroth order vector. They correspond to the main configurations which give the state of interest its major overall characteristics. In molecules, these correlations are essential for the correct description of bonding and dissociation. Their importance has been pointed out by many authors, although their practical establishment is not unique and varies from theory to theory.

*Example:* The  $O_2$   ${}^3\Sigma_g^- \rightarrow {}^3\Sigma_u^-$  transition.

From the pioneering work of Buenker and Peyerimhoff [21] we can deduce the FS as follows: For the ground state, the  $3\sigma^2 \pi_u^2 \pi_g^4$  configurations. For the excited valence-Rydberg states, the  $3\sigma^2 \pi_u^3 \pi_g^3$ ,  $3\sigma_g^2 \pi_u^4 \pi_g$  ( $3p\pi_u$ ),  $3\sigma_g \pi_u^2 \pi_g^4 3\sigma_u$  and  $3\sigma \pi_u^4 \pi_g^2 3\sigma_u$  configurations.

*b) «Double Jump of Orbital Momentum» (DJOM) for Single subshell Clusters*

This rule refers to the importance of *single* subshell substitutions with orbitals whose symmetry differs by two units of orbital momentum. We write symbolically for the interacting symmetries:

*Rule (DJOM):*  $l \rightarrow l + 2$

*Examples*

- 1)  $s \rightarrow d$ . E.g.  $Br^+ 4s4p^5 {}^3p^\circ \rightarrow 4p^5 \sigma_d {}^3p^\circ$
- 2)  $p \rightarrow f$ . E.g.  $Mn^{++} 3p^6 3d^5 {}^6S \rightarrow 3p^5 3d^5 \sigma_f {}^6S$
- 3)  $d \rightarrow g$ . E.g.  $Pd 5d^{10} 6s^2 6p^2 {}^3P \rightarrow 5d^9 6s^2 6p^2 \sigma_g {}^3P$

For computational purposes, the one electron functions  $\alpha$  can be expanded in terms of HF or virtual orbitals or both. (See section IIC).

*c) «Hole-Filling», «Symmetric Exchange of Orbital Symmetry» (SEOS)*

The hole-filling pair correlation effect is the most important one for excited states with a hole in one of the FS and especially the inner shells. In most cases, there is strong mixing with Rydberg or continuum states which gives rise to large anomalies in the photoabsorption spectra (e.g. see next section) and, should the energies allow it, to the process of autoionization. Also, for such states, *three* electron correlations are relatively much more important than for ground states [15].

Of the possible rearrangements, the most significant by far is that where one of the two correlating electrons loses one unit of orbital angular momentum while the other one gains it. This rule is symbolically written as:

*Rule (SEOS):*  $l^2 \rightarrow (l-1) \times (l+1)$   
 $l \times l' \rightarrow (l-1) \times (l'+1)$

(The hole has  $(l-1)$  symmetry).

The reason for this rule seems to be the fact that the radial functions of higher angular momentum  $(l+1)$  are usually symmetry orthogonal to the lower Hartree-Fock (HF) orbitals and nodeless and therefore overlap the HF region efficiently.

In order to demonstrate the utility and unifying nature of SEOS, below we present qualitative explanations and predictions for a number of seemingly unrelated systems and phenomena in the vapor or the solid state.

*Examples*1)  $p^2 \rightarrow sd$ 

E.g. a) The  $6s6p^4$  configuration in Bi. This should mix heavily with  $6s^26p^2v_d$  and influence the matrix elements involved in the parity nonconserving optical rotation problem [22]. This state was recently studied by Multi Configurational Dirac-Fock methods [23] but the SEOS correlation was not considered.

b) ns photoionization of the noble gases or  $ns^2np^a \rightarrow nsnp^{a+1}$  intrashell transitions [3, 11].

2)  $\epsilon np \rightarrow sd$ 

E.g. Electron correlation between the free electron ( $\epsilon p$ ) and the  $np^6$  core in alkali valence photoionization.

3)  $f^2 \rightarrow dg$ 

E.g. Creation of a hole in the 4d subshell in the rare earths [46], where absorption or emission dipole transitions in the discrete or the continuous spectrum will be strongly influenced by correlations of the type:  $4f^2 \rightarrow 4dv_g$  [40].

For molecules, an analogous rule can probably be given in terms of gerade-ungerade or bonding-antibonding exchange. For example, for the ethylene  $^1(\pi, \pi^*)$  state,  $\pi^*\sigma \rightarrow \sigma^*\pi$  substitutions have been found to be important [24].

*3. Extraordinary Photoabsorption Phenomena*

By making obvious those correlations which contribute to the photoabsorption intensities the most, FOTOS has led us to simple analyses of some extraordinary photoabsorption phenomena which characterize core or valence electron excitations in the discrete and continuous spectrum. These involve the unusual mixing of excited valence with degenerate or close lying scattering or Rydberg states which gives rise to the following phenomena:

*a) «Collective Excitations» [25a]*

Although the name «collective» takes a different meaning depending on the type of theory which is employed [25], we have reserved this term for situations where a particular energy region absorbs very strongly while the surroundings hardly at all. In order to explain this phenomenon from a many-body point of view, we considered the following:

If the excited state wave-function is written in the usual expansion form in terms of closely lying configurations  $\Phi_K$  (which are connected via the dipole operator to the ground state FS vector  $\Psi_0$ ),

$$\Psi_{\text{excited}} \simeq \sum_K \alpha_K \Phi_K \quad (11)$$

then, strong absorption to only a narrow part of the spectrum implies:

$$|\langle \Psi_0 | D | \Psi_{\text{exc}} \rangle|^2 \simeq \sum_K |\langle \Psi_0 | D | \Phi_K \rangle|^2 \quad (12)$$

In this case, a sufficient condition for a collective excitation is [25a]:

$$\alpha_k = \text{const.} \times \langle \Psi_0 | D_2 | \Phi_k \rangle \quad (13)$$

This condition applies to the continuous as well as to the discrete spectrum.

*b) Localized Exchange of Intensity [26, 27]*

In most open shell species, even in the low energy excitation spectrum there can be situations where, due to the proximity of two excited states of the same symmetry, there is an irregular behavior of the intensity as a function of the parameters of the Hamiltonian or from independent particle to the many-body description of the corresponding wave-functions. This phenomenon is explainable in terms of the Two-State Approximation (TSA) [26, 27] which shows how this irregular behavior results from a localized exchange of oscillator strength between the two states. As an example we take the oscillator strength for the photoexcitation of Cl III  $KL3s^23p^3 \ ^4S^\circ$  to the lowest two excited states of  $^4P^\circ$  symmetry, the valence  $3s3p^4$  and the Rydberg  $3s^23p^23d$ . The HF values (length form) are 0.685 and 2.9 respectively while the FOTOS values are 0.041 and 3.47 [ref. 6, p. 171]. This shows that electron correlation transfers oscillator strength mainly between adjacent states in this case. The experimental value for the valence state is 0.043 [6], in excellent agreement with FOTOS.

*c) Delocalized Exchange of Intensity [28, 6]*

These are situations where, in the many-body description the oscillator strength is spread almost equally over a large energy region covering many discrete and/ or continuum states. The «excess» oscillator strength comes from one or two Hartree-Fock states which, in exceptional cases (e.g. see the Be  $2s2p \ ^1P^\circ \rightarrow 2p^2 \ ^1D$  case, page 170, ref. 6) may lose *all* their oscillator strength to the Rydberg or continuum series.

#### *IV. Quantitative Applications of FOTOS*

##### *A. The Discrete Spectrum*

A number of atomic and molecular FOTOS bound-bound transition probabilities have been presented recently [6]. The accuracy is very good and in many cases even supercedes that of other many-body theories. The conclusion from our work thus far is that light ions are rather easy to treat while neutrals, light or heavy, always present difficulties related to near-degeneracies in the excited state and corresponding choice of basis functions.

In order to demonstrate the capabilities of FOTOS for accuracy at least in few electron systems, in this section we present recent results on the Li,  $Be^+ \ 1s^22s^2S \rightarrow 1s^22p \ ^3P^\circ$  transitions for which calculations from large CI as well as measurements have produced accurate values. The comparison which is given in Table 1 demonstrates that FOTOS, when applied with care and detail, is capable of high precision.

That the efficient FOTOS calculations can compare favorably with very extensive computations has also been demonstrated recently in the case of the

TABLE 1: Oscillator Strengths for the  $1s^2 2s \ ^2S - 1s^2 2p \ ^2P^0$  Transition. For these FOTOS calculations, the K-shell is included in the Fermi-Sea and all correlation vectors which are zeroth and first order in the overlap are kept.

		FOTOS	CI <sup>(c)</sup>	Hylleraas-CI <sup>(d)</sup>	Experiment
Li <sup>(a)</sup>	$f_L$	0.759	0.753	0.748	0.742 <sup>(e)</sup>
	$f_V$	0.740	0.773		
Be <sup>+(b)</sup>	$f_L$	0.500	0.505		0.54 <sup>(f)</sup>
	$f_V$	0.510	0.521		

a) A. Gaupp and D.R. Beck (unpublished).

b) Ref. 6.

c) A. Weiss, Astr. J. **138**, 1262, (1968).

d) J.S. Sims, S. Hagstrom and J.R. Ruble Jr., Phys. **A13**, 242 (1976).

e) A. Gaupp (unpublished).

f) I. Martinson, quoted in A. Lindgard and S.E. Nielsen, J. Phys. **B8**, 1183 (1975); this experiment probably has a larger uncertainty than our theoretical value.

TABLE 2: Transition Probabilities (in  $10^8 \text{ sec}^{-1}$ ) for the Li  $1s2p^2 \ ^2P$  decays to the Rydberg Li  $1s^2 2p, 3p, 4p \ ^2P^0$  states from FOTOS and from very large CI calculations.  $A_L$  = length form.  $A_V$  = velocity form.

	FOTOS [31]		Large CI [32]
	$A_L$	$A_V$	A
Li $1s2p^2 \ ^2P - 1s^2 2p \ ^2P^0$	208	189	$197 \pm 20$
-3p $\ ^2P^0$	13.5	13.9	$13 \pm 1$
-4p $\ ^2P^0$	3.8	4.0	$4 \pm 1$



study of the decay of the Li  $1s2p^2 \ ^2P$  state [31, 32]. Our predictions for the discrete transitions  $1s2p^2 \ ^2P \rightarrow 1s^2 \ 2p, 3p, 4p \ ^2P^o$ , which were made using an 11-and an 8-term expansion for initial and final state wave-functions [31], have been confirmed by Bungés 200 term CI [32] (Table 2).

## B. The Continuous Spectrum

### 1) Electron Correlation (EC) in the Continuum

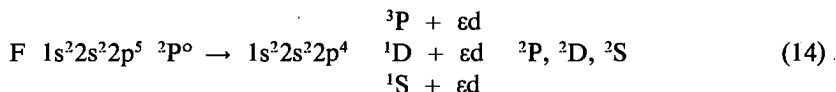
The phenomenon of photoionization involves the electronic continuum. Most of the theories treat this part of the spectrum very approximately. Thus, our present knowledge of the effect of electron correlation in the continuous spectrum, the interplay of resonances, interchannel coupling, core polarization etc. is limited. Furthermore, there are still conceptual problems such as the proper description of two simultaneously free electrons [33].

The problem of EC in the continuum differs from the much better studied problem of EC in the discrete spectrum in both the conceptual and computational aspects. On the conceptual side, a perusal of the literature indicates a lack of analysis of correlation effects. On the computational side, different methods must be applied, such as the K-matrix [34], R-matrix [35] and the novel Stieltjes-Tchebycheff [36] procedures.

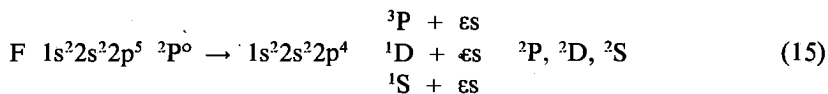
Below we emphasize the analysis of correlation effects in the continuum by extending and generalizing the subshell cluster expansion for the bound states. To do this we choose as an example the F atom for which the photoionization process which is of intermediate complexity has not been examined before. Obviously, the statements regarding the importance of certain correlations have a general character. Only the  $^2S$  channel is studied here since, due to the presence of the  $2s2p^6 \ ^2S$  autoionizing state it is the most interesting.

We assume a nonrelativistic Hamiltonian without spin-orbit forces.

The photoionization of the 2p shell of Fluorine yields an electron of s or d symmetry. As is well known [37], the transition probability for  $l \rightarrow l+1$  photoionization is much larger than for  $l \rightarrow l-1$ . Thus, the process which dominates the photoionization cross-section is:



while the minor one is:



The  $^3P$  channel opens at 17.4 eV above the ground state, the  $^1D$  channel opens

at 20.0 eV above and the  $^1S$  at 23.0 eV above [38].

In order to analyze and compute the electron correlation effects in the continuum, we extend the domain of application of the subshell cluster expansion which has proved useful and efficient for ground and excited discrete or autoionizing states [5, 29, 15]. Thus, for the exact function  $\Psi(E)$  at energy  $E$  we write formally:

$$\Psi(E) = \Phi_{HF}(E) + \Phi_{HF}^{-1} \sigma(r_1) + \Phi_{HF}^{-2} \Pi(r_1, r_2) + \dots \quad (16)$$

$\Phi_{HF}(E)$  is the Hartree-Fock function of the continuum states which are responsible for most of the photoabsorption. In the F case, knowledge of the  $l \rightarrow l+1$  rule suggests that the  $\epsilon d$  channel is the most important. Thus, for the  $^3S$  states we may choose as the HF zeroth order scattering state description:

$$\Phi_{HF}(E): 1s^2 2s^2 2p^4 (^1D, ^1S) \epsilon d \ ^3S \quad (17)$$

$\sigma$  and  $\pi$  are single and pair symmetrized subshell correlation functions which, if expanded in terms of orbitals, may contain bound as well as bound and scattering functions. (We note that single and pair symmetrized subshell functions may correspond to up to four spin-orbital excitations in the usual schemes of many-body theory).

Solution of the Schrödinger equation wavefunctions of the type of eq. 16 requires different techniques than those of the bound state problem. Our approach is based on the Fano theory of configuration-interaction (CI) in the continuum [39]. However, before the problem of how to solve the Schrödinger equation in the continuum, the usual and fundamental problem of «which configurations to include» arises. To solve this we apply the correlation rules of the electronic structure and photoabsorption theories presented here and elsewhere [5, 15, 16, 40]. These rules lead to an a priori identification of the important correlation effects with ease and consistency. Below, we outline their application to the  $F^+ + e^-$  continuum.

The important parts of the single subshell correlation functions  $\sigma$  are those which follow the  $l \rightarrow l+2$  correlation rule.

Thus, for a frozen K-shell, we have:

$$2s \rightarrow v_d = \sigma_{2s}(r_1) \quad (18a)$$

$$\epsilon d \rightarrow \epsilon s = \sigma_{\epsilon d}(r_1) \quad (18b)$$

The  $v_d$  is a virtual bound orbital computed variationally from a small configuration-interaction calculation in the presence of a few other important correlation vectors (section 2c).

The  $\epsilon s$  is a scattering orbital which represents the open channel of process (15) and gives rise to the interchannel mixing  $1s^2 2s^2 2p^4 \epsilon d \rightarrow 2s^2 2p^4 \epsilon s$ .

As outlined in section III, in excited states, the important parts of the pair subshell correlation functions are those which describe Fermi-Sea (FS) correlation, and those which correspond to «hole-filling» excitations. Of the hole-filling correlations, those which are FS or of the «symmetric exchange of orbital sym-

metry» types, (SEOS), are the most important and play a fundamental role in photochemistry and photophysics. For example, in the much studied photoionization of the noble gases [e.g. 41] the interaction

$$np^2 \rightarrow nsn' (\epsilon) d \quad (19)$$

where the quantum numbers  $n$ , and  $n'$  may or may not be the same, will always yield conspicuous effects on the  $ns$  photoionization. The same goes with the photoionization of the  $nd$  shells of the heavy atoms where the interaction

$$nf^2 \rightarrow n'd n'' (\epsilon) g \quad (20)$$

is crucial [40, 46].

In the present case we have:

$$\text{Fermi-Sea: } 2s^2 \rightarrow 2p^2 ({}^1S) \text{ (only for the } F^+ {}^1S \text{ term)} \quad (21a)$$

$$\text{SEOS: } 2sed \rightarrow p^2 \quad (21b)$$

The FS correlation gives rise to the configurations  $1s^2 2p^6 (\epsilon d, \epsilon s)$  which correspond to a two electron photoexcitation process (of the  $2s^2$  shell):

$$F 1s^2 2s^2 2p^5 2P^0 \rightarrow F^+ 1s^2 2p^6 + \bar{e} \quad (22)$$

The  $p$  symmetry in SEOS may characterize bound or continuum orbitals. The most important radial functions are those which overlap the initial configuration space the most. Thus, the expected significant subshell pair substitutions are:

$$2sed \rightarrow 2p^2 \quad (23a)$$

$$\rightarrow 2p3p \quad \Pi_{2sed}(r_1, r_2) \quad (23b)$$

$$\rightarrow 2pep \quad (23c)$$

The correlation in (23a) and (23b) gives rise to the configurations  $1s^2 2s 2p^6 {}^3S$  and  $1s^2 2p^5 3p {}^3S, {}^3P, {}^2D$  which represent autoionizing states. The correlation in (23c) gives rise to interchannel mixing,  $1s^2 2s^2 2p^4 \epsilon d \rightarrow 1s^2 2s 2p^5 \epsilon p$ . The scattering orbital  $\epsilon p$  represents the open channel of the  $2s$  shell:

$$F 1s^2 2s^2 2p^5 {}^2P^0 \rightarrow 1s^2 2s 2p^5 \begin{matrix} {}^3p^0 \\ {}^1p^0 \end{matrix} + \epsilon p \quad {}^2P, {}^2D, {}^2S \quad (24)$$

Here we observe that the photoionization rule  $l \rightarrow l + 1$  and the SEOS correlation rule  $l^2 \rightarrow (l - 1)(l + 1)$  complement each other in determining the major and minor interactions during photoabsorption. For example, the configuration  $2s 2p^6 {}^3S$  (or any configuration of this type with an  $s$  hole) interacts via the  $1/r_{ij}$  operator with the  $2s^2 2p^4 (nd, \epsilon d)$  channel much stronger than with the  $2s^2 2p^4 (ns, \epsilon s)$  channel (see e.g. ref. 6, p. 159 for the  $Ne^+$  case, pertinent to

the 2s photoionization). At the same time, the d channel also interacts with the 2p shell more strongly, via the electric dipole operator.

The previous correlation analysis gives rise, in a natural manner, to autoionizing configurations which affect the interchannel mixing and the photoionization probability in an unpredictable way. For example, the mixing of  $2s^2 2p^4 \epsilon d \rightarrow 2s^2 2p^4 \epsilon s$  is affected by the  $2s 2p^6$  configuration just like the weak mixing between  $2s 2p^6$  and  $2p^5 \epsilon p$  is enhanced by the presence of  $2s^2 2p^4 \epsilon d$  (eqs. 23), at least for energies above the 2s threshold.

In closing, we note that our approach to the photoabsorption related electron correlation problem in the discrete and the continuous spectrum is general and applicable throughout the periodic table. On the computational side, most of the theory has been programmed and will be applied to a variety of systems as soon as we have the necessary computer time.

2) *Application: The F  $2s^2 2p^5 \ ^2P^0 \rightarrow [2s^2 2p^4 (\ ^1D, \ ^1S) \ \epsilon d, \ \epsilon s, \ 2s 2p^6] \ ^2S$  Photoionization Cross-Section*

The photoionization cross section of the F atom has not been studied from a many-body point of view before. In this section, we present results from an approximate FOTOS application to the  $\ ^2P^0 \rightarrow \ ^2S$  channel in the region 0.1–1.0 a.u. above the  $\ ^1D$  threshold.

The F-S for initial and final states in this energy region are:

$$\begin{aligned} |^2P^0 \text{ ground state} \rangle &: 1s^2 2s^2 2p^5 \ ^2P^0 \\ |^2S \text{ excited states} \rangle &: [1s^2 2s 2p^6, (1s^2 2s^2 2p^4 \ ^1D) \ d] \ ^2S \end{aligned}$$

Application of the FOTOS procedure yields the FOTOS wave functions:

$$|^2P^0\rangle_{\text{FOTOS}} : K 2s^2 2p^5, 2s 2p^5 v_d, 2s 2p^4 v_p v_d, 2s^2 2p^3 v_s v_d, 2s^2 2p^3 v_d^2, 2s^2 2p^4 v_p, 2s^2 2p^4 v_f, 2p^6 v_p, 2s 2p^5 v_s \quad (25a)$$

$$|^2S\rangle_{\text{FOTOS}} : 2s^2 2p^4 n d, \ \epsilon d, 2s^2 2p^4 n s, \ \epsilon s, 2s 2p^6, 2s 2p^5 3p, 2s 2p^4 v_d \epsilon d, 2p^6 n s, \ \epsilon s, 2s 2p^5 \epsilon p, 2s 2p^4 n d(\epsilon d), 2s 2p^4 n s v_d \quad (25b)$$

For the  $|^2P^0\rangle$  state, the virtual orbitals  $v_e$  are computed variationally as described in section IIc and ref. 15. For the  $|^2S\rangle$  state we make the approximation, for reasons of computer time and size limitations, of keeping only the  $2s 2p^6 \ ^2S$  autoionizing state and the  $2s^2 2p^4 \ n d, \ \epsilon d, 2s^2 2p^4 n s, \ \epsilon s$  channels (see the discussion on correlation in the continuum). Furthermore, instead of computing the K-matrix [34], we employed the following model, where the coupling of the channels is assumed to occur only via the  $2s 2p^6$  configuration [41]:

$$\begin{aligned} \langle n d, \ \epsilon d | H | n s, \ \epsilon s \rangle &= 0 \\ \langle n d, \ \epsilon d | H | 2s 2p^6 \rangle &= V_{1n}, \ V_{1\epsilon} \\ \langle n s, \ \epsilon s | H | 2s 2p^6 \rangle &= V_{2n}, \ V_{2\epsilon} \end{aligned} \quad (26)$$

where  $n = 3, 4, 5$  and  $\epsilon = [0, 9 \text{ a.u.}]$ .

The solution of this model is carried out by applying the Altick and Moore [43] methods. The zeroth order discrete state,  $2s 2p^6$ , has a HF energy  $E = -$

14.8 eV above the experimental  $2p^4 \ ^1D$  d threshold. The energy of the resonance is the solution of the transcendental equation:

$$E-E_0 = F(E) = \sum_n \frac{|V_{1n}|^2}{E-E_{1n}} + \sum_n \frac{|V_{2n}|^2}{E-E_{2n}} + \\ + \text{P.V.} \int_{I_1} dE' \frac{|V_{1E'}|^2}{E-E'} + \text{P.V.} \int_{I_2} dE' \frac{|V_{2E'}|^2}{E-E'} \quad (27)$$

which yields  $F(E) = -3.0\text{eV}$ .

In the actual calculations the rest of the Rydberg series were included as an appendage of the continuum using the relation  $V_{in} = n^{-3/2} V_{ie}$  ( $\epsilon=0$ ). In this way, the range of the continuum is extended below threshold. This extended continuum is now replaced by a finite sum by choosing a mesh of energy points up to an energy of 9 a.u. The principal value integrals are calculated by a generalized Simpson's rule [43] that is,  $V_{iE}$  is expanded as  $E'f_1(E) + E'f_2(E) + f_3(E)$  where  $f_j(E)$  are linear combinations of the values of  $V_{iE'}$  at the mesh points and the resulting integrals  $\text{P.V.} \int dE' (E')^j / (E-E')$  are calculated exactly.

Fano's theory gives a resonant continuum of the form:

$$\Psi_{iE} = \cos D_E \frac{(V_{iE} u_{iE} + \lambda V_{2E} u)}{(V_{iE}^2 + \lambda V_{2E}^2)^{1/2}} - \frac{\sin D_E}{\pi (V_{iE}^2 + \lambda V_{2E}^2)^{1/2}} \\ \Phi_0 + \text{P.V.} \int dE' \frac{V_{iE'}}{E-E'} U_{iE'} + \text{P.V.} \int dE' \frac{V_{2E'}}{E-E'} U_{2E'} \quad (28)$$

where  $\Phi_0$  is the autoionizing state and  $D_E$  is the phase shift given by

$$\cot D_E = - \frac{E-E_0 - F(E)}{\pi (V_{iE}^2 + \lambda V_{2E}^2)^{1/2}}$$

The value of  $\lambda$  is 0 or 1 depending on whether the value of  $E$  is below or above the  $^1S$  threshold. It also gives a non-resonant continuum (above the  $^1S$  threshold) of the form:

$$\Psi_{2E} = \frac{V_{iE}}{(V_{iE}^2 + V_{2E}^2)^{1/2}} u_{2E} - \frac{V_{2E}}{(V_{iE}^2 + V_{2E}^2)^{1/2}} u_{iE} \quad (29)$$

We observe that the state with the higher transition amplitude ( $\epsilon d$ ) has the smaller coefficient in this combination. Therefore, the interaction of the two channels through the autoionizing state plays a significant role in redistributing the transition probabilities in the  ${}^2S$  final state.

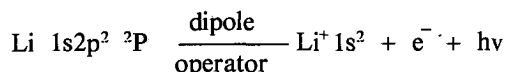
The cross-section  $\sigma(E)$  is then proportional to:

$$\sigma(E) \sim |\langle {}^2P^0 | D | \Psi_{1E} \rangle|^2 + |\langle {}^2P^0 | D | \Psi_{2E} \rangle|^2 \quad (30)$$

The results are given in fig. 1. Because of the presence of the  $2s2p^6 {}^2S$  configuration, the absorption just above threshold increases dramatically giving rise to a rather wide resonance whose width is  $\Gamma = 3.1\text{eV}$  and the Fano asymmetry parameter  $q=2.25$ . We note that, because of the omission of most of the energy contributing correlation energy, the exact position of this resonance is still uncertain [30].

### 3) Application: Radiative Autoionization of the Li $1s2p^2 {}^2p$ state

«Radiative autoionization» is a one photon two electron decay process of an excited state which is embedded in an electronic continuum of opposite parity [44]. For the Li  $1s2p^2 {}^2P$  state, this decay mode is:



Contrary to the photoionization process, the information for this *emission* into the continuum phenomenon is contained in the lifetime of the  $1s2p^2 {}^2P$  state [44]. A FOTOS analysis indicates that electron correlation is not very crucial for this transition. The determining factor is essentially the nonorthonormality between the HF functions of initial and final states.

Using free Coulomb functions with effective  $Z$ 's for the  $\epsilon p$  continuum and a HF representation of the autoionizing state  $[1s(2s2p)^3P] {}^2P^0$  we computed the spontaneous transition probability for radiative autoionization to be [44]:  $19.1 \times 10^8 \text{ sec}^{-1}$  in the length and  $26.2 \times 10^8 \text{ sec}^{-1}$  in the velocity form [45]. This amounts to about 10% of the total lifetime. We note that because of the smallness of the  $\langle 1s\epsilon p | H | 2s2p \rangle$  matrix element (not a SEOS correlation, large K-L shell separation) the coupling of the  ${}^2P^0$  autoionizing state to the continuum is small and does not affect the spectrum.

### V. Synopsis

The theory of transition probabilities we have presented has the following characteristics:

- 1) It takes into account:
  - a) Multiplet symmetry — By doing a term-dependent SCF Hartree-Fock calculation.
  - b) Relaxation — For the same reason as in (a).
  - c) Interchannel coupling

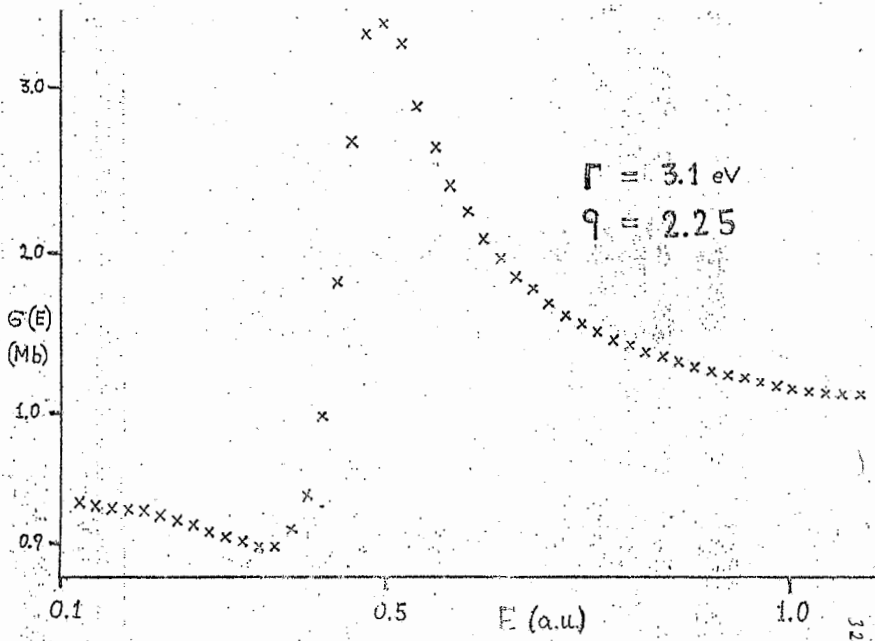


FIG. 1: Photoionization of Fluorine to the  $^2S$  channel:  $F 2s^2 2p^5 \ ^2P^0 \rightarrow 2s^2 2p^4 \ (^1D, \ ^1S) \ \epsilon d, \ \epsilon s \ ^2S$ . The cross-section in the region 0.1 a.u. (above the  $^1S$  threshold) - 1.1 a.u. is dominated by a resonance corresponding to the  $F 2s 2p^6 \ ^2S$  autoionizing state. The parameters for the width and asymmetry ( $\Gamma$ ,  $q$ ) are given on the figure. The ground state was represented by the FOTOS wavefunction of eq. 25a while the excited states were obtained within the model of eq. 26 which neglects a few FOTOS correlation vectors and the interchannel  $\epsilon d \rightarrow \epsilon s$  coupling.

d) Multiply excited states, resonances and Rydberg states.

2) By looking directly at the transition amplitude and taking advantage of symmetry and notions of variation-perturbation theory, it reduces the magnitude of computation- as compared with other approaches - considerably.

3) It is applicable to atoms, small molecules, nuclei, impurities in solids and on surfaces and in general to systems with sufficient localization and symmetry.

4) Its extension to a *Relativistic FOTOS* is straight forward [6], especially in view of the relativistic - correlation theory now being developed [15, 40].

5) It identifies and computes the important correlation effects in initial and final states at the same level of approximation.

6) It avoids overkill computations (e.g. big CI) and is not an algorithm, like e.g. the RPA and its variants, where the emphasis is on the correct numerical solution of a standard set of equations.

7) Because of points 2, 5 and 6, it is electronic structure oriented, thus contributing to the real physical understanding of the dynamics of the photoabsorption process.

### Acknowledgments

The computations of the F photoionization cross-section were carried out on the IBM 125 computer of the Bothosakis Foundation whom we thank for their generosity. We also thank Mr. G. Aspromallis for his computational assistance on the Fluorine photoionization problem. A summary of this work was presented by C.A. Nicolaides at the Nobel Symposium on «Many-Body Theory of Atomic Systems», Aspenäs garden, Sweden, June 6-13, 1979.

### Περίληψη

*Πολυ-Ηλεκτρονική θεωρία Πιθανοτήτων Μεταβάσεως στο Διακεκριμένο και Συνεχές Φάσμα για Συστήματα με Συμμετρία.*

Παρουσιάζουμε τα ουσιώδη χαρακτηριστικά μιάς ελαστικής και αποτελεσματικής θεωρίας για σχετικές ταχύτητες φωτοαπορροφήσεως. Έκμεταλλευόμενη την συμμετρία του συστήματος και του τελεστού μεταβάσεως, αυτή η θεωρία προβλέπει απλά και με συνέπεια τις σπουδαίες συσχετιστικές συστάδες ενός και ζεύγους υποφλοιδών που επιδρούν επί της ενεργού διατομής της φωτοαπορροφήσεως. Έτσι, δείχνουμε ότι τό παλιό και φαινομενικά πολύ μπλεγμένο πρόβλημα, έννοιολογικά και ύπολογιστικά, των πιθανοτήτων μεταβάσεως μπορεί να αναχθή σε μικρές ύπολογιστικές αναλογίες για κλειστούς όσο και για άνοικτούς φλοιδούς. Επί πλέον, μιά γενική συσταδική ανάπτυξη ύποφλοιδών και η εφαρμογή άπλών κανόνων επιτρέπουν την a priori αναγνώριση των κυριότερων συσχετιστικών επιδράσεων στο διακεκριμένο όσο και στο συνεχές φάσμα που επηρεάζουν εμφανώς διάφορες πειραματικές μετρήσεις της ηλεκτρονιακής δομής και δυναμικής όπως η ύπερλεπτή ύψη και οι ενεργοί διατομές φωτοαπορροφήσεως. Έχουν ήδη γίνει πολλές εφαρμογές αυτής της θεωρίας



πὸ συμφωνοῦν μὲ ἀκριβεῖς πειραματικὲς τιμές. Ἐδῶ περιέχονται δύο νέες ἐφαρμογές: 1) Ὁ πολὺ ἀκριβὴς ὑπολογισμὸς τῶν δυνάμεων ταλαντώσεων γιὰ τὶς μεταβάσεις  $1s^2 2s \ ^2S$  —  $1s^2 2p \ ^2P^0$  στὸ Li καὶ  $Be^+$  τὰ ὁποῖα ἀναλύονται σὰν προβλήματα τριῶν σωμάτων καὶ 2) Ὁ φωτοιονισμὸς τῆς θεμελιώδους καταστάσεως  $^2P^0$  τοῦ F στὸν  $^2S$  δίαυλο λαμβανομένων ὑπ' ὄψη καὶ τῶν ἐπιδράσεων τῆς  $2s 2p \ ^6 \ ^2S$  αὐτοιονιζομένης καταστάσεως.

## References

1. I. Martinson, in «Excited States in Quantum Chemistry», C.A. Nicolaides and D.R. Beck, eds., p. 1, Reidel (1978).
2. J.C. Browne, in «Energy, Structure and Reactivity», D.W. Smith and W.B. Mcrae eds. Wiley (1973).
3. C.A. Nicolaides and D.R. Beck, Chem. Phys. Letts. **36**, 79 (1975).
4. D.R. Beck and C.A. Nicolaides, Phys. Letts. **56A**, 265 (1976).
5. C.A. Nicolaides and D.R. Beck, J. Chem. Phys. **66**, 1982 (1977).
6. C.A. Nicolaides and D.R. Beck in «Excited States in Quantum Chemistry» p. 143 Reidel 1978; C.A. Nicolaides and G. Theodorakopoulos, Int. J. Qu. Chem. **145**, 315 (1980).
7. P. Westhaus and O. Sinanoglu, Phys. Rev. **183**, 56 (1969).
8. C.A. Nicolaides and O. Sinanoglu, Phys. Letts. **33A**, 178 (1970).
9. D.R. Beck and O. Sinanoglu, Phys. Rev. Letts. **28**, 934 (1972).
10. C.A. Nicolaides and D.R. Beck, J. Phys. **B6**, 535 (1973).
11. C.A. Nicolaides, Chem. Phys. Letts. **21**, 242 (1973).
12. I. Öksüz and O. Sinanoglu, Phys. Rev. **181**, 42 (1969).
13. H.J. Silverstone and O. Sinanoglu, J. Chem. Phys. **44**, 1899 (1966).
14. C.A. Nicolaides and D.R. Beck, Phys. Rev. **A18**, 1307 (1978).
15. D.R. Beck and C.A. Nicolaides in «E.S.Q.C» p. 105, Reidel 1978.
16. D.R. Beck and C.A. Nicolaides, Int. J. Qu. Chem. **58**, 17 (1974).
17. J.E. Hansen, Phys. Rev. **A15**, 810 (1977).
18. D.R. Beck and C.A. Nicolaides, Phys. Letts. **65A**, 293 (1978).
19. C.A. Nicolaides and D.R. Beck, Can. J. Phys. **53**, 1224 (1975).
20. R.J. Buenker and S.D. Peyerimhoff, Chem. Phys. Letts. **29**, 253 (1974).
21. R.J. Buenker and S.D. Peyerimhoff, Chem. Phys. **8**, 324 (1975).
22. M.J. Harris, C.E. Loving and P.G.H. Sandars, J. Phys. **B11**, L749 (1978).
23. S.J. Rose, I.P. Grant and N.C. Pypèr, J. Phys. **B11**, 3499 (1978).
24. L.E. McMurchie and E.R. Davidson, J. Chem. Phys. **66**, 2959 (1977).
25. C.A. Nicolaides and D.R. Beck, J. Phys. **B9**, L259 (1976).
26. C.A. Nicolaides and D.R. Beck, Chem. Phys. Letts. **53**, 87 (1978).
27. D.R. Beck and C.A. Nicolaides, Chem. Phys. Letts. **53**, 91 (1978).
28. D.R. Beck and C.A. Nicolaides, Phys. Letts. **61A**, 227 (1977).
29. C.A. Nicolaides and D.R. Beck, Int. J. Qu. Chem. **14**, 457 (1978).
30. C.A. Nicolaides, Phys. Rev. **A6**, 2078 (1972); Nucl. Inst. Methods **110**, 231 (1973).
31. C.A. Nicolaides and D.R. Beck, Phys. Rev. **A17**, 216 (1978).
32. C.F. Bunge, Phys. Rev. **A19**, 936 (1979).
33. U. Fano, in «Photoionization and other probes of Many-electron interactions», p. 11 ed. F.J. Willeumier, Plenum (1976).
34. U. Fano and F. Prats, Proc. Natl. Acad. Sci. India **A33**, 553 (1963).
35. e.g. P.G. in «Atomic Processes and Applications» eds. P.G. Burke and B.L. Moiseiwitsch, N.H. (1976).
36. P.W. Lenghoff, Int. J. Qu. Chem. **11**, 301 (1977).
37. U. Fano and J. W. Cooper, Rev. Mod. Phys. **40**, 441 (1968).
38. C.E. Moore «Atomic Energy Levels» vol. 1 NBS 467.
39. U. Fano, Phys. Rev. **124**, 1865 (1961).

40. D.R. Beck and C.A. Nicolaides, *Chim. Chronika*, in press; *Int. J. Qu. Chem.* **145**, 323 (1980).
41. M.Ya. Amusia, *Comm. At. Mol. Phys.* **8**, 61 (1979).
42. A complete study of the  $F\ 2p^5\ ^2P^0 \rightarrow ^2S, ^2D, ^2P$  photoabsorption is in progress and will be reported elsewhere.
43. P.L. Altick and E.N. Moore, *Phys. Rev.* **147**, 59 (1966).
44. C.A. Nicolaides and D.R. Beck, *Phys. Rev.* **A17**, 2116 (1976).
45. C.A. Nicolaides and D.R. Beck, *Chem. Phys. Letts.* **35**, 202 (1975).
46. B. Sountag, *J. Physique, Colloque C4*, **39**, 9, (1978).

## **STRUCTURAL ANALYSIS OF CHLORINATED ORGANIC COMPOUNDS BY NUCLEAR QUADRUPOLE RESONANCE SPECTROSCOPY<sup>1</sup>**

DINA GEGIOU

*Research Department, General Chemical State Laboratory, 16 A. Tsoha Street, Athens 602, Greece.*

FANI MILIA

*Physics Department, Nuclear Research Center «Democritos», Athens, Greece.*

### **Summary**

Nuclear Quadrupole Resonance (NQR) Spectroscopy has been used to demonstrate the difference in the chemical environment of the <sup>35</sup>Cl atoms in a number of chlorinated organic compounds with emphasis on chlorinated pesticides. Assignment of signals to specific chlorine atoms has been made utilizing spectra-structure correlation charts and other available data. Some of the problems arising in the interpretation of the NQR spectral lines are discussed.

**Key Words:** Structural analysis, chlorinated pesticides, and NQR spectroscopy.

### **Introduction**

<sup>35</sup>Cl Nuclear Quadrupole Resonance (NQR), although known for quite some time, has been used lately for the structural analysis of chlorinated organic compounds. This development was determined mainly by the improvement of spectrometers. Structural information can be obtained from the spectra of chlorinated compounds by a method similar to that used in proton resonance. In cases where conventional spectroscopic methods, such as infrared spectroscopy, mass spectroscopy, and proton resonance, yield ambiguous results, the chlorine NQR spectroscopy can help to settle certain structures by detailed statements regarding the linkage of the individual chlorine atoms in the molecule.

In the present work we have studied the NQR spectra of a number of chlorinated organic compounds and combining the results with appropriate literature data we attempt to assign each individual chlorine atom. Emphasis is given to chlorinated pesticides and to commercially available model compounds of piece-wise similar structure, because of their analytical interest.

The four pesticides investigated Aldrin, Endrin, and Endosulfan a and b all contain six chlorine atoms but three pairs of chemically different C-Cl bonds:

a) the two chlorine atoms on the bridgehead carbon atoms, b) the two vinylic chlorine atoms, and c) the two chlorine atoms of the dichloromethylene group. In a previous publication<sup>2</sup> the chlorine atoms on the bridgehead carbon atoms were assigned with certainty to absorb at lower field as compared to the other two kind of chlorines, but the other two groups were tentatively assigned, because spectroscopic data were insufficient for meaningful correlations. To help our interpretation five more chlorinated organic compounds have been studied at various temperatures; the NQR spectra of some of them are reported for the first time.

### Experimental

The samples of Aldrin and Endrin used in the present work were analytical grade (99% purity) from Shell Chemical Co., New York. The samples of the two isomers of Endosulfan were also analytical grade (99% purity) from Hoechst A.G., Frankfurt, Germany. The samples of 1, 2, 3, 4, 7, 7, -hexachlorobicyclo [2.2.1] -2,5-heptadiene (technical grade), hexachloro-2,4-cyclohexadienone (98% purity), 2, 3-dichloro-5,6-dicyano-1,4-benzoquinone (98% purity), dichloromaleic anhydride, and perchloro-2-cyclobuten-1-one (96% purity) were from Aldrich. Tetrachlorothiophene (97% purity) was supplied by EGA-Chemie KG. All the samples were used without further purification.

The NQR spectra were obtained by using a Decca-Radar NQR spectrometer. Samples (0.5-1g) were placed in a glass tube (1cm dia) and positioned in the spectrometer coil. When closely spaced lines were suspected, side-band suppression by slow variation on the quench frequency was used, for better distinction between line and side-band. For some of the compounds the temperature dependence of the frequency was measured from room temperature down to liquid nitrogen temperature to detect possible phase transitions. Frequency measurements were accurate to  $\pm 0.01$  MHz and temperature measurements to  $\pm 1^\circ\text{C}$ .

### Results and discussion

The <sup>35</sup>Cl NQR frequencies of 2,3-dichloro-5,6-dicyano-1,4-benzoquinone (I), dichloromaleic anhydride (II), and tetrachlorothiophene (III) all containing only vinylic chlorine atoms are reported in Table I and compared with the literature values where such values have been reported. In (I) the two vinylic chlorine atoms resonate at 38.34 and 38.37 MHz (77°K). In (II) the vinylic chlorine atoms resonate at 37.96 and 38.04 MHz (77°K). The frequency versus temperature plot for (II), shown in Figure 2, suggests that at 273°K the two chlorine atoms become equivalent. Compound (III) exhibits at room temperature the expected four signals (36.89, 36.91, 37.65, and 37.70 MHz, 290°K) corresponding to the four chlorine atoms bound in the molecule, but only three signals at liquid nitrogen temperature (37.52, 38.48, and 38.54 MHz). Relative intensities of the resonance frequencies at low temperature

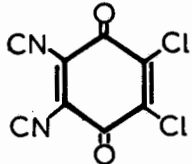
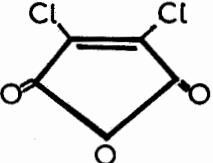
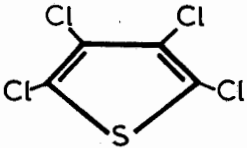
Compound	Structure	Resonance frequency MHz (this work)	Literature <sup>4</sup> values
2,3 Dichloro-5,6- -dicyano-1,4-benzo- quinone (I)		38,34, 38,37 (77°K)	38,013 , 37,945 (86°K)
Dichloromaleic anhydride (II)		37,96, 38,04 (77°K)	
Tetrachlorothiophene (III)		37,52 , 37,52 } (77°K) 38,48 , 38,54 }  36,89 , 36,91 } (290°K) 37,65 , 37,70 }	37,52 , 37,52 } (86°K) 38,50 }  36,91 , 36,93 } (294°K) 37,74 }

TABLE I: <sup>35</sup>Cl Pure Quadrupole Resonances of Some Organic Compounds Containing Vinyllic Chlorine Atoms (at Various Temperatures)

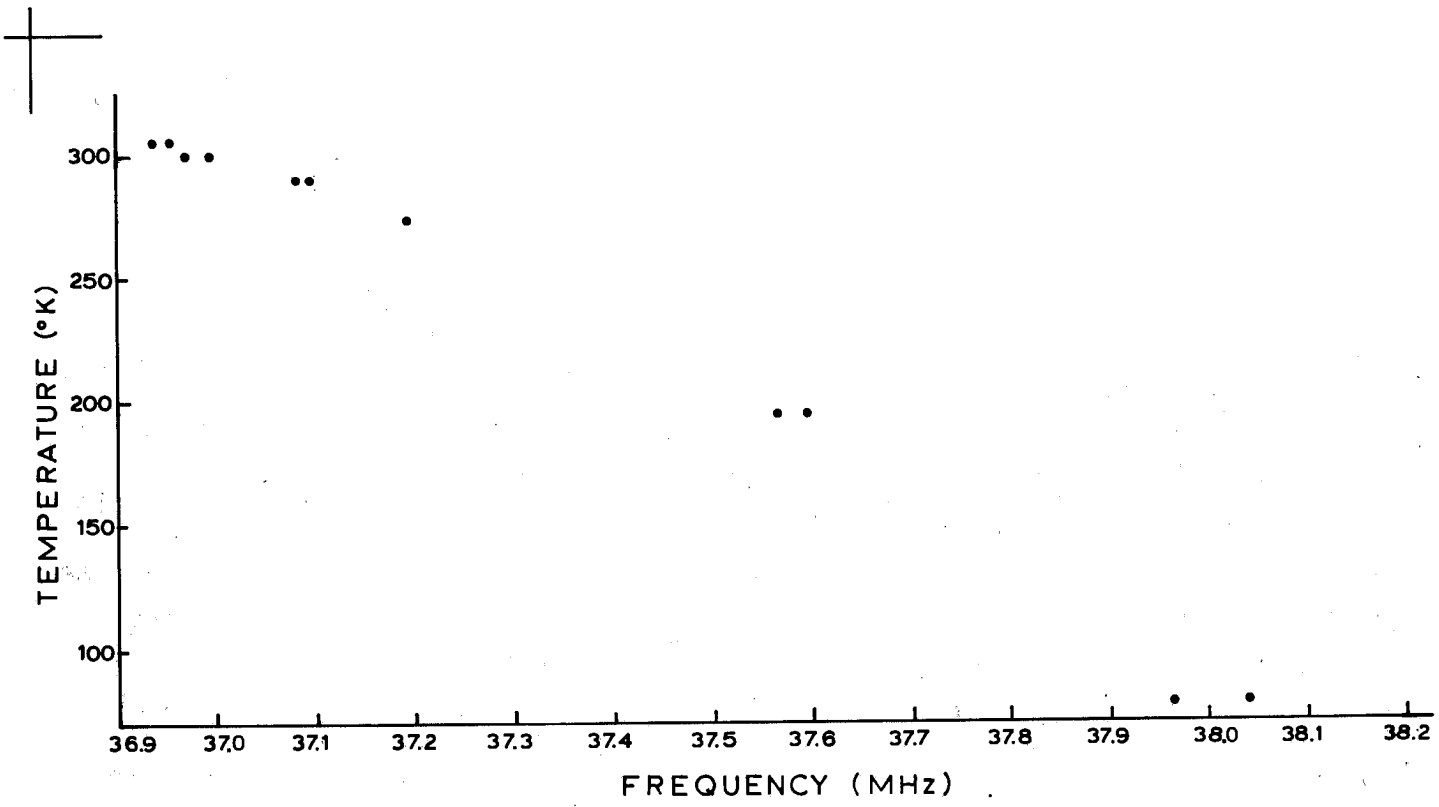


FIG. 1: The NQR frequency of  $^{35}\text{Cl}$  as a function of temperature in dichloromaleic anhydride.

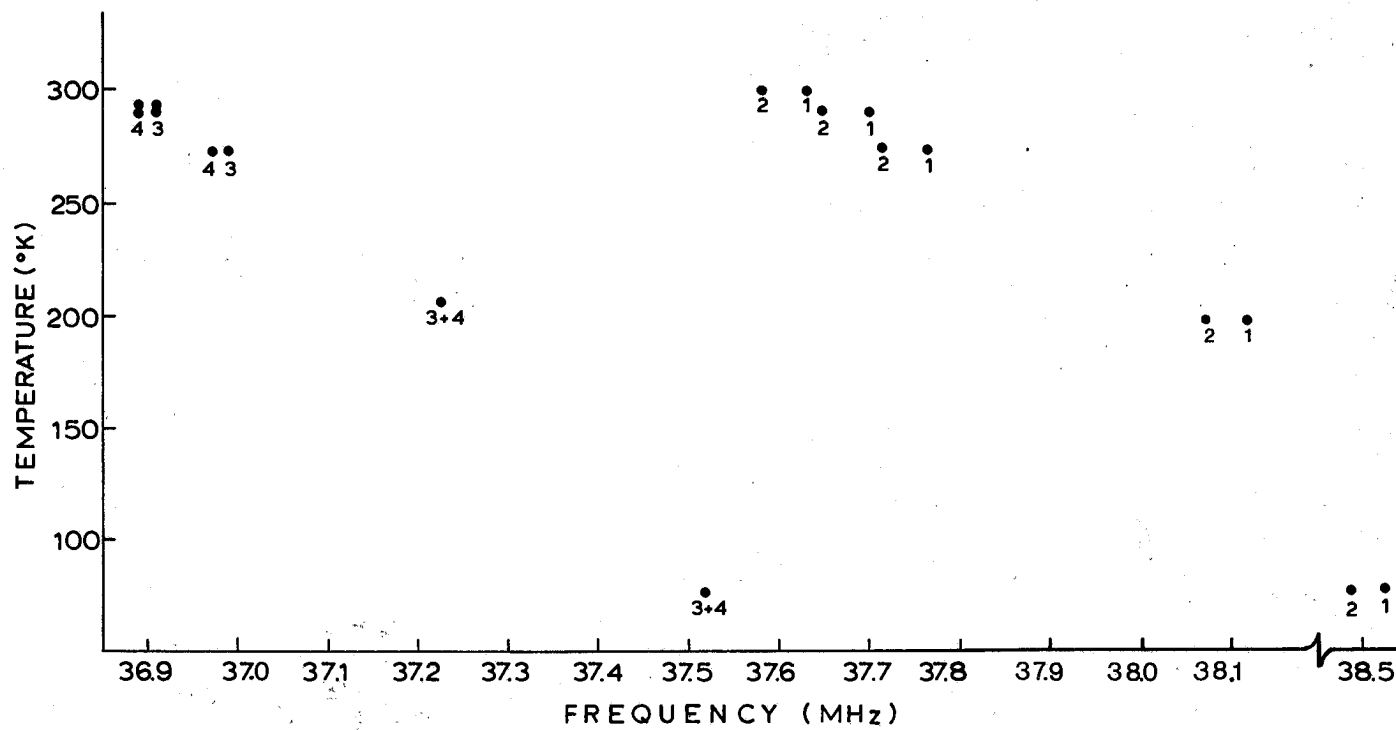


FIG. 2: The NQR frequency of  $^{35}\text{Cl}$  as a function of temperature in tetrachlorothiophene.

suggest that the line at 37.52 MHz is an un-resolved doublet. The frequency versus temperature plot shown in Figure 3 appears normal. In general, as the temperature is raised, the frequencies diminish corresponding to the averaging effect of the increasing amplitudes of thermal oscillations of the molecules. The NQR spectrum of (III) has been reported previously<sup>3</sup>, but only three resonance frequencies have been observed at room temperature and two frequencies at low temperature; probably because of instrumental insensitivity the frequency of only three chlorine atoms could be observed.

Further, perchloro-2-cyclobuten-1-one (IV) and hexachloro-2,4-cyclohexadienone (V), both containing vinylic chlorine atoms and chlorine atoms of the dichloromethylene group, have been investigated. Compound (IV) is a liquid at room temperature, thus it has been studied only at 193°K and 77°K. The NQR spectra of (IV) and (V) at 77°K are shown in Table II; together, for reasons of comparison, are given the spectra of two other chlorinated compounds (VI and VII) from literature available data which both contain similar groups of chlorine atoms<sup>4,5</sup>. Compound (IV) yields the expected four lines. Since the molecule contains equal chlorine atoms in each chemically different group, assignment cannot be based on multiplet grouping of the lines. According to theoretical calculations CNDO/2 the lower frequency lines are assigned to the vinylic chlorine atoms<sup>6</sup>. Among the two lower frequency lines the lowest may be assigned to the  $\alpha$ -vinylic chlorine atom on the basis of the mesomeric effect. All four frequencies observed for (IV) are below 38 MHz. The low frequency of the allylic chlorine atoms is attributed to the contribution of some aromatization. Compound (V) yields six NQR lines divided into four and two line groups. Thus, the four lower frequency lines are assigned to the four vinylic chlorine atoms and the other two lines to the chlorine atoms of the dichloromethylene group. The assignment of the spectra of (IV) and (V) is in good agreement with the assignment made for comparison substances (VI) and (VII) shown in Table II.

We have also investigated the <sup>35</sup>Cl pure quadrupole resonances of the cyclo-diene chlorinated pesticides Aldrin, Endrin, and Endosulfan a and b which contain, in addition to a pair of vinylic and a pair of chlorine atoms of the dichloromethylene group, two bridgehead chlorine atoms. The spectrum of Aldrin exhibits at room temperature three resonance signals, while at lower temperatures the six signals as expected by the number of chlorine atoms in the molecule. Previously<sup>2</sup> only one signal was observed at room temperature. The spectrum of Endrin exhibits both at room and low temperatures the expected six signals. Roll and Biro<sup>2</sup> observed previously only five lines. With Endosulfan a only one frequency line is observed at room temperature, but the expected six lines at liquid nitrogen temperature. Broadening of lines beyond detection at elevated temperatures can arise from a variety of reasons. Finally, Endosulfan b yields both at room and at low temperatures twelve frequency lines for the six chlorine atoms in the molecule; the spectrum thus suggests that there are two unequivalent molecules of this compound per unit cell of the crystal. The resonance frequencies are given in Table III.



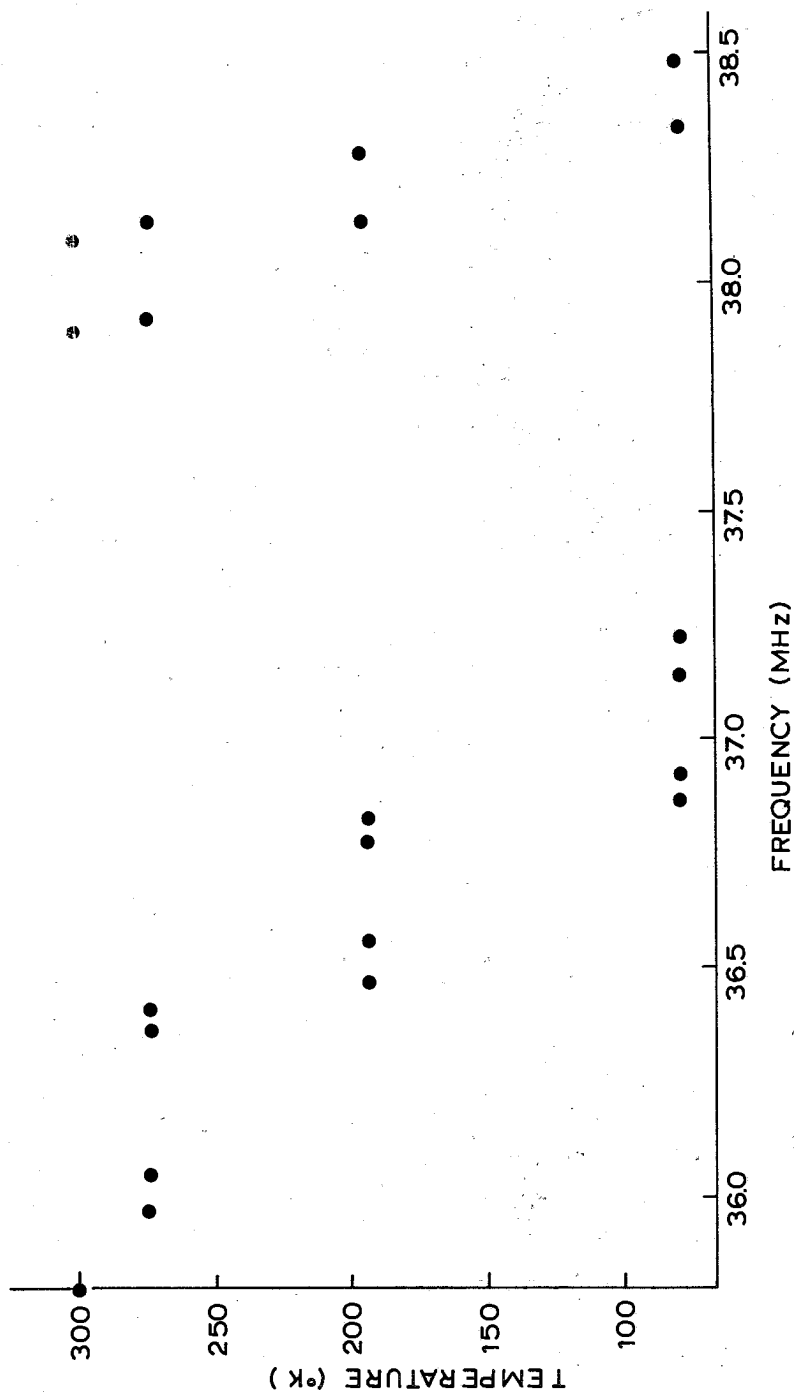


FIG. 3: The NQR frequency of  $^{35}\text{Cl}$  as a function of temperature in Aldrin.

Compound	Structure	Frequency MHz (77°K)	
Perchloro-2 cyclobuten-1-one (IV)		36.69, 37.27 ← $\gg$ C-Cl 37.63, 37.75 ← $\gg$ C-Cl <sub>2</sub>	This work
Hexachloro-2,4- cyclohexadienone (V)		37.36, 37.92 } ← $\gg$ C-Cl 38.07, 38.17 } 38.57, 38.62 ← $\gg$ C-Cl <sub>2</sub>	
Hexachlorocyclo- pentadiene (VI)		37.46, 37.28 } ← $\gg$ C-Cl 37.28, 36.95 } 39.10, 38.88 ← $\gg$ C-Cl <sub>2</sub>	Decca <sup>5</sup>
(VII)		38.59, 38.80 ← $\gg$ C-Cl 39.19, 40.35, 40.66 } ← $\gg$ C-Cl <sub>2</sub> 40.69, 40.78, 41.23 } 48.27 ← =N-Cl	

TABLE II: <sup>35</sup>Cl Pure Quadrupole Resonances of Some organic Compounds Containing Vinylic Chlorine Atoms and Chlorine Atoms of the Dichloromethylene Group

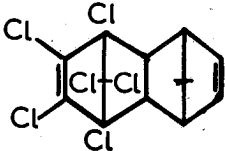
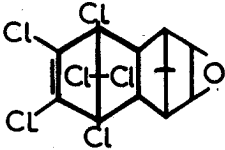
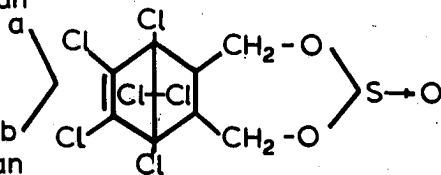
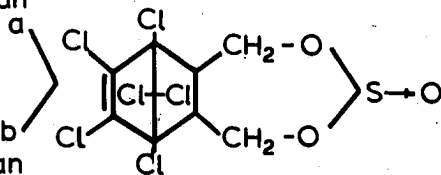
Compound	Structure	Resonance frequency MHz (this work)	Literature <sup>2</sup> value
Aldrin		36.86, 36.92, 37.22 } (77°K) 37.14, 38.38, 38.48 }	37.9 (295°K)
Endrin		35.93, 36.14, 36.18 } (300°K) 36.43, 37.19, 37.86 }	35.9, 36.1 } (295°K) 36.3, 37.0 } 37.7
Endosulfan		36.92, 37.07, 37.30 } (77°K) 37.48, 38.37, 38.92 }	
Endosulfan		36.72, 36.91, 37.05 } (77°K) 37.15, 37.19, 37.24 } 37.26, 37.35, 37.69 } 38.08, 38.79, 39.16 }	

TABLE III: <sup>35</sup>Cl Pure Quadrupole Resonances of Some Cyclohexene Chlorinated Pesticides (at Various Temperatures)

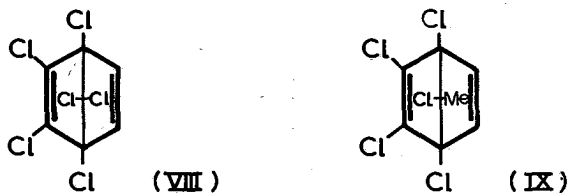
The NQR frequency versus temperature plot for Aldrin, shown in Figure 4, presents no discontinuities and therefore no phase transitions from room temperature down to liquid nitrogen temperature. The resonance frequency decreases at higher temperatures in qualitative agreement with Bayer's theory<sup>7</sup>.

Previous assignment<sup>2</sup> based on spectra-structure correlation charts attributed the chlorine atoms on the bridgehead carbon atoms with certainty to absorb at lower field as compared to the other two kind of chlorines. Thus, for all four compounds, the bridgehead chlorine atoms resonate at lowest frequency; 36.86 and 36.92 MHz (77°K) for Aldrin, 35.93 and 36.14 MHz (300°K) for Endrin, 36.92 and 37.07 MHz (77°K) for Endosulfan a, and 36.72, 36.91, 37.05, and 37.15 MHz (77°K) for Endosulfan b.

Following the reasoning outlined above for compounds (IV) and (V), the assignment of the resonance frequencies of the remaining chlorine atoms can be made as shown in Figure 5. The two higher lying frequency lines are attributed to the dichloromethylene group chlorine atoms; 38.38 and 38.48 MHz (77°K) for Aldrin, 37.19 and 37.86 MHz (300°K) for Endrin, 38.37 and 38.92 MHz (77°K) for Endosulfan a, and 37.69, 38.08, 38.79, and 39.16 MHz (77°K) for Endosulfan b. Thus, the vinylic chlorine atoms should resonate at lower frequencies as compared to the chlorine atoms of the dichloromethylene group; 37.22 and 37.14 MHz (77°K) for Aldrin, 36.18 and 36.43 MHz (300°K) for Endrin, 37.30 and 37.48 MHz (77°K) for Endosulfan a, and 37.19, 37.24, 37.26, and 37.35 MHz (77°K) for Endosulfan b.

This assignment is of course still tentative and differs from that of Roll and Biros. The previous assignment was based on the fact that vinylic chlorine atoms occur at higher frequencies than aliphatic chlorine atoms. However, we believe that the effect of the accumulation of chlorine atoms on the same carbon atom was underestimated in that reasoning.

Attempts to support further our assignment by studying the NQR spectra of a model compound where one chlorine atom on the dichloromethylene group would be replaced by a methyl group have not been successful. Specifically in 1, 2, 3, 4, 7, 7-hexachlorobicyclo [2.2.1] -2,5-heptadiene (VIII) one chlorine atom of the dichloromethylene group was replaced by a methyl



group with methyl-lithium<sup>8</sup>, but with the methylated product (IX) no NQR spectrum could be detected.

The present results extend the set of cyclodiene chlorinated pesticides and show the applicability and usefulness of the NQR spectroscopy in the analysis of organic compounds.

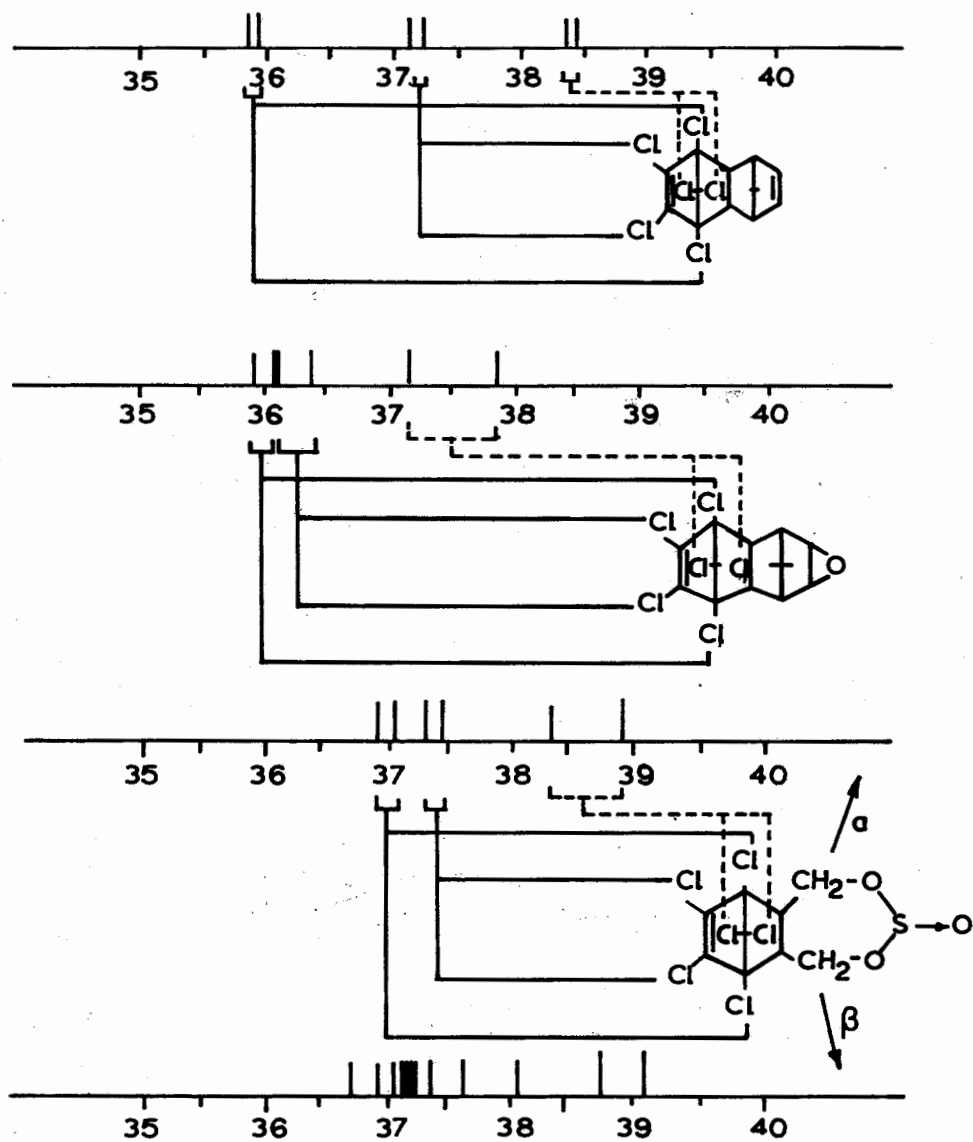


FIG. 4: Structure assignment of the  $^{35}\text{Cl}$  NQR lines of Aldrin, Endrin, and Endosulfan a and b.

## Περίληψη

Δομική ανάλυση γαμοριών οργανικών ενώσεων με φασματοσκοπία πυρηνικών τετραπολικών συντονισμών

Χρησιμοποιείται η φασματοσκοπία του πυρηνικών τετραπολικών συντονισμών για τη διάκριση του χημικού περιβάλλοντος ατόμων<sup>35</sup>Cl σε άρθια γαμοριών οργανικών ενώσεων με έμφαση σε όργανα χαμηλού γύρω φυτόφθμακα. Η απόδοση των συχνοτήτων σε ειδικά άτομα χαμηλού γύρω με τη βοήθεια πινακων συχνοτήτων φασμάτων — δομής και άλλων βιβλιογραφικών στοιχείων. Συζητούνται τάλος όργανα προβλήματα του ανκρόπου στην έρηνεια των φασματικών γράμων του πυρηνικού τετραπολικού συντονισμού.

## References and Notes

1. Presented in part at the 2nd Specialized Colloque Ampere, 25-29 August, 1975, Budapest, Hungary.
2. Roll, D.B., and Biros, F.J.: Anal. Chem. **39**, 918 (1967).
3. Dewar, M.J.S., and Lucken, E.A.C.: J. Chem. Soc., 426 (1959).
4. Fitzky, H.G.: Advances in Nuclear Quadrupole Resonance, Vol. 1, Heyden, London (1973).
5. Radio Frequency Spectroscopy, p. 44. Decca Radar Ltd, Instrument Division, Walton-on-Thames, Surrey, England.
6. Unpublished results.
7. Bayer, H.: Z. Physik, **130**, 227 (1951).
8. Alexander, R., and Davies, D.L.: J. Chem. Soc. Perkin I, 83 (1973).

## Acknowledgments

We would like to thank Mr Marios Voudouris for his skilful technical assistance.

## THE KINETICS OF THE DEOXYRIBONUCLEIC ACID-RIBONUCLEIC ACID HYBRIDIZATION WITH SIMULTANEOUS SELF-ANNEALING OF RIBONUCLEIC ACID

NICHOLAS A. KATSANOS and HELEN THOMOU

*Physical Chemistry Laboratory, University of Patras, Patras, Greece and*

*Department of Biology, N.R.C. «Democritos», Aghia Paraskevi, Athens, Greece*

### Summary

The kinetics of the self-annealing of RNA in solution and of the DNA-RNA hybridization reaction have been studied in the presence of the RNA self-annealing. The time-course of both reactions follows a simple first-order law with the same apparent rate constant, which does not depend either on temperature or on RNA concentration. It is shown that single stranded DNA exhibits the same kinetic behaviour towards self-annealed and non-annealed complementary RNA.

Detailed mechanisms for both above reactions are proposed and theoretical integrated rate equations, derived from these mechanisms, are consistent with the experimental findings. These mechanisms are based on the formation of weakly bound complexes, sensitive to RNase, which are formed between mutually complementary RNA strands, and between DNA and (RNA)<sub>2</sub>.

It is further shown that the infinity values of the hybridization reaction lead theoretically to the well known double reciprocal relation between hybridization and RNA concentration.

**Key-words:** Deoxyribonucleic acid/ Ribonucleic acid/ DNA-RNA hybridization/ RNA self-annealing.

### Introduction

In a previous paper<sup>1</sup> we reported a contribution to the theory of the equilibrium of the DNA-RNA hybridization reaction. Some new data at various temperatures, analyzed by means of a new equation derived there, led to the tentative conclusion that DNA, which is immobilized on membrane filters, exhibits the same equilibration behaviour towards solutions of single RNA and of self-annealed (RNA)<sub>2</sub>. This finding encouraged us to further investigate the DNA-RNA hybridization reaction by studying the way of approach to equilibrium, i.e. the kinetics of its attainment. Since the formation of hybrids between DNA and complementary RNA takes place in the presence of an apparently competing self-annealing of single RNA to form double stranded (RNA)<sub>2</sub>, the kinetics of the latter reaction in the absence of DNA was studied first.

## Materials and Methods

The materials used, the method of preparation of DNA, the synthesis of labelled RNA *in vitro*, the self-annealing of RNA, and the proportion of DNA retained on the filters used in hybridization runs, have been described elsewhere<sup>1</sup>. The hybridization procedure was also the same, except that each kinetic run comprised samples incubated for varying times with the same amount of <sup>3</sup>H-labelled RNA in 4 × SSC\* solution.

The amount of denatured DNA in all samples was 5μg, and the final volume of each hybridization mixture 250 mm<sup>3</sup> (μl).

## Results and Discussion

### *Self-annealing reaction of RNA*

The kinetics of this reaction was studied at two temperatures by determining the fraction of acid-precipitable RNA which became resistant to RNase as a function of time.

The unexpected finding of this type of experiments was that the results can best be fitted into the rate law of a reversible reaction which is first-order in both directions, whereas a mechanism of the type  $2\text{RNA} \rightleftharpoons (\text{RNA})_2$  would lead to a rate law which is second-order in the forward and first-order in the reverse directions.

The integrated kinetic equations for these two cases are easily derived as follows. We call  $c/\mu\text{g}\cdot\text{cm}^{-3}$  the concentration of RNA in the annealed form at time  $t$ , and  $c_{\text{tot}}/\mu\text{g}\cdot\text{cm}^{-3}$  the total concentration of RNA (annealed + non-annealed), which remains constant with time. Then, for a reversible reaction which is first-order in both directions,

$$\frac{dc}{dt} = k_1 (c_{\text{tot}} - c) - k_{-1}c \quad (1)$$

where  $k_1$  and  $k_{-1}$  are the rate constants for the forward and the backward directions, respectively. Dividing eqn. (1) throughout by  $c_{\text{tot}}$  and denoting the fraction  $c/c_{\text{tot}}$  by  $f_t$ , we obtain, after some rearrangement,

$$\frac{df_t}{dt} + kf_t = k_1 \quad (2)$$

where  $k = k_1 + k_{-1}$ .

This differential equation can be solved by conventional methods, or most easily by Laplace transformation with initial condition  $f_t = f_0$  at  $t = 0$ . The result is

---

\* 4 × SSC means four times the concentration of saline/sodium citrate, i.e. 0.6M-NaCl/0.6M-sodium citrate.



$$f_t = \frac{k_1}{k} + (f_0 - \frac{k_1}{k}) \cdot \exp(-kt) \quad (3)$$

Calling  $f_\infty$  the equilibrium value of  $f_t$ , we find from eqn. (2)  $f_\infty = k_1/k$ , since at equilibrium  $df_t/dt = 0$ . Substituting  $f_\infty$  for  $k_1/k$  in eqn. (3), rearranging and taking logarithms we have finally

$$\ln(f_\infty - f_t) = \ln(f_\infty - f_0) - kt \quad (4)$$

For a reversible reaction which is second-order in the forward direction, with rate constant  $k_2$ , and first-order in the backward direction, with rate constant  $k_{-1}$ , the rate equation is

$$\frac{dc}{dt} = k_2 (c_{\text{tot}} - c)^2 - k_{-1} c \quad (5)$$

or, after division by  $c_{\text{tot}}^2$ ,

$$\frac{df_t}{dt} = k_2 c_{\text{tot}} (1 - f_t)^2 - k_{-1} f_t \quad (6)$$

Using the equilibrium condition  $df_t/dt = 0$  we can eliminate  $k_{-1}$  by means of  $f_\infty$ . The resulting equation can then be integrated by the method of partial fractions giving finally

$$\ln \left( \frac{1 - f_t f_\infty}{f_\infty - f_t} \right) = \ln \left( \frac{1 - f_0 f_\infty}{f_\infty - f_0} \right) + \frac{1 - f_\infty^2}{f_\infty} \cdot c_{\text{tot}} k_2 t \quad (7)$$

Both integrated rate equations (4) and (7) can be tested by using their left-hand side to plot the experimental data against  $t$ , whereby a linear plot can decide in favour of the one or the other rate law. These plots are shown in Fig. 1 and it is seen that the annealing data follow the rate equation of a reversible reaction which is first-order in both directions [eqn. (4)], rather than second-order in the forward and first-order in the reverse directions [eqn. (7)]. A deviation of the time dependence of the RNA self-annealing from a second-order law has also been observed by Geiduschek *et al*<sup>2</sup>.

A mechanism explaining the time-course of the self-annealing reaction must also take into account two other facts. First, that the RNA used by us was prepared *in vitro* by transcription of native (double-stranded) DNA and it is a well-known fact that *in vitro* conditions both strands of DNA are transcribed producing two kinds of RNA strands which are mutually complementary<sup>3</sup>.

Second, that the acid-precipitable RNA was a large fraction (51-56%) of the total, and of this a large fraction (54-92%, depending on the individual preparation) became RNase resistant when the self-annealing reaction reached equilibrium.

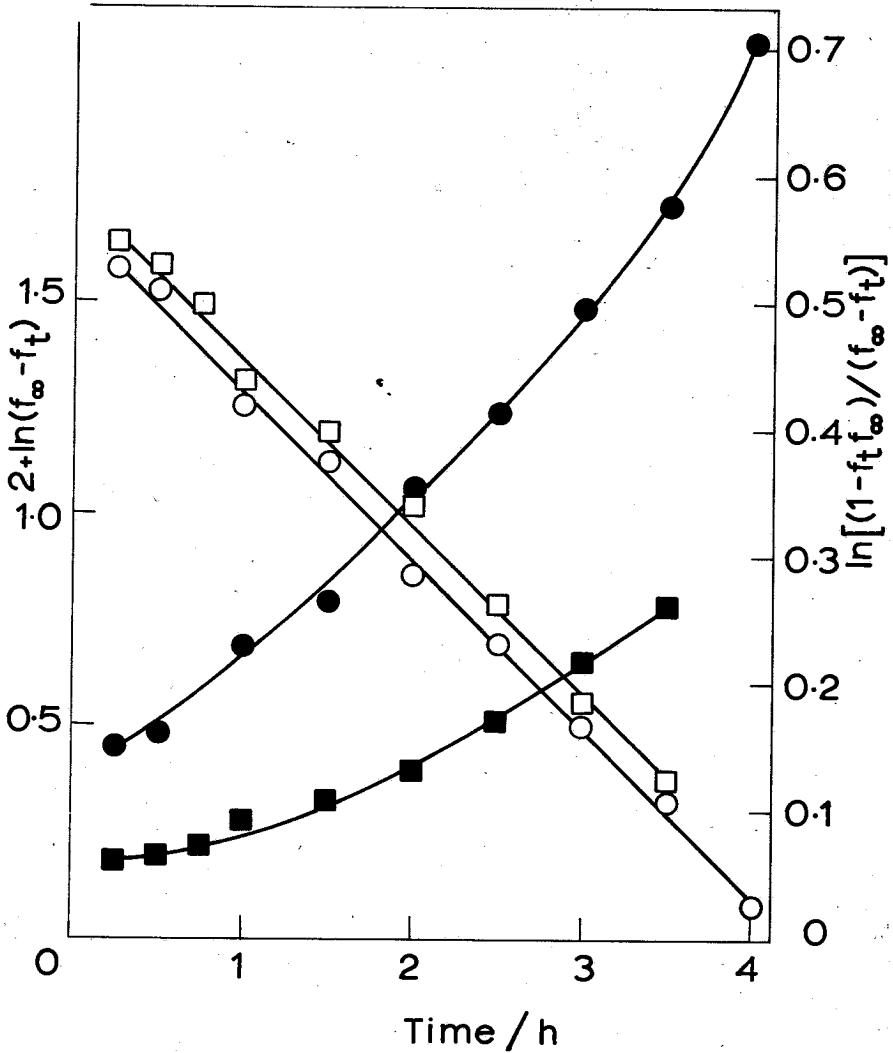


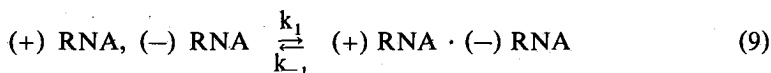
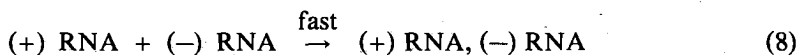
FIG. 1. Data for self-annealing reaction of RNA plotted according to eqns. (4) and (7). The RNA solutions in 4×SSC, pH 7.0, at a concentration of 80  $\mu\text{g}/\text{cm}^3$ , were incubated at constant temperature, immediately after preparation. At various time intervals four 50  $\text{mm}^3$  samples were withdrawn from the solution and diluted to 2×SSC pH 7.0. Two of them were digested with heat-treated pancreatic ribonuclease (20  $\mu\text{g}/\text{cm}^3$ ) for 20 min at 37°C, while the other two served as controls of the total acid-precipitable RNA. Each sample was then precipitated by addition of 0.1  $\text{cm}^3$  of bovine serum albumin (4  $\text{mg}/\text{cm}^3$  in water) and 0.1  $\text{cm}^3$  of 50% (w/v) trichloroacetic acid. After mixing, 3  $\text{cm}^3$  of 5% trichloroacetic acid was added, and after standing for 10 min on ice, it was centrifuged at 2000 g for 10 min at 4°C. The pellet formed was drained, dissolved in 0.3  $\text{cm}^3$  of 1M - NaOH and transferred to a vial containing 0.5  $\text{cm}^3$  of 1M

- HCl. The tube was rinsed with 0.2 cm<sup>3</sup> of water, which was also transferred to the vial. Finally, 10 cm<sup>3</sup> of a scintillation mixture was added, containing 1 part of Triton X - 100 and 2 parts of toluene-based scintillator [0.42% 2,5-diphenyloxazole, 0.021% 1,4-bis-(5-phenyloxazol-2-yl)benzene]. The resulting sample was counted in a Beckman liquid-scintillation counter, corrections for background radiation etc. being made. The counter had an efficiency of 20% for tritium.

The fraction  $f_i$  of RNA in the annealed form at each time was calculated by dividing the mean counting rate of the two samples (c.p.m.) treated with RNase, by the mean counting rate of the two respective control samples (without enzymic digestion). Little change of  $f_i$  was observed after about 6 h, and after 10 h the value of  $f_i$  remained fairly constant. The mean of three or four such values was taken as the  $f_\infty$  value.

O, ●, incubation at 67°C; □, ■, incubation at 75°C; empty symbols represent first-order plots according to eqn. (4) (left ordinate), while filled-in symbols are second-order plots according to eqn. (7) (right ordinate).

A mechanistic hypothesis, consistent with all facts above, is that mutually complementary strands of RNA, which for convenience we denote by (+) RNA and (-) RNA, associate very rapidly by a few hydrogen bonds between complementary bases or otherwise to form a loosely and weakly bound complex, (+) RNA, (-) RNA, sensitive to RNase. This then transforms slowly to a proper double-stranded structure (+) RNA · (-) RNA, resistant to RNase:



However, first-order kinetics can be explained, not only by eqns. (8) and (9), but also by assuming that the self-annealing reaction involves folding of the RNA chain back on itself in a number of places, so that pairs of complementary bases may come together and become linked by hydrogen bonds. This type of secondary structure, however, must be ruled out, since the molecular weight of self-annealed RNA is much bigger than that before annealing (Fig. 2). Polyacrylamide-gel electrophoresis can easily break a weak association such as (+) RNA, (-) RNA but not a highly ordered, DNA-like secondary structure such as (+) RNA · (-) RNA. The two structures shown on both sides of eqn. (9) will then move with quite different rates upon electrophoresis.

The melting curve of the RNA used in this study was reported earlier by us<sup>1</sup> and it is a further confirmation of an ordered secondary structure such as that assumed by Geiduschek *et al.*<sup>2</sup>

We can summarize the results of the self-annealing reaction as follows. Less than 50% of the RNA synthesized *in vitro* on a DNA template from eukariotic cells using the RNA polymerase of *M. Lysodeikticus* consists of small fragments non-precipitable in acid solution under the conditions described

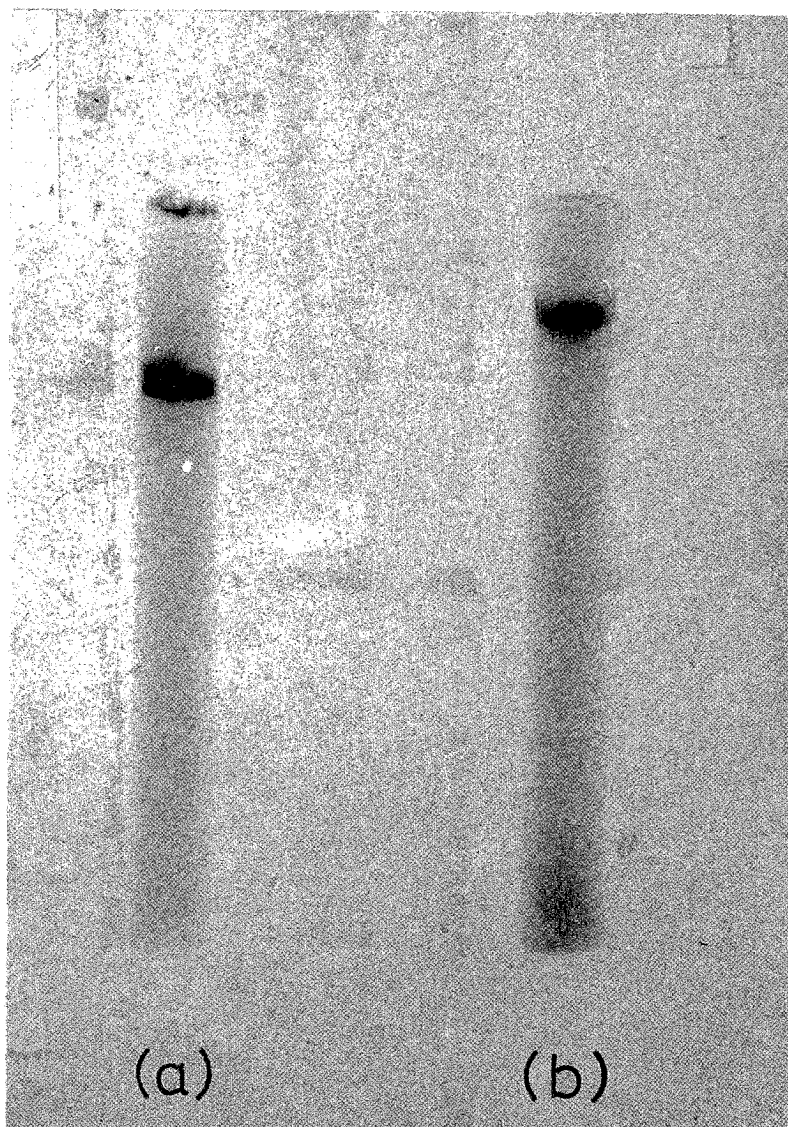


FIG. 2. *Relative molecular size estimation of RNA before and after self-annealing at 67°C.*

RNA synthesized *in vitro* as described by Thomou & Katsanos<sup>1</sup> was dissolved in 0.01 M-Tris/HCl, pH 7.5 and subjected to electrophoresis on polyacrylamide-gel (2.4%, w/v, acrylamide and 0.12% bisacrylamide; the method was that of Loening<sup>10</sup>, slightly modified by using 2 mA per gel for 45 min).

(a), un-incubated RNA; (b), RNA incubated at 67°C for 18 h. The two samples were run simultaneously.

in the legend of Fig. 1. This portion of RNA may result from the transcription of that part of the genome which occurs in only a few copies, or it is due to degradation of the initial product occurring during the isolation procedure. Of the remaining fraction of the total RNA, consisting of more than 150 nucleotides per molecule<sup>1</sup>, a large proportion is self-complementary and follows a first-order self-annealing reaction which can be explained by eqns. (8) and (9). The final product is most probably a double-stranded ordered structure.

The rate constant of the self-annealing reaction  $k = k_1 + k_{-1}$ , calculated from the first-order plots of Fig. 1 is  $(1.11 \pm 0.02) \cdot 10^{-4} \text{ s}^{-1}$  at 67°C, and  $(1.10 \pm 0.03) \cdot 10^{-4} \text{ s}^{-1}$  at 75°C. Similar values were obtained with solutions containing 50 and 100  $\mu\text{g}/\text{cm}^3$  RNA.

#### *Hybridization of RNA with DNA*

If only single-stranded RNA molecules could hybridize with single-stranded complementary DNA, then the self-annealing reaction of RNA would compete with the DNA-RNA hybridization, and the rate of the last reaction would be different if kinetic experiments on hybridization were performed with unincubated and pre-incubated RNA solutions. This, however, does not seem to be the case, as is evidenced from Fig. 3, where hybridization data are presented as first-order plots. The apparent rate constant from the slope of both plots is  $(1.20 \pm 0.03) \cdot 10^{-4} \text{ s}^{-1}$ , their difference lying beyond the second decimal point.

It is thus shown that single-stranded immobilized DNA exhibits the same *kinetic* behaviour towards solutions of self-annealed and of non-annealed complementary RNA. A similar observation was reported by Nygaard & Hall<sup>4</sup> who found no decrease in the DNA-RNA hybridization rate when RNA was boiled for 5 min or pre-incubated for 2h at 67°C. However, their RNA was isolated from T2-infected cultures of *E. coli* and it is not certain that it contained self-complementary RNA.

The possibility that the hybrids with DNA are not formed by the self-complementary acid-precipitable form of RNA, but from the non-precipitable small fragments of RNA, was excluded by performing the following experiment. RNA was precipitated by 5% trichloroacetic acid as described in the legend of Fig. 1 and the supernatant solution, containing the non-precipitable RNA fraction ( $59 \mu\text{g}/\text{cm}^3$ ), was used for hybridization with DNA at 67°C, in  $4 \times \text{SSC}$ . The reaction was followed for 16h, samples being treated as described in the legend of Fig. 3 at various time intervals. The amount of RNA bound to the filters was found to be invariably less than 0.31%, whereas in a control experiment with total RNA ( $56 \mu\text{g}/\text{cm}^3$ ), without prior precipitation by acid, 3.1% of the RNA input was finally bound to the filters.

In contrast to Nygaard & Hall<sup>4</sup> who used conventional second-order kinetics to analyse their hybridization data in solution, Bishop<sup>5</sup> introduced a linear double reciprocal plot presentation,  $1/\text{hybridization}$  against  $1/\text{time}$ , for his results on nitrocellulose membrane filters with complementary RNA in considerable excess over DNA. The same presentation was extensively used by

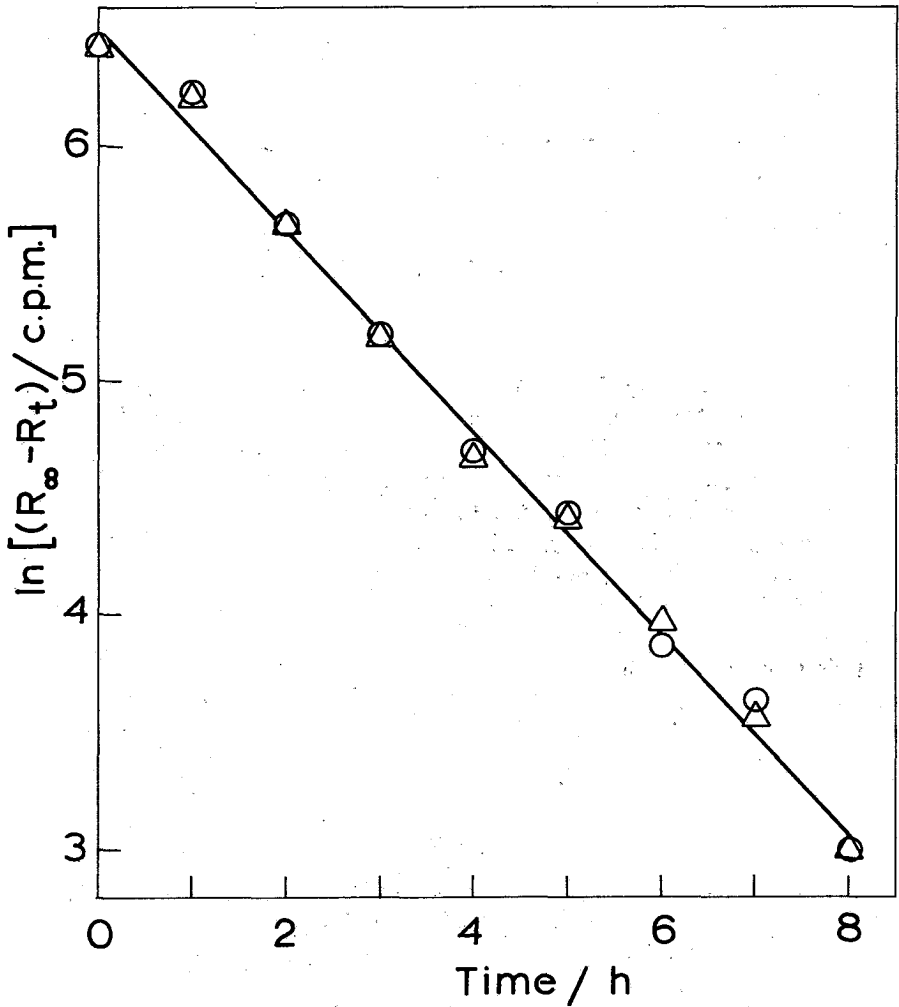


FIG. 3: Time-course of hybridization between RNA and DNA at 67°C, before and after self-annealing of RNA at the same temperature.

For details, see under 'Hybridization procedure' in Thomou & Katsanos<sup>1</sup>. Each kinetic run comprised samples maintained at  $67.0 \pm 0.05^\circ\text{C}$  for varying times and always with  $30 \mu\text{g}$  of  $^3\text{H}$ -labelled RNA in  $4\times\text{SSC}$ , pH 7.0 solution ( $250\text{mm}^3$ , specific activity  $540 \text{ c.p.m./}\mu\text{g}$  RNA). The RNA solution was either un-incubated (O), or pre-incubated ( $\Delta$ ) at  $67.0^\circ\text{C}$  for 18 h before being used in the hybridization run.

The data are presented as first-order plots,  $R_t$  representing the radioactivity (c.p.m.) of RNA bound to the filters as a hybrid with DNA at time  $t$ , and  $R_\infty$  being the equilibrium value of  $R_t$  (mean of four values obtained after 10, 12, 14 and 16 h and differing by only a few c.p.m.). This  $R_\infty$  value was 689 and 691 c.p.m. for un-incubated and pre-incubated RNA, respectively (counted with an efficiency of 20%).

Birnstiel *et al*<sup>6</sup> for their hybridization data with a variety of RNA species. For equal initial concentrations of DNA and RNA the linear dependence of  $1/\text{hybridization}$  on  $1/\text{time}$  follows directly from the relevant integrated second-order rate equation, but when the initial concentrations of DNA and RNA are different, another integrated second-order equation holds, which predicts a curved double reciprocal plot. However, Young & Paul<sup>7</sup> have shown that in this case the plot of  $1/\text{hybridization}$  against  $1/\text{time}$  has two asymptotes, one of which (for small values of time) has a linear double reciprocal form.

The time-course of the hybridization reaction in our case cannot be adequately described by double reciprocal plots, since such plots have a pronounced curvature. All our results conform to a first-order law (Fig. 3 and 4) and the deviation from this law is very small, as judged from the standard errors of the relevant linear regression coefficients. An easy explanation of this would be that we are dealing with a pseudo first-order process, since RNA in considerable excess compared to DNA was used, so that the RNA concentration did not change appreciably with time because of the hybridization. However, a pseudo first-order equation would have the initial RNA concentration incorporated into the apparent rate constant, thus predicting a linear relationship between these two variables. Our results do not bear out such a relationship, since kinetic experiments with different RNA concentrations give the same value for the apparent first-order rate constant, within the limits of experimental error (cf. results in Table I).

TABLE I. Values for the apparent rate constant ( $k_{app}$ ) at various temperatures and two RNA concentrations ( $c_{tot}$ ), calculated from first-order plots of the hybridization data. The errors given with the values of  $k_{app}$  are standard errors, calculated from regression analysis.

Temp./°C	$10^4 k_{app}/s^{-1}$	
	$c_{tot} = 112 \mu\text{g}\cdot\text{cm}^{-3}$	$c_{tot} = 56 \mu\text{g}\cdot\text{cm}^{-3}$
60	$1.03 \pm 0.02$	$1.18 \pm 0.04$
65	$1.08 \pm 0.01$	—
70	$1.05 \pm 0.03$	—
75	$1.07 \pm 0.03$	—
80	$1.03 \pm 0.03$	$1.13 \pm 0.02$

These two experimental findings, namely (a) the same time-course of the reaction with un-incubated and pre-incubated RNA solutions, and (b) the first-order kinetics with a rate constant non-dependent on RNA concentration, indicate that the mechanism of the DNA-RNA hybridization reaction is complex. Any mechanism being proposed must also take into consideration two additional facts: (c) the peculiar dependence of the reaction rate on temperature, which in some cases passes through a maximum<sup>4</sup> and in other cases remains constant with temperature (present results, Fig. 4 and Table I); (d) that the infinity values of the hybridization reaction should theoretically lead to the linear double reciprocal relation,  $1/\text{hybridization}$  against  $1/\text{RNA concentration}$ , or to other more refined equations<sup>1</sup> used to analyse equilibrium data.

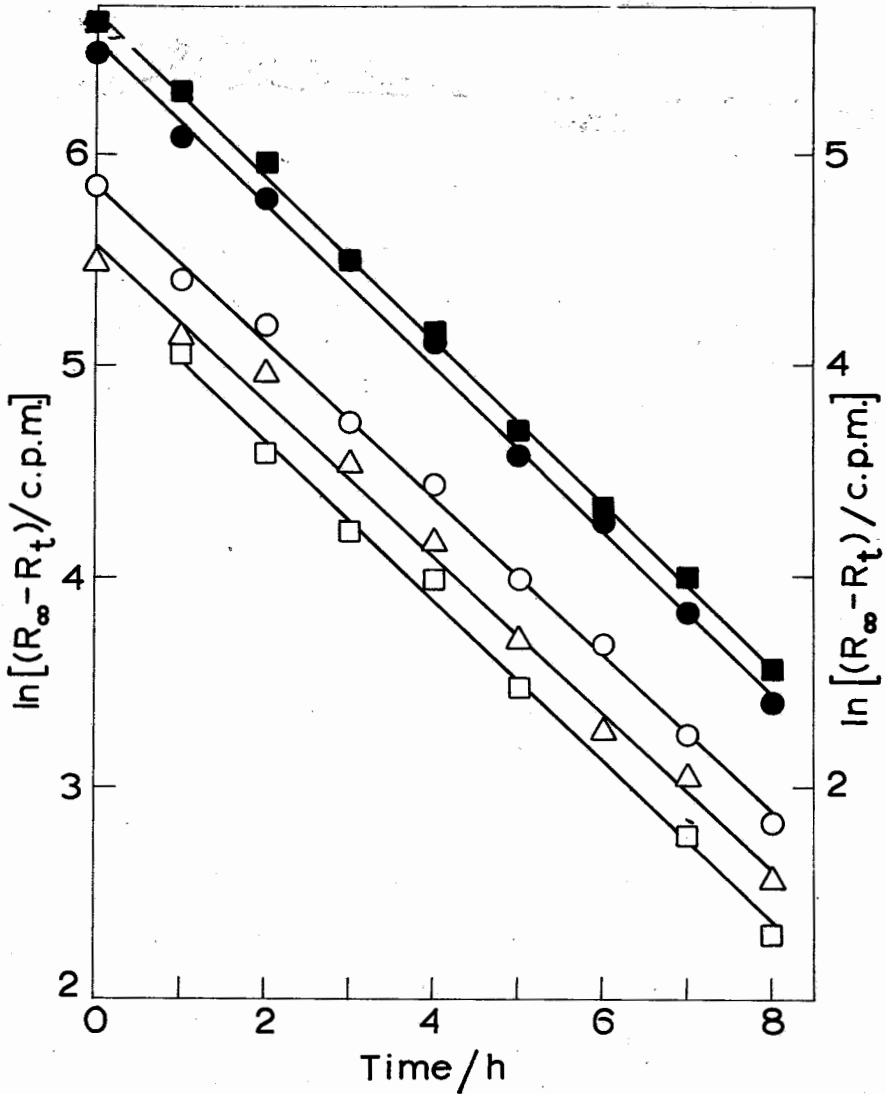


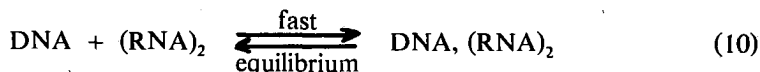
FIG. 4. First-order plots of hybridization data at various temperatures.

For details, see Thomou & Katsanos<sup>1</sup> under 'Hybridization procedure'. Each kinetic run comprised samples maintained at a stabilized temperature ( $\pm 0.05^\circ\text{C}$ ) for varying times (0 to 16h) and always with a 250 mm<sup>3</sup> solution containing 28  $\mu\text{g}$  of <sup>3</sup>H-labelled RNA in 4 $\times$ SSC pH 7.0 (250 c.p.m./ $\mu\text{g}$  RNA).  $R_t$  and  $R_\infty$  have the same meaning as in Fig. 3.

O, 60°C; ■, 65°C; □, 70°C ●, 75°C; Δ, 80°C. Empty symbols belong to left ordinate, and filled-in symbols to right ordinate.



We put forward the following mechanistic hypothesis and then show that it is consistent with all above (a) to (d) experimental facts: (+) RNA, (-) RNA or (+) RNA · (-) RNA [cf. eqn. (9)], which we denote by  $(\text{RNA})_2$ , forms a loose intermediate complex with single-stranded DNA, the bonds of this complex being sensitive to RNase, thus



This intermediate species transforms slowly with a rate constant  $k_3$  to the final hybrid, which is resistant to RNase:



We assume that the final formation of the hybrid is reversible, and so we write for the unimolecular decomposition of the hybrid



concluding the mechanism by associating the single-stranded RNA from eqn. (11) with that from eqn. (12) according to eqn. (8). A similar mechanism involving an unstable intermediate more sensitive to RNase than the final hybrid has been postulated by Spiegelman *et al*<sup>9</sup>. However, their intermediate differed from that proposed by us here in that it was formed between DNA and single-stranded RNA.

Instead of using initial rates, as is usually done in biochemical kinetics, we follow the general practice of classical kinetics, namely we derive from the proposed mechanism above [eqns. (10) - (12)] a theoretical rate equation which we integrate by using the approximation that the total RNA concentration,  $c_{\text{tot}}/\mu\text{g} \cdot \text{cm}^{-3}$  (annealed + non-annealed) remains constant at all times, because of the very small fraction of RNA becoming hybridized (it never exceeded 5.3% at equilibrium). The integrated theoretical rate equation is then compared to experimental data. We feel that this procedure is preferable, since it describes the kinetics of the process over a large fraction of the whole reaction period and not only over a small initial fraction of time when the reaction is far removed from equilibrium.

Let  $\theta_i$  be the fraction of reactive sites in DNA which are in the form of intermediate complex  $\text{DNA}, (\text{RNA})_2$  at time  $t$ , and  $\theta_f$  the respective fraction in the form of the final hybrid  $\text{DNA} \cdot \text{RNA}$ . Then, equilibrium (10) is described by the equation

$$K \simeq \frac{\theta_i}{(1 - \theta_i - \theta_f) c_{\text{tot}}} \quad (13)$$

with the approximation previously mentioned for  $c_{\text{tot}}$  and assuming that the equilibrium constant is about the same for both (+) RNA, (-) RNA and (+) RNA · (-) RNA.

The rate of formation of the final hybrid is calculated from eqns. (11) and (12) as

$$\frac{d\theta_t}{dt} = k_3\theta_i - k_4\theta_t$$

or, substituting  $\theta_i$  from eqn. (13) and rearranging,

$$\frac{d\theta_t}{dt} + (k' + k_4)\theta_t = k' \quad (14)$$

where

$$k' = k_3 \cdot \frac{Kc_{\text{tot}}}{1 + Kc_{\text{tot}}} \quad (15)$$

Eqn. (14) has the same form as eqn. (2) with a similar solution:

$$\theta_t = \frac{k'}{k' + k_4} + \left(\theta_0 - \frac{k'}{k' + k_4}\right) \cdot \exp[-(k' + k_4)t] \quad (16)$$

Thus, the equilibrium value of the hybrid is

$$\theta_{\infty} = \frac{k'}{k' + k_4} \quad (17)$$

and the time-course of the reaction is described by a first-order law which in linear form is

$$\ln(\theta_{\infty} - \theta_t) = \ln(\theta_{\infty} - \theta_0) - (k' + k_4)t \quad (18)$$

The experimentally measured quantity is the radioactivity  $R_t$  / c.p.m. bound to the filter after an incubation time  $t$ , and if  $R_m$  / c.p.m. is the maximum radioactivity which would be attached to the filter if all reactive sites were blocked, we can set  $\theta_t = R_t / R_m$ . Substituting this relation for  $\theta$  in eqn. (18) one obtains

$$\ln(R_{\infty} - R_t) = \ln(R_{\infty} - R_0) - (k' + k_4)t \quad (19)$$

This typical first-order equation coincides with that used to plot the hybridization data in Figs. 3 and 4. The new element in eqn. (19), however, is that it discloses the physical meaning of the apparent rate constant, which is equal to  $k' + k_4$  or, using eqn. (15),

$$k_{app} = k_3 \left( \frac{Kc_{tot}}{1 + Kc_{tot}} \right) + k_4 \quad (20)$$

The integrated theoretical rate equation (18), or its equivalent eqn. (19), with the auxiliary definitions [eqns. (15), (17) and (20)] can explain all experimental facts previously listed under (a) to (d). Thus, the same time-course of the reaction with un-incubated and pre-incubated RNA is a consequence of the assumption that  $K$  and  $k_3$  have approximately the same values for both forms of  $(RNA)_2$ . This is not an unreasonable assumption if we admit that  $(RNA)_2$  is bound to DNA in the complex by physical forces or by a few hydrogen bonds between complementary bases not already involved in bonding the two complementary RNA strands. The first-order kinetics has already been explained by the form of eqn. (19), and the non-dependence of  $k_{app}$  on RNA concentration can be due to the fact that this is a composite rate constant as eqn. (20) indicates. It may be that  $Kc_{tot}$  has a large value so that unity can be neglected compared with it in the denominator. Under this condition  $k_{app} \approx k_3 + k_4$ , an expression independent of  $c_{tot}$ . Alternatively,  $k_4$  may be much larger than the whole first term in eqn. (20), so that it predominates.

We come now to the dependence of the reaction rate on temperature. Equilibrium (10) is expected to be exothermic, because it is an association reaction. The equilibrium constant  $K$  of such a reaction will decrease as temperature increases and so the expression in parentheses ( ) in eqn. (20) will decrease with increasing temperature. The rate constants  $k_3$  and  $k_4$  on the other hand always increase with temperature, although this increase may be very small if the activation energy is small. Thus  $k_{app}$  is a combination of physical constants some of which decrease while others increase with increasing temperature, and this could result in the behaviour of the rate reported by Nygaard & Hall<sup>4</sup>, passing through a maximum with increasing temperature. As to our results being virtually independent of temperature, this could be due to a predominating value of  $k_4$  which probably changes little with temperature. Lastly, the  $\theta_\infty$  value as given by eqn. (17) leads to the expected double reciprocal relation between hybridization and RNA concentration. Setting  $\theta_\infty = x/x_m$ , where  $x$  is the amount of RNA hybridized at equilibrium and  $x_m$  the maximum amount of RNA hybridized with a given amount of DNA, and substituting this relation for  $\theta_\infty$  in eqn. (17), we obtain after inversion and rearrangement

$$\frac{1}{x} = \left( 1 + \frac{k_4}{k_3} \right) \cdot \frac{1}{x_m} + \frac{k_4}{k_3} \cdot \frac{1}{Kx_m} \cdot \frac{1}{c_{tot}} \quad (21)$$

Other more exact forms of this equation are easily obtained, e.g. by multiplying throughout with  $c_{tot}$  and correcting the RNA concentration by subtracting from it  $x/V$ ,  $V$  being the volume of the solution, an equation is obtained having the same form with eqn. (11) in the paper of Thomou & Katsanos<sup>1</sup>. It is to be noted, however, that in all these equations the slope and the intercept have a slightly different meaning than usually ascribed to them, since they are now multiplied by  $k_4/k_3$  or by  $1 + k_4/k_3$ .

The results reported here are somehow at variance with those on hybridization kinetics reported by others, but this is almost certainly due to the different origin of the DNA and/or RNA used, and also to the different conditions of experimentation. As examples, we mention the work of Bishop<sup>5</sup> who used DNA from bacteriophages T4 and  $\lambda$ , denatured by alkali in  $6\times SSC$ , and the work of Birnstiel *et al*<sup>6</sup> who used a high concentration (50% or more) of formamide in their hybridization media.

As to the intermediate complex between DNA and  $(RNA)_2$  postulated in eqn. (10) and forming the basis for the proposed hybridization mechanism, one can reinforce this idea by referring to the isolation of complexes formed between eukariotic DNA and RNA which are sensitive to RNase<sup>9</sup>.

One final worth mentioning observation is that the DNA - RNA rate constants of the hybridization reaction are not significantly different from the rate constant of the RNA - RNA self-annealing reaction. A similar observation has been reported by Bishop<sup>5</sup>, and an analogous similarity in rates between DNA - RNA hybridization and DNA - DNA renaturation by Nygaard and Hall<sup>4</sup>. All these rate equalities are probably due to the fact that the same type of bonds are formed or broken in the rate determining steps of the above reactions.

## Περίληψη

*Κινητική τής αντίδρασης ύβριδισμού τού Δεσοξυριβονουκλεϊνικού οξέος με τού ριβονουκλεϊνικό οξύ με σύγχρονη αυτο-σύνδεση τού ριβονουκλεϊνικού οξέος*

Έμελετήθη ή κινητική τής αυτο-συνδέσεως τού RNA σε διαλύματα, καθώς και ή κινητική τού ύβριδισμού τού DNA με τού RNA παραλλήλως πρὸς τήν αντίδραση αυτο-συνδέσεως τού RNA. Καί οί δύο αντίδρασεις ακολουθοῦν ἀπλό κινητικό νόμο πρώτης τάξεως, με τήν αὐτή φαινόμενη σταθερά ταχύτητος, ή ὅποια δέν ἐξαρτᾶται οὔτε ἀπό τήν θερμοκρασία, οὔτε ἀπό τήν συγκέντρωση τού RNA. Τό μονόκλωνο DNA ἔχει τήν αὐτή κινητική συμπεριφορά ἔναντι τού δικλῶνου καί τού μονοκλῶνου συμπληρωματικού RNA.

Προτείνονται λεπτομερεῖς μηχανισμοί καί γιά τις δύο ἀνωτέρω ἀντιδράσεις, ἀπό τούς ὁποίους ἐξάγονται ὀλοκληρωμένες θεωρητικές ἐξισώσεις ταχύτητος, πού συμβιβάζονται με τὰ πειραματικά εδρήματα. Οί μηχανισμοί αὐτοί στηρίζονται στόν σχηματισμό ἀσθενῶν συμπλόκων, εὐαισθηστων στήν RNάση, πού σχηματίζονται μεταξύ συμπληρωματικῶν ἀλύσσεων RNA, καθώς καί μεταξύ DNA καί  $(RNA)_2$ .

Περαιτέρω, δείχνεται ότι οι τιμές ισορροπίας της αντίδρασης ύβριδισμού οδηγούν θεωρητικώς στην γνωστή διπλώς αντίστροφη σχέση μεταξύ βαθμού ύβριδισμού και συγκεντρώσεως του RNA.

### References

1. Thomou, H. and Katsanos, N.A.: *Biochem. J.* **153**, 241 (1976).
2. Geiduschek, E.P., Moohr, J.W. and Weiss, S.B.: *Proc. Natl. Acad. Sci. U.S.A.* **48**, 1078 (1962).
3. Davidson, J.N.: *The Biochemistry of Nucleic Acids*, (7th edition), p. 301, Chapman and Hall, London (1972).
4. Nygaard, A.P. and Hall, B.D.: *J. Mol. Biol.* **9**, 125 (1964).
5. Bishop, J.O.: *Biochem. J.* **113**, 805 (1969).
6. Birnstiel, M.L., Sells, B.H. and Purdom, I.F.: *J. Mol. Biol.* **63**, 21 (1972).
7. Young, B.D. and Paul, J.: *Biochem. J.* **135**, 573 (1973).
8. Spiegelman, G.B., Haber, J.E. and Halvorson, H.O.: *Biochemistry* **12**, 1234 (1973).
9. Kang, C.-Y. and Temin, H.M.: *Nature New Biology* **242**, 206 (1973).
10. Loening, U.E.: *Biochem. J.* **102**, 251 (1967).

### Acknowledgment

The authors acknowledge the assistance of Mrs. Margaret Barkoula.

## **A MODIFICATION OF THE A.O.A.C. DRYING OVEN METHOD FOR TOTAL SOLIDS DETERMINATION IN MILK AND MILK PRODUCTS**

JOHN D. EFSTATHIOU,

*Product Process Development, General Mills, Inc. Mpls, MN 55427 U.S.A.*

### **Summary**

Milk, fortified milk, and a number of other dairy products were analyzed for total solids content by using a modification of the A.O.A.C. drying oven technique. The products were also analyzed by using the Mojonnier and Apollo Microwave Oven methods. The modified drying oven method was evaluated and compared to the other two methods as to accuracy, testing time required and cost. It was found that the new method was more accurate and consistent than the Apollo, comparable in accuracy ( $\pm 0.05\%$ ) to the Mojonnier, and less expensive and time consuming than both reference methods.

*Key words: Vacuum Oven, Mojonnier, Apollo Microwave Oven.*

### **Introduction**

The commonly used procedures for determining the total solids (T.S.) of milk and milk products may be classified as either indirect or direct methods. The indirect methods depend upon the principle that there is a general parallelism between the solids-not-fat (S.N.F.) and the fat content of milk and in some cases the specific gravity of the milk. The direct methods on the other hand involve the principle of evaporating the moisture from a weighed sample of milk and re-weighing the residue.

The indirect methods generally have the advantages of speed, ease of operation and low cost, but tend to vary in precision and are necessarily limited to fluid products. The direct methods have the advantages of accuracy and applicability to solid as well as fluid products, but are generally higher in cost and more time consuming. The official A.O.A.C. (Association of Official Agricultural Chemists) method<sup>1</sup> for example requires an excess of three hours to determine the solids content of a dairy product.

The most widely accepted method for total solids determination of milk and milk products is that of the Mojonnier. However, due to high cost of the necessary equipment, frequently this method is not available and applicable in milk plant laboratories. In most cases, a simple microwave oven with an

analytical scale are being used. The Apollo Moisture Tester employs infrared heat to evaporate the moisture, and further simplifies the procedure by automatically registering the moisture lost from a sample of known weight. This method is simple but expensive and not that accurate and consistent as the Mojonnier.

We attempted to develop a method for T.S, determination of milk and milk products that is accurate, simple, fast and inexpensive.

### Materials and Methods

**Samples:** Milk, milk solids not-fat (M.S.N.F.) fortified lowfat milk, butter-milk, yogurt, ice cream, soft serve ice cream and ice milk shake were used in this study.

**Methods:** Samples were divided in three subsamples and analyzed in triplicate by Mojonnier as described in the Laboratory Manual of the Milk Industry Foundation<sup>2</sup>, and the Apollo Microwave Oven Method following manufactures' instructions<sup>3</sup>.

The modified A.O.A.C. Drying Oven Total Solids Determination Method employs the same principles as the Mojonnier method. The samples were mixed thoroughly by pouring several times from one vessel to another. A one gram sample was weighed accurately to the fourth decimal place into an aluminum foil solids dish that had been previously heated in a vacuum oven at 212°F (100°C) under 25 psi vacuum and subsequently cooled in a dessicator and weighed. The weight of the dish plus the sample (sample must be cool or evaporation will prohibit accurate weighing) and the weight of the dish were recorded. One milliliter (ml) of distilled water from an automatic burette was added and the mixture of sample and water were spread evenly over the bottom of the dish by gently tilting it with a tong. The dish was placed on a hot plate at 356°F (180°C) and heated until all visible moisture was driven off and the residue began to turn light brown. Occasionally, a tong was used to press the dish gently against the hot plate to insure uniform evaporation. The dish was transferred to a vacuum oven at 212°F (100°C) for 10 minutes at 25 psi vacuum. At the end of this period the dish was transferred into a cooling dessicator for 1 min. and then weighed to fourth decimal place. The percent total solids were calculated using the formula:

$$\% \text{ Total Solids} = \text{weight of solids} / \text{weight of sample} \times 100$$

### Results and discussion

Twenty eight samples of milk solids not-fat fortified milk, butter milk, yogurt, ice cream, soft serve ice cream and ice milk shake mixes were analyzed for T.S. content in triplicate by using the Mojonnier, Apollo Microwave Oven and Modified A.O.A.C. Drying Oven methods.

Table I presents the mean total solids content of these products who were grouped in three categories according to their T.S. content, in order to reduce large statistical error due to sampling. Data were statistically analyzed by using

Mojonnier readings as independent variable (x) and Vacuum Oven or Apollo Microwave Oven determinations as dependent variables (y).

TABLE I. Total Solids Content Determinations by Mojonnier, Modified Vacuum Oven and Apollo Microwave Oven Methods.

Sample	Mean % Total Solids		
	Mojonnier	Vacuum Oven	Apollo
Group 1			
1	11.100	10.920	10.990
2	11.480	12.440	11.640
3	11.445	11.620	11.275
4	11.890	11.870	11.300
5	11.705	12.115	11.640
6	12.370	12.380	12.100
7	11.415	11.430	12.155
8	11.525	11.550	12.140
9	15.750	15.710	15.870
Group 2			
10	19.705	19.725	18.460
11	24.155	24.165	24.990
12	24.950	24.770	25.400
13	28.390	27.200	26.785
14	26.215	25.510	24.755
15	26.680	26.375	25.530
16	21.185	20.895	20.390
17	24.750	24.980	23.320
18	26.500	26.780	27.150
Group 3			
19	36.560	37.050	37.405
20	37.750	36.165	35.700
21	40.370	40.475	37.385
22	37.790	37.860	38.275
23	34.520	33.270	32.050
24	33.625	33.570	32.675
25	30.335	30.255	31.840
26	34.820	33.325	33.275
27	31.550	31.990	32.450
28	36.550	37.090	37.700

Correlation coefficient between the Mojonnier and Apollo methods was 95.81% as compared to 97.02% for Mojonnier vs Vacuum Oven (Table II) for the first group of products. As the total solids content of the products increased the correlation coefficient between Mojonnier and Vacuum Oven remained stable, 98.67% and 96.35% for groups two and three respectively (Table II). For the same groups however, the correlation coefficient between



Mojonnier and Apollo was reduced as the total solids content increased, 93.97% and 83.57% for groups two and three respectively.

TABLE II. *Statistical Analysis*

Group No.	Method	$\bar{x}$	$\bar{y}$	S.D.	Variance	Correlation Co-efficient
Group 1	Mojonnier	12.22		1.42	1.80	
	Vacuum Oven		12.07	1.39	1.72	.9702
	Apollo		12.12	1.46	1.91	.9581
Group 2	Mojonnier	24.72		2.75	6.74	
	Vacuum Oven		24.48	2.57	5.91	.9867
	Apollo		24.08	2.90	7.51	.9397
Group 3	Mojonnier	35.38		3.04	8.33	
	Vacuum Oven		35.10	3.11	8.73	.9635
	Apollo		34.87	9.65	6.33	.8357

In addition, statistical analysis of the triplicate readings for each method (data not shown) produced correlation coefficients of 99.2% between Mojonnier readings, 99.05% for Vacuum Oven and 96.5% for Apollo determinations.

Data presented here show that the Vacuum Oven method for T.S. determination of dairy products is more accurate than the Apollo Microwave Oven method and compatible to the Mojonnier.

Considering the fact that up to twelve samples can be analyzed simultaneously within 30 minutes for complete results as compared to one sample every 15 minutes for the Apollo it makes the method more applicable for routine testing in a quality control laboratory.

Initial investment for the system is approximately, \$1,500 as compared to \$7,000 for the Apollo and \$12,000 for a Mojonnier.

Overall, we feel that the method is accurate enough, fast and inexpensive to lend readily itself to both large and especially small quality control laboratories.

### Περίληψη

*Προσδιορισμός του ξηρού υπολείματος γάλακτος και προϊόντων γάλακτος δια παραλλαγής της επίσημου Α.Ο.Α.Σ. μεθόδου*

Το ξηρό υπόλειμμα γάλακτος και προϊόντων γάλακτος προσδιορίστη δια των μεθόδων Mojonnier και Apollo Microwave Oven<sup>2,3</sup>, καθώς και παραλλαγής της επίσημου μεθόδου της Association of Official Agricultural Chemists (A.O.A.C.).

Ἡ νέα μέθοδος βασίζεται εἰς τὴν γρήγορη ἐξάτμιση τοῦ μεγαλύτερου ποσοστοῦ ὕδατος εἰς τὸ προϊόν ἐπὶ θερμαινομένης πλακῶς (180°C). Τὸ δείγμα κατόπιν μεταφέρεται εἰς κλίβανον θερμοκρασίας 100°C ὑπὸ ἀρνητικὴν πίεσιν (25 psi) ἐπὶ 10' ὅπου τὸ ὕδωρ ἐξατμίζεται πλήρως.

Ἡ μέθοδος εἶναι ἀκριβῆς (συχνότητα εὐθυγράμμου συμμεταβολῆς με Mojonnier 96,35 - 98,67%), ἀπλῆ, γρήγορη (15') καὶ τὸ κόστος τῶν ἀπαιτουμένων ὀργάνων πολὺ μικρότερο (20%) αὐτοῦ τῶν δύο ἄλλων μεθόδων.

---

### References

1. Official Methods of Analysis of the Association of Official Agricultural Chemists, 12th Ed. Washington, D.C., Par. 16.032, p. 256, 1975.
2. Laboratory Manual: Methods of Analysis of Milk and its Products, 3rd Ed., Milk Industry Foundation, Washington, D.C., Ch. 17, p. 283, 1959.
3. Operation Manual for Apollo Microwave Laboratory, Apollo Microwave Products Co, Crystal Lake, Illinois, 1977.

## THE REMOVAL OF ORGANIC ENTRAINMENT IN COPPER SOLVENT EXTRACTION BY FLOTATION

KOSTAS A. MATIS

Mitropoleos 60, Thessalonika, Greece

### Summary

Advance electrolytes entraining organic droplets have been shown to deposit poor quality copper. Additionally, the high cost of solvents makes necessary to remove the organic entrainment. The flotation process was studied in this paper as a means of separating the organic entrainment, before the electrolyte is entering the tankhouse. Two techniques were tested, dispersed-air and electrolytic flotation. Preliminary experimental results were found very promising.

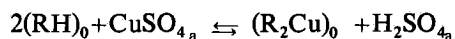
**Key Words:** Advance electrolytes, organic entrainment, solvent extraction, dispersed-air flotation, electroflotation.

### Introduction

Solvent extraction is a well established process in hydrometallurgy. Twenty years ago this unit process was relatively unknown and restricted in application to the nuclear field and to some less common metals. The process was considered expensive and unlikely to be of general interest without the development of cheap extractants, available for commercial use. Nowadays, however, solvent extraction is one of the most important processes in hydrometallurgy for separation, purification and concentration of metal ions.

The most important solvent extraction reagent development in the field has been that of the copper extractants. The incentive for this development was the ability to extract copper from dump leach liquors, mine waters etc. and final production of high grade cathode copper, thus avoiding the traditional cementation process (1). The development of hydroxyoxime LIX reagents by Henkel Corporation (formerly General Mills Inc.) is now history as is the successful commercial applications which followed. This success has led to the entrance of other companies on the scene.

Solvent extraction of copper follows a reaction of the form:



where the subscript shows the aqueous or organic phase. When the arrow is to the right the reaction represents the loading part of the process, and when it is to the left, the stripping part. Figure I shows a flowsheet of the process. Each of the above mentioned parts is generally accomplished in more than one stages, while in each stage there is a mixer and a settler.

In extraction processes it is necessary to minimize droplet entrainment in the bulk phases from the settling zone. A way to prevent the problem of organic entrainment is by controlling the conditions in the mixing zone and the axial velocity through the settler. This paper deals with the problem after it occurs.

In a recent work (2) solvent extraction was proposed for the recovery of copper concentrated in incinerated municipal sewage sludge. However, the costs estimation in this field of metal recovery from effluents was not attractive, as it was found that the solvent loss in the raffinate represented a figure greater than the gain in copper recovered (3).

This perhaps can not be valid for a leach solution rich in copper, but due to the relatively high cost of the solvent, efficient coalescence devices are necessary to reduce the organic loss. A relatively issue is also the environmental effects of the reagents loss, which was discussed in reference (4).

Additionally, it has been observed (5) that cathodes electrowon from electrolytes containing organic entrainment exhibit a brown material, deposited usually at the air/electrolyte interface, and referred to as organic burn.

The problem was contained by methods as centrifugation, and filter coalescers (as coke beds) after large storage vessels, the latter being used for the release of gross entrainment. However, centrifugation is a rather expensive technique, and settlers have usually a small throughput per unit volume. A literature survey showed that flotation has not attracted considerable attention for this purpose on a commercial scale (6), (7). In the references mentioned very few details were reported.

Flotation is known from the field of mineral processing, where various minerals are separated from the undesirable portion of an ore. In recent years, the process has been applied also in effluent treatment (8).

In the laboratory study two techniques of bubbles generation were tried. In the first case, the electrolytic flotation was tested, where fine bubbles of hydrogen and oxygen are formed by electrolysis. While in the second, bubbles were formed by forcing air through porous media (dispersed-air flotation). Dissolved-air flotation, which is the dominant flotation method in wastes treatment, was not tried as it was believed that it offers disadvantages for this application.

### Experimental Work

In the experiments that were undertaken a single mixer-settler was used to generate the entrainment (called also haze). This was perspex, having a mixer chamber with dimensions 80 mm wide, 80 mm deep and 75 mm long, and a

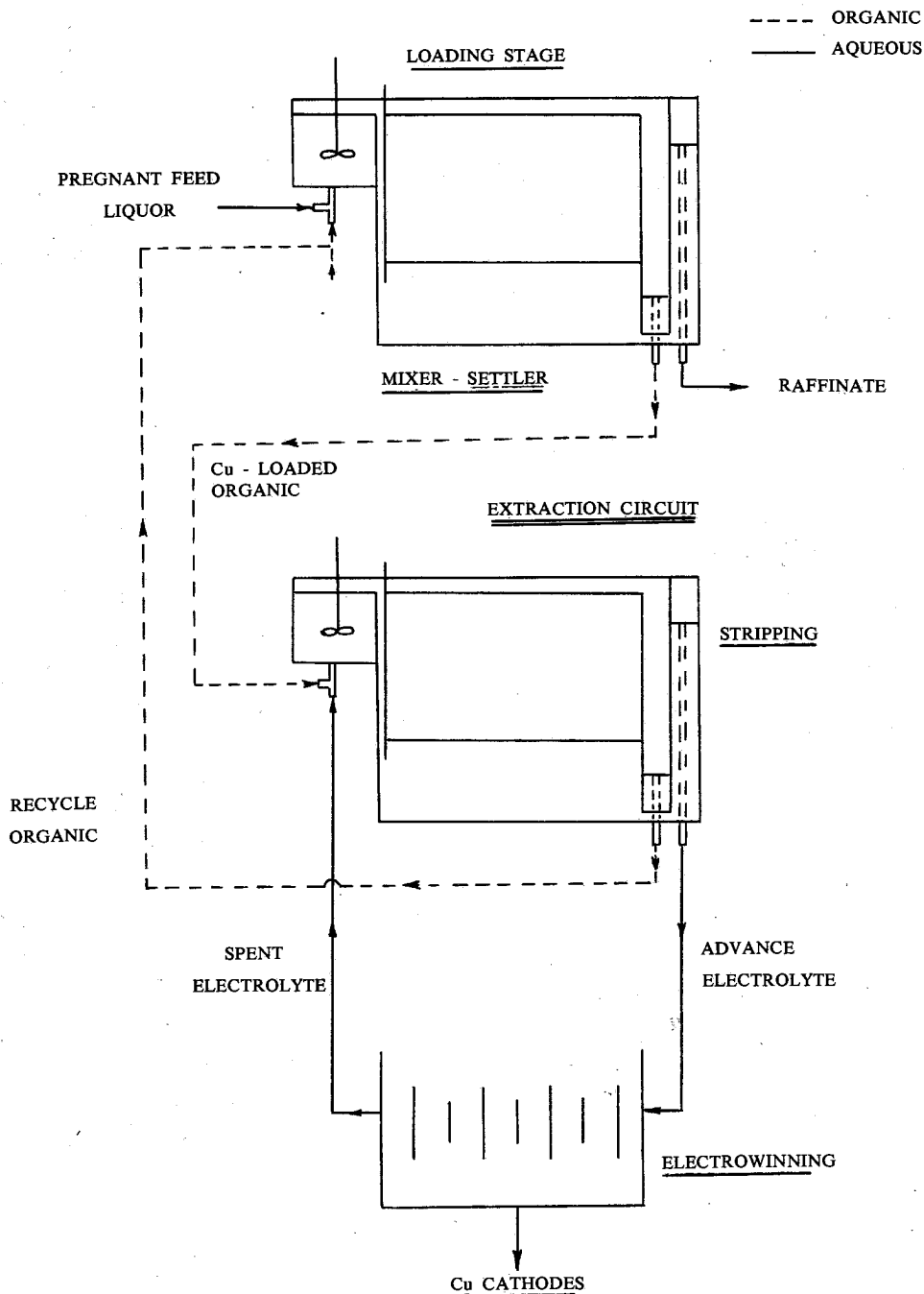


FIG. 1. Schema of copper solvent extraction.

settler chamber 80 mm wide, 280 mm deep and 255 mm long. It was a miniature of a commercial one (see the figure).

The aqueous phase was a solution containing 30 kg/m<sup>3</sup> copper as copper sulphate and 150 kg/m<sup>3</sup> sulphuric acid. The organic phase was 40% v/v LIX 65N in Escaid 100 loaded to about 6 kg/m<sup>3</sup> copper. LIX 65N is an aromatic hydroxyoxime that exhibits slow kinetics of extraction (9).

A double shrouded, radial flow, flat blade impeller was used, and the stirrer tip speed was approximately 3 m/s. The mixing retention time was 180 w; the organic phase was continuous, and the organic/aqueous ratio was 2:1. The dispersion discharging from the mixer chamber flowed into the settler down and adjustable vertical baffle. While, the organic was flowing from the settler over a weir.

Analysis for the organic concentration was done in a Grating Infrared Spectrophotometer. The idea was to scan the carbon-hydrogen stretch peak in at 2930 cm<sup>-1</sup>. The samples were initially extracted with trifluoro-trichloroethane, which was the reference liquid.

The flotation tests (dispersed-air) were carried out batchwise in a perspex tank, 1 m tall and with internal diameter of 146 mm. The sampling point was near the base plate, which was flanged and removable. In the electrolytic flotation tests a set of two horizontal and parallel electrodes was fitted near the bottom of a 0.9 m high column, having an internal diameter of 95.2 mm (in this case only). A stainless steel grid, with a wire diameter of 0.92 mm, was the anode and a graphite plate was the cathode. The applied current density was 300 A/m<sup>2</sup> and the cell voltage was 1.7 V. A concentration reduction from 150 to 32ppm was effected after two hours. In Figure 2 the change of organic concentration with time is shown.

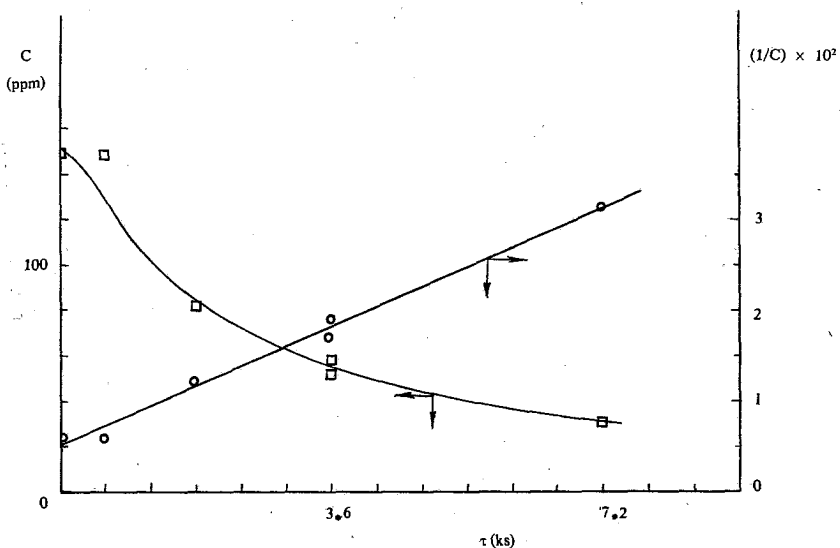
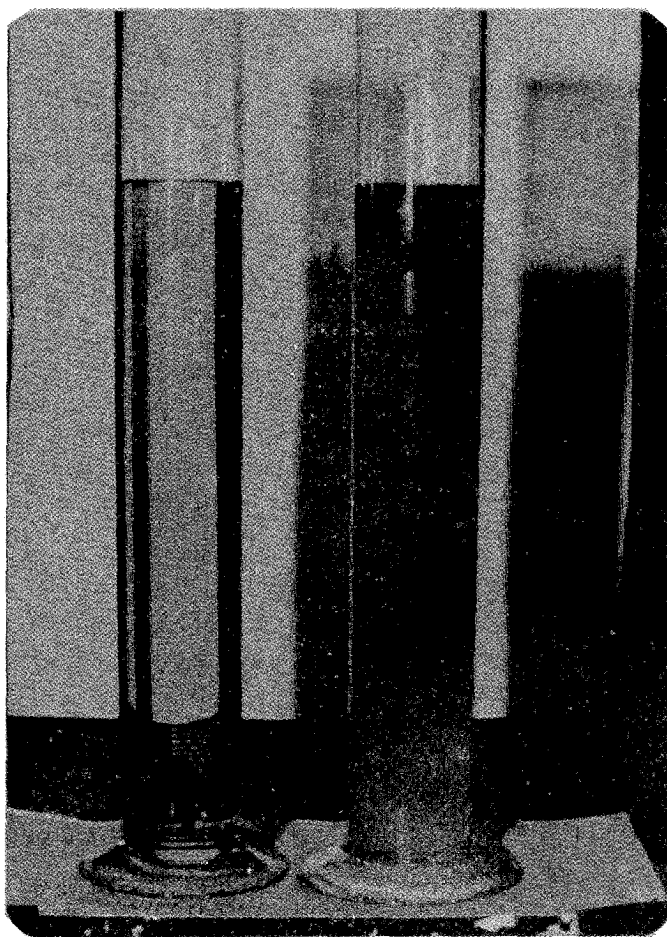


FIG. 2. Changes of concentration with time during electroflotation.

Preliminary considerations on the kinetics are also shown in the figure. The second-order equation was found in agreement with the data. This, if established, could be a useful tool in process design. The electrolytic interference in the process can be overcome by electrodes separated by a membrane (10).

For comparison reasons, a study of the stability of the dispersion and the effect of time on it was carried out in a two liter cylinder. A solution generated by extraction and having an organic concentration of 268 ppm was left to rest. After 54 ks, a sample from the top gave a concentration of 91 ppm, which means that 66% settled.

In dispersed-air flotation tests a compressor and a porous dome, made from carborundum, were used; the latter having porosity 150-250  $\mu\text{m}$ , and dimensions 98 mm diameter, 89 mm height and 16 mm wall thickness. The air flow



Photograph. Aqueous extraction effluent before (on the right) and after (on the left) flotation.

during the experiments was  $2.58 \times 10^4 \text{ m}^3/\text{s}$ , and the excess air pressure, under the porous plate, was around 80 mm Hg. These were variables established earlier when treatment of paint dilutions was undertaken (8).

The tests gave a concentration reduction of 97.4% with a retention time of approximately 300 s, as the organic concentration was found to change from 233 ppm initially to 6 ppm. The results are really promising. The photograph shows two samples before and after treatment. The advantage of dispersed-air flotation is that it does not interfere with electrowinning, and offers a simple way for the removal of the organic entrainment. The work has been continued (11).

### Περίληψη

*Ο άποχωρισμός τής οργανικής συγκράτησης στη διαλυτική εκχύλιση του Χαλκού με επίπλευση*

Η διαλυτική εκχύλιση είναι σήμερα μιá από τις πιό σπουδαίες μεθόδους διεργασίας στην ύδρομεταλλουργία για τó διαχωρισμό, καθαρισμό και συγκέντρωση τών μεταλλικών ιόντων. Ίδιαίτερη πρόοδος έγινε στην έξαγωγή του χαλκού, με τελικό άποτέλεσμα τήν παραγωγή καθόδων χαλκού ψηλού βαθμού καθαρότητας, που έπιτεύχθηκε με τή βελτίωση στόν τομέα τών διαλυτικών και εύρεια χρησιμοποίηση σε έμπορικé κλίμακα.

Ένα πρόβλημα που παρουσιάζεται στη μέθοδο είναι ή συγκράτηση οργανικής φάσης που συνεπάγεται μιá οικονομική επιβάρυνση λόγω του κόστους τών διαλυτικών, κι επίσης παραγωγή καθόδων μικρότερης καθαρότητας. Η επίπλευση έχει δοκιμασθεί σαν λύση σε προκαταρκτικά πειράματα, που όμως έδωσαν πολú θετικά άποτελέσματα. Δύο μέθοδοι επίπλευσης χρησιμοποιήθηκαν: ή επίπλευση με διασκορπισμένο άερα και ή ήλεκτρολυτική επίπλευση.

### References

1. Flett D.S.: «Solvent extraction in hydrometallurgy», Chem. & Ind. 706 (1977).
2. Jowett A. et al.: «Recovery of metal values from an incinerated municipal sewage sludge», in «The Application of Chemical Engineering to the Treatment of Sewage and Industrial Liquid Effluents», I. Ch. E. Symp., Univ. York, Apr. 16-17, Series No. 41, (1975).
3. Fletcher A.W.: «Metal recovery from effluents - Some recent developments», *ibid*, p. TI.
4. Ritchey G.M. et al.: «Some comment on the loss and environmental effects of solvent extraction reagents used in metallurgical processing», Proc. Int. Solv. Extr. Conf. 74, p. 2873, Lyon. Sept. 8-14, (1974).
5. Eggett G. and Hopkins W.R.: «The solving of problems associated with copper recovery from solvent extraction produced electrolytes», in «Interaction between Solvent Extraction and Electrochemical Technology», S.C.I. Symp. London, Nov. 24 (1975).
6. Merifold R.C. and Jensen W.H.: «The separation and recovery of Ni and Cu from a laterire-ammonia leach solution by liquid ion exchange», Proc. ISEC '74, p. 1231.



7. Ettel V.A. et. al: «Solvent extraction of base metals using in sith neutralization with lime» Proc. ISEC '77, Sept. 9-16, Toronto.
8. Matis K.A.: «A Study of Flotation Techniques in Effluent Treatment», M. Sc. Thesis, Chem. Eng., Univ. Newcastle (1975).
9. Christie P.G. et al: «The liquid-liquid extraction of copper (II) and iron (III) from chloride solutions using Lix 64N in kerosene», Proc. ISEC '74, p. 685.
10. Matis K.A.: «Treatment of industrial liquid wastes by electroflotation», Water Pollut. Control, to be published.
11. Amigo P.A.: Ph D. Thesis (under completion), Chem. Eng., Univ. Newcastle.

## ETUDE DE CATALYSEURS $\text{Co}/\text{Al}_2\text{O}_3$ ET $\text{CoMo}/\text{Al}_2\text{O}_3$ PAR SPECTROSCOPIE DE PHOTOELECTRONS, REFLEXION DIFFUSE ET MICROSCOPIE ANALYTIQUE

P. CAJARDO, A. LYCOURGHOTIS\*, F. DELANAY, P. GRANGE, B. DELMON

*Groupe de Physico-Chimie Minerale et de Catalyse*

*Universite Catholique de Louvain*

*Place Croix du Sud, 1*

*1348 Louvain-la Neuve*

*Belgique*

### Resume

L'emploi complémentaire de la spectroscopie de photoélectron (X.P.S.), réflexion diffuse (D.R.S.) et de la microscopie électronique (AEM) permet d'identifier la nature et l'état de dispersion de phase active dans deux précurseurs de catalyseurs d'hydrodésulfuration [ $\text{Co}/\text{Al}_2\text{O}_3$ ,  $\text{CoMo}/\text{Al}_2\text{O}_3$ ].

D.R.S. confirme la présence de Mo (VI) en symétrie tétraédrique et octaédrique, la présence de  $\text{CoAl}_2\text{O}_4$  dans le système  $\text{CoMo}/\text{Al}_2\text{O}_3$  et son absence dans le système  $\text{Co}/\text{Al}_2\text{O}_3$ . La formation de l'oxyde de cobalt,  $\text{Co}_3\text{O}_4$ , a été détecté dans ce dernier.

La présence de  $\text{CoAl}_2\text{O}_4$ , un composé non désirable dans le catalyseur d'hydrodésulfuration, semble liée à l'état de dispersion du cobalt.

**Key Words:** hydrodesulfurization catalysts, X.P.S., D.R.S. AEM

### 1. Introduction

Deux catalyseurs  $\text{Co}/\text{Al}_2\text{O}_3$  (Al-1,00) et  $\text{CoMo}/\text{Al}_2\text{O}_3$  (Al-0,35) ont été étudiés par spectroscopie d'électron, réflexion diffuse et microscopie électronique. Les facteurs 1,00 et 0,35 correspondent à la composition atomique  $r = \text{Co}/(\text{Co}+\text{Mo})$  de ces catalyseurs. Une attention particulière a été portée sur l'étude du cobalt.

### 2. Methodes Experimentals

#### 2.1. Préparation des catalyseurs

L'alumine ( $\gamma/\text{Ketjen}$ ) utilisée comme support a une surface spécifique de  $160 \text{ m}^2 \text{ g}^{-1}$  et un volume poreux de  $0,46 \text{ cm}^3 \text{ g}^{-1}$ . Avant imprégnation, cette alumine est séchée à  $500^\circ\text{C}$  pendant 15 heures.

Le cobalt et le molybdène ont été déposés par double imprégnation. Le paramolybdate d'ammonium est tout d'abord dissous dans un excès d'eau. L'

---

\*Present address: Physical Chemistry Laboratory, University of Patras, Patras, Greece.

alumine est ensuite progressivement ajoutée. La suspension obtenue est agitée trois jours à température ambiante. Le solide obtenu est séché à 100°C, décomposé à 300°C puis calciné à 500°C. Dans une seconde étape le cobalt est imprégné «à sec» à partir d'une solution de nitrate de cobalt. Le produit est décomposé à 300°C puis calciné 24 h à 500°C.

La quantité de phase active déposée sur le support est de 15% en poids d'oxyde.

## 2.2. Spectroscopie de réflexion diffuse

Un spectromètre Beckman Acta IV fut employé. La référence étant une pastille d'alumine utilisée comme support.

## 2.3. XPS

Un spectromètre Vacuum Generators ESCA 2 équipé d'un accumulateur Tracor Northern NS 560 a permis d'analyser ces échantillons. La radiation excitatrice est la raie  $K\alpha$ , (1486,6eV) de l'aluminium. La raie  $4f_{7/2}$  (82,8eV) fut utilisée comme référence.

## 2.4. Microscopie électronique et microsonde

Le microscope électronique Jeol 100C était équipé d'un spectromètre à dispersion d'énergie (Kevex). Les échantillons dispersés dans l'eau sont déposés sur une grille de cuivre puis recouverts d'un film de carbone.

## 3. Resultats experimentaux

### 3.1. Spectroscopie de réflexion diffuse

La figure 1 permet de comparer les spectres des composés modèles et des catalyseurs. Les spectres ont été analysés dans le domaine 200-800 nm (fig. 1a) et 800-1840 nm (fig 1b).

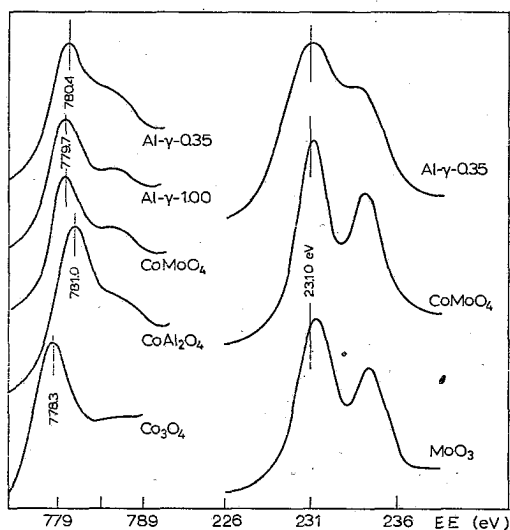


FIG. 1.: Spectres XPS du cobalt et du molybdène.

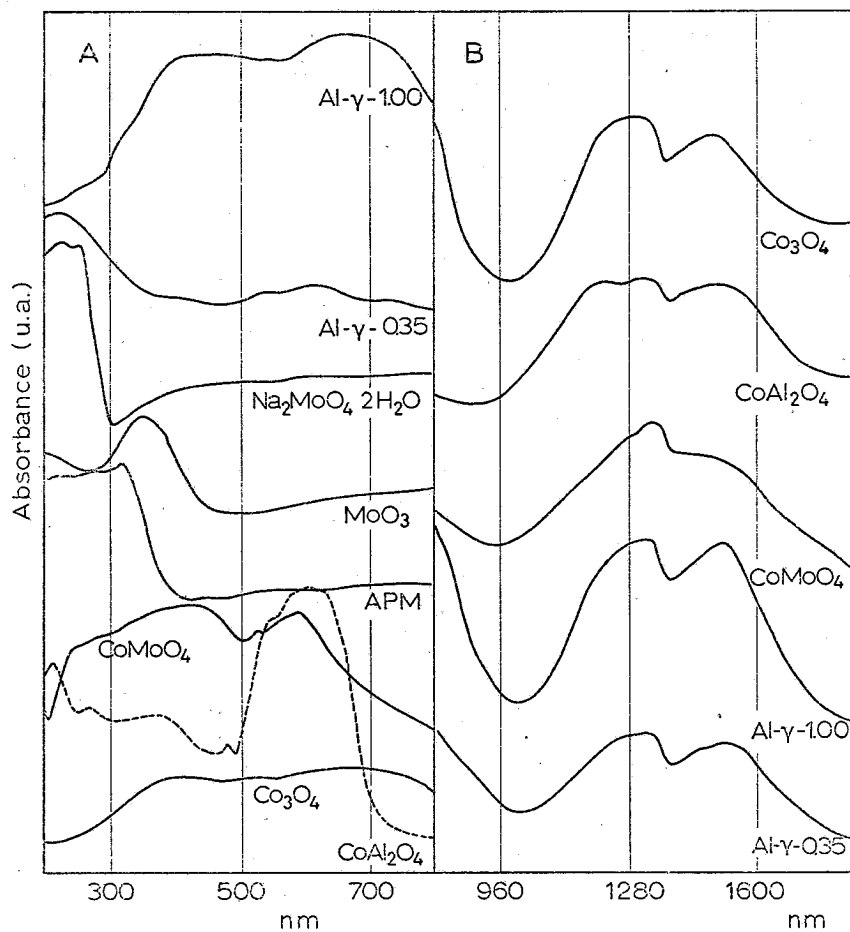


FIG. 2.: Spectres de réflexion diffuse.

### 3.2. XPS

La figure 2 illustre les spectres XPS du molybdène ( $\text{Mo}_{3d}$ ) et du cobalt ( $\text{Co}^{2p}$ ) des catalyseurs étudiés et des composés massiques ( $\text{MoO}_3$ ,  $\text{Co}_3\text{O}_4$ ,  $\text{CoMoO}_4$ ,  $\text{CoAl}_2\text{O}_4$ ). On observe que la résolution des bandes  $\text{Mo}_{3d_{5/2}}$  est plus faible dans le cas du catalyseur supporté que pour celui des composés massiques.

### 3.3. Microscope électronique et microsonde

Les figures 3 et 4 illustrent les échantillons  $r = 0,35$  et  $r = 1,00$ . Une analyse par EPMA a permis de différencier trois régions dans le catalyseur Al-

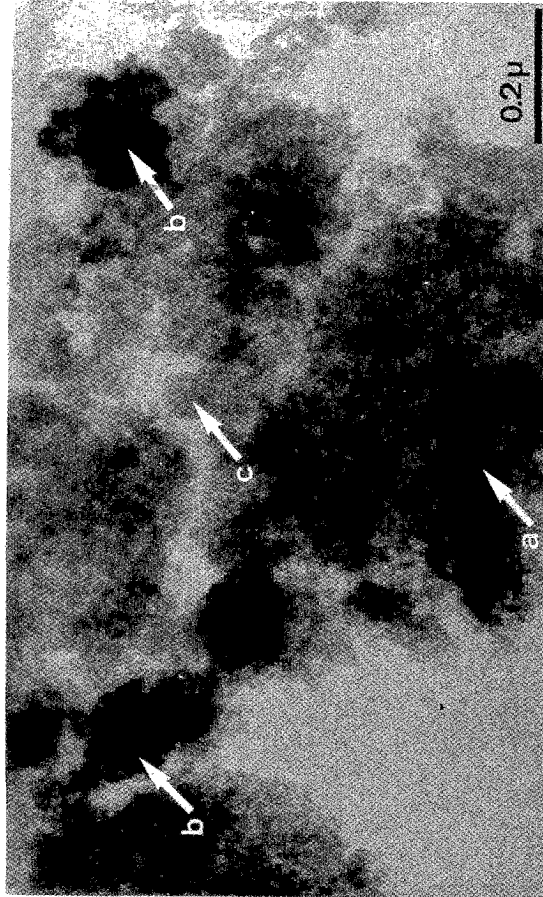


FIG. 3.: Microscopie électronique et analyse EPMA du catalyseur Al-0,35.

0,35. En effet on observe de gros cristallites qui à l'analyse par diffraction des électrons s'avère être du molybdate de calcium. Une deuxième série de particules est constituée de cristallites d'oxyde de cobalt.

Il existe des zones qui ne présentent pas de structure cristalline visible. Cependant, une analyse EPMA révèle la présence de cobalt et de molybdène très dispersés dans les proportions  $\text{Co/Mo} = 1/1$ .

La figure 4 montre une photographie STEM du catalyseur Al-1,00. Les taches correspondent, par analyse EPMA, à des cristallites de cobalt. Une analyse par diffraction des électrons confirme la présence de  $\text{Co}_3\text{O}_4$ . Toutefois, à la

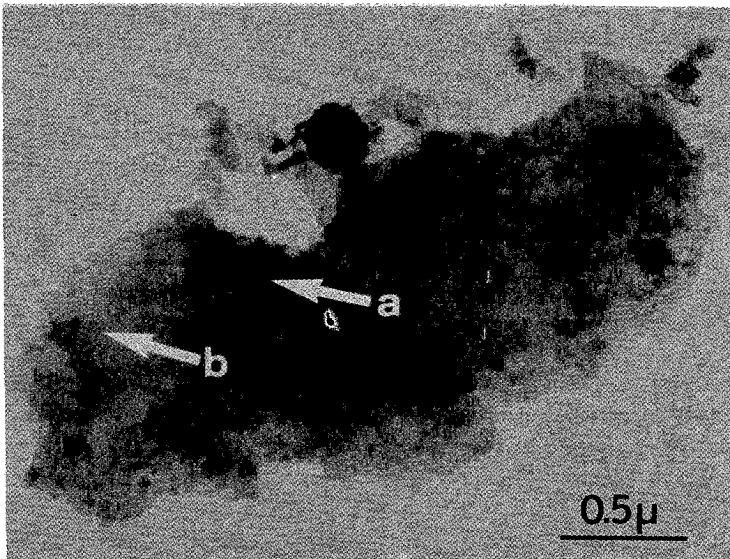
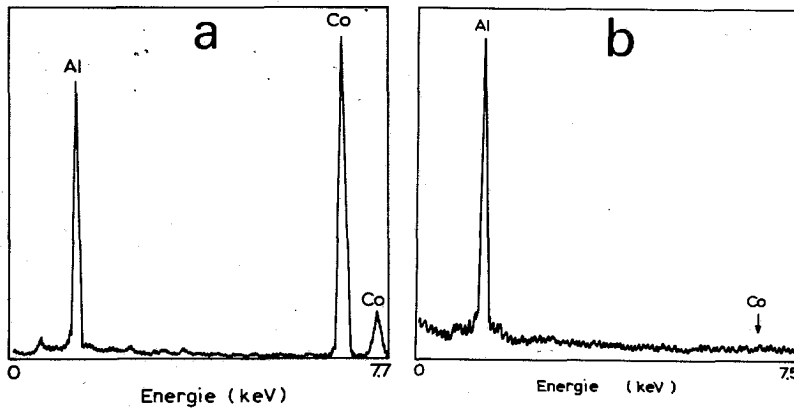


FIG. 4.: Microscopie électronique et analyse EPMA du catalyseur Al-1,00.

différence de ce qui a été observé dans le cas du catalyseur 0,35, il n' a pas été possible de mettre en évidence de cobalt non cristallisé bien dispersé à la surface de l' alumine.

#### 4. Discussion

##### 4.1. Spectroscopie de réflexion diffuse

##### 4.1.1. Catalyseur Al-0,35

La spectroscopie de réflexion diffuse donne des informations sur la nature et la symétrie des espèces présentes à la surface des catalyseurs.

La figure 1 montre par exemple que le molybdène dans le catalyseur Al-0,35 se trouve à la fois en coordination tétraédrique et octaédrique. En effet, si l'on compare les spectres à ceux de  $\text{Na}_2\text{MoO}_4 \cdot 2\text{H}_2\text{O}$ ,  $\text{MoO}_3$  et  $(\text{NH}_4)_6\text{Mo}_7\text{O}_{24} \cdot 4\text{H}_2\text{O}$  (dans lesquels le molybdène est soit octaédrique soit tétraédrique), on observe une large bande d'adsorption située en 200 et 300 nm due au molybdène dans un environnement tétraédrique (2,3,7). Cependant, cette bande d'adsorption est beaucoup plus large que théoriquement prévu et débute aux environs de 400 nm.

C'est précisément dans cette zone que débute la bande d'absorption du Mo(VI) en coordination octaédrique du paramolybdate. Elle présente un maximum d'absorption entre 300 et 500 nm.

L'attribution des bandes dues au cobalt est la suivante. La triple bande d'absorption située aux environs de 600 nm est due au Co (II) de la spinelle  $\text{CoAl}_2\text{O}_4$  (2.6). La similitude de la forme du spectre de ce composé modèle et du catalyseur Al-0,35, dans cette région, est particulièrement évidente. La situation est plus compliquée dans le domaine 800-1840 nm. En effet, les différences entre les spectres de  $\text{Co}_3\text{O}_4$ ,  $\text{CoAl}_2\text{O}_4$  et  $\text{CoMoO}_4$  ne sont pas très importantes. Cependant, la grande similitude du spectre du catalyseur et du composé  $\text{Co}_3\text{O}_4$  permet de supposer qu'outre la présence de Co(II) sous forme  $\text{CoAl}_2\text{O}_4$ , il existe du Co (II) comparable à Co(II) dans  $\text{Co}_3\text{O}_4$ . L'absence de Co(II) dans le catalyseur (présent dans  $\text{Co}_3\text{O}_4$ ) est renforcée par la faible valeur de l'intensité du satellite comparé à l'intensité du pic principal du niveau  $\text{Co}_{2p_{3/2}}$  mesuré par XPS.

#### 4.1.2. Catalyseur Al 100

La similitude des spectres de  $\text{Co}_3\text{O}_4$  et de ce catalyseur démontre la présence d'oxyde de cobalt dans ce solide.

Il faut remarquer l'absence de la triple bande à 600 nm caractéristique de  $\text{CoAl}_2\text{O}_4$ .

### 4.2. XPS

#### 4.2.1. Catalyseur Al 0,35

L'analyse XPS est un bon complément de l'étude de la surface de ces solides. En effet, cette technique fournit non seulement des informations sur le degré d'oxydation superficiel des éléments mais aussi sur le type d'interaction que cet élément peut avoir avec ses voisins. Une bonne illustration des possibilités de cette méthode est donnée dans la figure 2 qui représente le spectre du niveau 3d du molybdène du catalyseur et des composés modèles. L'énergie de liaison du molybdène dans le catalyseur est de 231. eV, c'est-à-dire voisine de celle du Mo(VI) de  $\text{MoO}_3$  et  $\text{CoMoO}_4$ . Cependant, les bandes  $\text{Mo}_{3d_{3/2}}$  et  $\text{Mo}_{3d_{5/2}}$  sont bien moins résolues pour le catalyseur. Ce phénomène peut avoir pour le moins 3 causes:

(i) l'existence d'un effet de charge, (ii) l'existence de différents degrés d'oxydation du molybdène, (iii) l'existence de différents Mo(VI) (différente coordina-

tion, adsorption sur différents sites de l'alumine). Il est possible d'éliminer la première hypothèse car la conductivité électrique n'est pas meilleure pour les composés modèles qui présentent cependant une bonne résolution.

La deuxième hypothèse peut être retenue car il a déjà été mentionné la présence de Mo(V) dans la littérature (8). Cependant, la concentration de cette espèce est très faible et ne devrait pas modifier le spectre XPS. La troisième hypothèse est plus raisonnable. Elle est corroborée par spectroscopie de réflexion diffuse et par EPMA.

Le spectre du niveau  $\text{Co}_{2p}$  du catalyseur montre la présence de Co (II) en surface. En effet, le spectre est similaire à ceux de  $\text{CoAl}_2\text{O}_4$  et  $\text{CoMoO}_4$ . Cependant, l'analyse XPS ne permet pas de différencier ces deux composés.

#### 4.2.2. Catalyseur Al-1.00

La forme du spectre de la bande  $\text{Co}_{2p}$  est différente de celle du solide Al-0,35. Dans ce cas, l'énergie de liaison (780.4eV) est voisine de celle de  $\text{Co}_3\text{O}_4$ . De plus, l'intensité du satellite associée au pic principal est plus faible. Ceci est une indication de la présence de Co(III) diamagnétique qui ne présente pas de satellite.

#### 4.3. Microscopie et microrsonde électronique

Les résultats AEM confirment ceux obtenus par les autres techniques.

La formation de  $\text{CaMoO}_4$  a un caractère parasite et est dû vraisemblablement à la présence de trace de Ca dans les réactifs.

Le phénomène le plus surprenant, mis en évidence par cette technique, concerne la dispersion du cobalt. Quand celui-ci est imprégné seul sur l'alumine, il se produit une ségrégation et la formation de grosses particules de  $\text{Co}_3\text{O}_4$ . Par contre, lorsqu'il est déposé sur une monocouche de molybdène (1-9) sur alumine la dispersion du cobalt est facilitée.

#### 5. Conclusions

Ce travail permet d'illustrer sur un exemple pratique, l'emploi complémentaire de différentes techniques pour l'identification des structures de catalyseur.

L'analyse XPS a permis une analyse globale de la surface des solides. La spectroscopie de réflexion diffuse confirme la présence de Mo(VI) en symétrie tétraédrique et octaédrique, la présence de  $\text{CoAl}_2\text{O}_4$  dans le catalyseur Al-0,35 et son absence dans le solide Al-1,00. De l'oxyde de cobalt  $\text{Co}_3\text{O}_4$  a été détecté dans ce dernier. La microscopie électronique précisant la composition de chaque région de l'échantillon.

Un point très intéressant est lié à la formation de l'aluminate de cobalt. La présence de ce composé non désirable dans le catalyseur d'hydrodésulfuration semble liée à l'état de dispersion du cobalt. Lorsque la dispersion du cobalt est favorisée par la présence de molybdène sous forme de monocouche, la concentration en alumine croît de manière parallèle.



Nous remercions les «Services de la Programmation Scientifique de Belgique» pour leur aide financière durant cette étude.

### Περίληψη

*Μελέτη τών καταλυτῶν  $Co/Al_2O_3$  καὶ  $CoMo/Al_2O_3$  με φωτοηλεκτρονικὴ φασματοσκοπία, φασματοσκοπία διαχύτου ἀνακλάσεως καὶ ἀναλυτικῆς μικροσκοπίας.*

Ἡ ταυτόχρονη ἐφαρμογὴ τῆς φωτοηλεκτρονικῆς φασματοσκοπίας δι' ἀκτίνων X (X.P.S.) τῆς φασματοσκοπίας διαχύτου ἀνακλάσεως (D.R.S.) καὶ τῆς ἀναλυτικῆς ἠλεκτρονικῆς μικροσκοπίας (AEM) ἐπέτρεψαν τὴ διερεύνηση τῆς φύσεως καὶ τῆς διασπορᾶς τῆς ἐνεργοῦ φάσεως σὲ δύο καταλυτικὰ συστήματα, ποὺ χρησιμοποιοῦνται στὴν ὑδροαποθείωση τοῦ πετρελαίου [ $Co/Al_2O_3$ ,  $CoMo/Al_2O_3$ ].

Ἡ φασματοσκοπία διαχύτου ἀνακλάσεως ἐπιβεβαιώνει τὴν ὑπαρξὴ Mo (VI) τόσο σὲ τετραεδρική, ὅσο καὶ σὲ ὀκταεδρική συνεντρία. Δείχνει ἐπίσης ὅτι τὸ κοβάλτιο σχηματίζει  $CoAl_2O_4$  στὸ  $CoMo/Al_2O_3$  καὶ  $Co_3O_4$  στὸ  $Co/Al_2O_3$ .

Ὁ σχηματισμὸς τοῦ  $CoAl_2O_4$  χημικοῦ εἶδους μὴ ἐπιθυμητοῦ στοὺς καταλύτες ὑδροαποθείωσης, φαίνεται νὰ συνδέεται μετὰ τὴν κατάσταση διασπορᾶς τοῦ κοβαλτίου.

---

### References

1. G.C.A. Schuit, B.C. Gates, A.I. Ch. E. Journal, **19**, 417, 1973.
2. J.H. Ashley, P.C.H. Mitchell, J. Chem. Soc., 2821, 1968.
3. Idem, 2730, 1969.
4. P.K. Gour, S.M. Upadhyat, J.S. Tiwari, P.K. Ghosh, N.B. Bhattacharyya, S.P. Sen, J. Res. Inst. Catalysis, Hakkaido Univ., **25**, 91, 1977.
5. J. Grimblot, J.P. Bonnelle, J. Electr. Spect. Relat. Phenom. **9**, 449, 1976.
6. M. Lo Jacono, A. Cimino. G.C.A. Schuit, Gazzetta Chim., Ital., **103**, 1281, 1973.
7. G.T. Pott, W.H.I. Stork, Preparation of Catalysts (B), Delmon, P.A. Jacobs, G. Poncelet, Eds) Elsevier Amsterdam, 537, 1976.
8. J. Masson, J. Nechtschein, Bull. Soc. Chim. Fr. **10**, 3933, 1978.
9. W.K. Hall, M. Lo Jacono, Vlth Int. Congress on Catalysis (G.C. Bond, P.B. Wells, F.C. Tompkins, Eds) The Chemical Society Burlington House, London, 246, 1976.

## **SYNTHESIS OF NEW N-SUBSTITUTED METHOXY-PHENETHYLAMINES AND THEIR PHARMACOLOGICAL ACTION ON C.N.S.**

TH. SIATRA-PAPASTAIKOUDI, A. PAPADAKI-VALIRAKI, G. TSATSAS (Chemistry),  
Z. PAPADOPOULOU-DAIFOTI, CH. SPYRAKI, D. VARONOS (Pharmacology)

\* *Laboratory of Pharmaceutical Chemistry, University of Athens, 104, Solonos Street, Athens (144), Greece.*

\*\* *Laboratory of Experimental Pharmacology, University of Athens, Goudi, Athens (609), Greece.*

### **Summary**

The synthesis of N-alkylamino-acetyl methoxy- $\beta$ -phenylethylamine derivatives is described.

These N-substituted derivatives are prepared from the analogous  $\beta$ -phenethylamines by adding chloroacetylchloride followed by the addition of aliphatic and heterocyclic amines.

The toxicity and the possible central pharmacological action of these compounds was studied on experimental animals.

**Key Words:** Derivatives of methoxy-phenethylamine.

### **Introduction**

The central stimulant properties of the phenethylamines may be associated with particular conformation of these flexible molecules.

Comparison of the pharmacological and chemical data suggests that the action on  $\alpha$ -adrenergic receptors of phenethylamines will be substantially reduced in these compounds in which the N-substitution will be voluminous.

In contrast voluminous N-substitution<sup>(1-2)</sup>, will increase the  $\beta$ -adrenomimetic action<sup>(4-6)</sup>. The 3, 4 dihydroxy substitution on the benzole ring, seems to be substantial for the adrenergic properties of the molecule.

In the present work various 2,3 3,4 or 3,4,5 methoxy substituted  $\beta$ -phenethylamines were prepared and their pharmacological activity have been determined. The synthesized and tested compounds correspond to the general formulas I, II, III.

The procedure followed for the preparation of the series of compounds is shown in the Fig. (I).

The parent compounds for the synthesis of the 2,3 and 3,4 substituted derivatives were *o*-vanilline and isovanilline, **1**, **1a**.

Methylation of these compounds with dimethyl sulfate in alkaline medium, gave the respective substituted benzaldehydes<sup>(8,9)</sup> **2**, **2a**, which were converted to the corresponding nitrostyrenes<sup>(10)</sup> **3**, **3a**, with the aid of nitromethane. Reduction of the above mentioned nitrostyrenes with zinc in hydrochloric acid<sup>(10,11)</sup> or lithium aluminium hydride<sup>(12)</sup> gave the respective  $\beta$ -phenethylamines, **4**, **4a**.

However, in case of the preparation of 3,4,5 trimethoxy phenethylamine (mescaline) the 3,4,5 trioxybenzoic acid (gallic acid) **5**, was used as starting material.

Methylation of this compound with dimethyl sulfate<sup>(8,9)</sup> and esterification of the methylated derivative gave the 3,4,5 trimethoxy benzoic ethylester<sup>(13)</sup> **6**. Reduction of this ethylester with lithium aluminium hydride gave 3,4,5 trimethoxy benzylalcohol<sup>(14)</sup> **7**. Reaction of the above alcohol with chloride gave the correspondin benzylchloride<sup>(17)</sup> **8** which further reacted with potassium cyanide and gave the nitrile<sup>(14)</sup> **9**. This nitrile was reduced to mescaline **10**, by lithium aluminium hydride<sup>(12)</sup>.

Besides the above mentioned procedure which gives relatively good yields mescaline could be obtained from 3,4,5 trimethoxy-benzaldehyde **12** which was obtained from *p*-toluolo-sulfonylo-N (3,4,5 trimethoxy-benzoyl) hydrazine<sup>(16)</sup> **11**.

Reaction of this substituted benzaldehyde with nitromethane gave the 3,4,5 trimethoxy nitrostyrene<sup>(17)</sup> **13**, which by reduction gave mescaline<sup>(13)</sup>.

Reaction of the substituted phenethylamines with chloracetyl-chloride in alkaline media gave the chloracylamino derivatives 14, 14a, 14 $\beta$  which on reaction with various amines yielded I, II, III.

## Experimental Part

### *N*-chloroacetyl- $\beta$ - (dimethoxy 2,3-phenethylamine).

Chloroacetylchloride (5,5ml/0,07 mol), was added dropwise to a stirred mixture of dimethoxy 2,3  $\beta$ -phenethylamine (15,5g/0,06 mol), 100ml chloroform and sodium bicarbonate 13,3g (0,12 mol). The mixture was stirred for 30 min and then was washed with diluted hydrochloric acid followed by water until neutral reaction. The solution was then dried over anhydrous sodium sulfate and the solvent was evaporated. The crystalline product was collected.

All the chloracylamino derivatives of the series were prepared with the procedure mentioned above and gave the following m.p. yields and analyses:



All the bases of this series were prepared with the same procedure mentioned above.

In the following tables (I, II, III) the compounds prepared are listed with their constants and analyses.

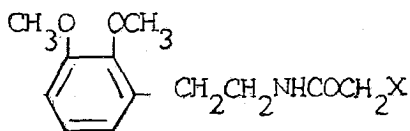


TABLE I

X	Yield	Nr Ref.	Salt	F°C	Analysis					
					Calc. %			Found %		
					C	H	N	C	H	N
CH <sub>3</sub> (CH <sub>2</sub> ) <sub>3</sub> NH	85	1390	picrate	118-120 <sup>(a)</sup>	50,6	5,6		50,6	5,6	
CH <sub>3</sub> (CH <sub>2</sub> ) <sub>3</sub> NH		1391	chlorhydrate	113-6 <sup>(a)</sup>	58,0	8,3	8,5	58,4	8,3	8,4
(C <sub>2</sub> H <sub>5</sub> ) <sub>2</sub> N	95	1379	picrate	154-7 <sup>(a)</sup>	50,5	5,6		51,0	5,6	
(C <sub>2</sub> H <sub>5</sub> ) <sub>2</sub> N		1387	chlorhydrate	103-5 <sup>(a)</sup>	58,1	8,2	8,5	58,7	8,2	8,0
N-(CH <sub>2</sub> ) <sub>2</sub> -O-(CH <sub>2</sub> ) <sub>2</sub>	92	1382	picrate	196-201 <sup>(a)</sup>	49,2	5,0	8,1	49,4	5,5	8,3
N-(CH <sub>2</sub> ) <sub>2</sub> -O-(CH <sub>2</sub> ) <sub>2</sub>		1386	chlorhydrate	171-2 <sup>(a)</sup>	55,7	7,3		55,7	7,3	
N-(CH <sub>2</sub> ) <sub>4</sub> -CH <sub>2</sub>	98	1383	picrate	177-181 <sup>(a)</sup>	51,6	5,5		51,3	5,2	
N-(CH <sub>2</sub> ) <sub>2</sub> -(CH <sub>2</sub> ) <sub>2</sub>	93	1380	picrate	170-2 <sup>(a)</sup>	50,7	5,2		51,0	5,3	
N-(CH <sub>2</sub> ) <sub>2</sub> -(CH <sub>2</sub> ) <sub>2</sub>	89	1392	oxalate	105-110 <sup>(b)</sup>	56,7	6,9	7,3	56,9	6,9	

a= Me<sub>2</sub>CO

b= EtOH

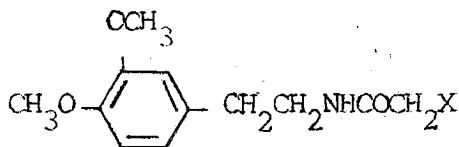


TABLE II

X	Yield	No Ref.	Salt	F°C	Analysis					
					Calc. %			Found %		
					C	H	N	C	H	N
(C <sub>2</sub> H <sub>5</sub> ) <sub>2</sub> N	85	1381	picrate	158-9 <sup>(a)</sup>	50,5	5,6		50,2	5,8	
(C <sub>2</sub> H <sub>5</sub> ) <sub>2</sub> N		1393	oxalate	102 <sup>(b)</sup>	56,3	7,3	7,3	56,8	7,3	7,3
N-(CH <sub>2</sub> ) <sub>2</sub> O-(CH <sub>2</sub> ) <sub>2</sub>	83	1389	picrate	169-172 <sup>(a)</sup>	49,2	5,0		49,3	5,2	
N-(CH <sub>2</sub> ) <sub>2</sub> O-(CH <sub>2</sub> ) <sub>2</sub>		1395	chlorhydrate	148-150 <sup>(a)</sup>	55,6	7,5	8,0	56,0	7,2	8,2
N-(CH <sub>2</sub> ) <sub>4</sub> -CH <sub>2</sub>	97	1388	picrate	173-6 <sup>(a)</sup>	51,6	7,3	8,1	51,6	7,5	8,2
N-(CH <sub>2</sub> ) <sub>4</sub> -CH <sub>2</sub>		1394	chlorhydrate	141-3 <sup>(b)</sup>	59,5	8,0	8,1	59,2	8,0	8,0

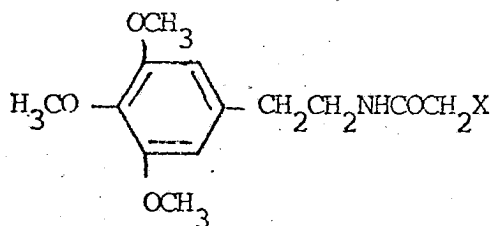


TABLE III

X	Yield	No Ref.	Salt	F°C	Analysis					
					Calc. %			Found %		
					C	H	N	C	H	N
N-(CH <sub>2</sub> ) <sub>4</sub> -CH <sub>2</sub>	95	2212	picrate	191-5	51,0	5,5		51,0	5,3	
N-(CH <sub>2</sub> ) <sub>4</sub> -CH <sub>2</sub>	82	2260	chlorhydrate	191-5 <sup>(a)</sup>	58,0	7,8	7,5	58,2	7,9	7,7
N(CH <sub>2</sub> ) <sub>2</sub> -O-(CH <sub>2</sub> ) <sub>2</sub>	85	2258	chlorhydrate	161 <sup>(a)</sup>	54,5	7,3	7,5	54,0	7,4	7,3

### Pharmacological Part

The experiments were performed on mice, male albino Swiss, of 28 ± 2gr.

Animals were always treated intraperitoneally with the salts of the test compounds (Nr. Ref.: 1391, 1387, 1386, 1392, 1393, 1395, 1394) dissolved in isotonic sodium chloride, while the control group with the vehicle only. Before any treatment the animals were housed for 8 days under the same conditions, water and food ad libitum; temperature 22 ± 2°.

The dose levels were chosen on a logarithmic scale. The effects obtained from the dose of 30mgr/kg were the most potent.

### Test Methods

#### Acute toxicity in mice

The number of deaths within groups of ten mice, 28 ± 2gr of male sex, during the 24 hours period following a single i.p. injection was used to determine the acute toxicity.

The LD<sub>50</sub> was calculated graphically in mortality percentage according to the administered dose <sup>(18)</sup>.

#### Behavioural observations

Behavioural observations were carried out in mice according to the general screening procedure described by Irwin<sup>(19)</sup> <sup>(20)</sup>. Groups of five animals were injected i.p. with each of the test compounds in the selected dose and observed 30 minutes afterwards for 3 hours.

### Motor Activity

Mice were housed in individual cages for 1 or 2 hours prior to i.p. dosing. Their movements are registered with the aid of a motor activity cage (Ugo Basile Nr: 7401) mounted on springs so that all the slightest movements of the animal cause the cage to oscillate slightly and thus to close the electrical circuit of a counter. The number of movements of the animal during every 15 minutes for 3 hours are recorded<sup>(21)</sup>.

### Stereotypy

Groups of 5 animals were injected i.p. with each compound and were observed 1 and 2 hours after administration. Searching movements of the head, circling, walking backwards and grooming were recorded<sup>(22)</sup>.

### Body Temperature

Five male mice were used each compound and dose. The test compounds were given i.p. and the mean temperature of the animals was determined at intervals 1, 2, 3, and 4 hours thereafter. A control group was also used.

### Results and Discussion

The i.p. LD<sub>50</sub> of the test compounds in male mice are listed in Table IV.

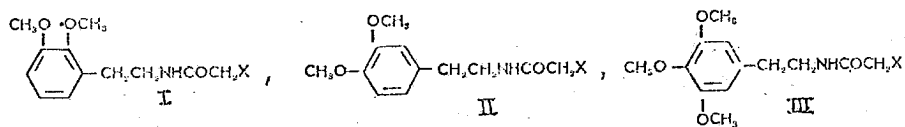
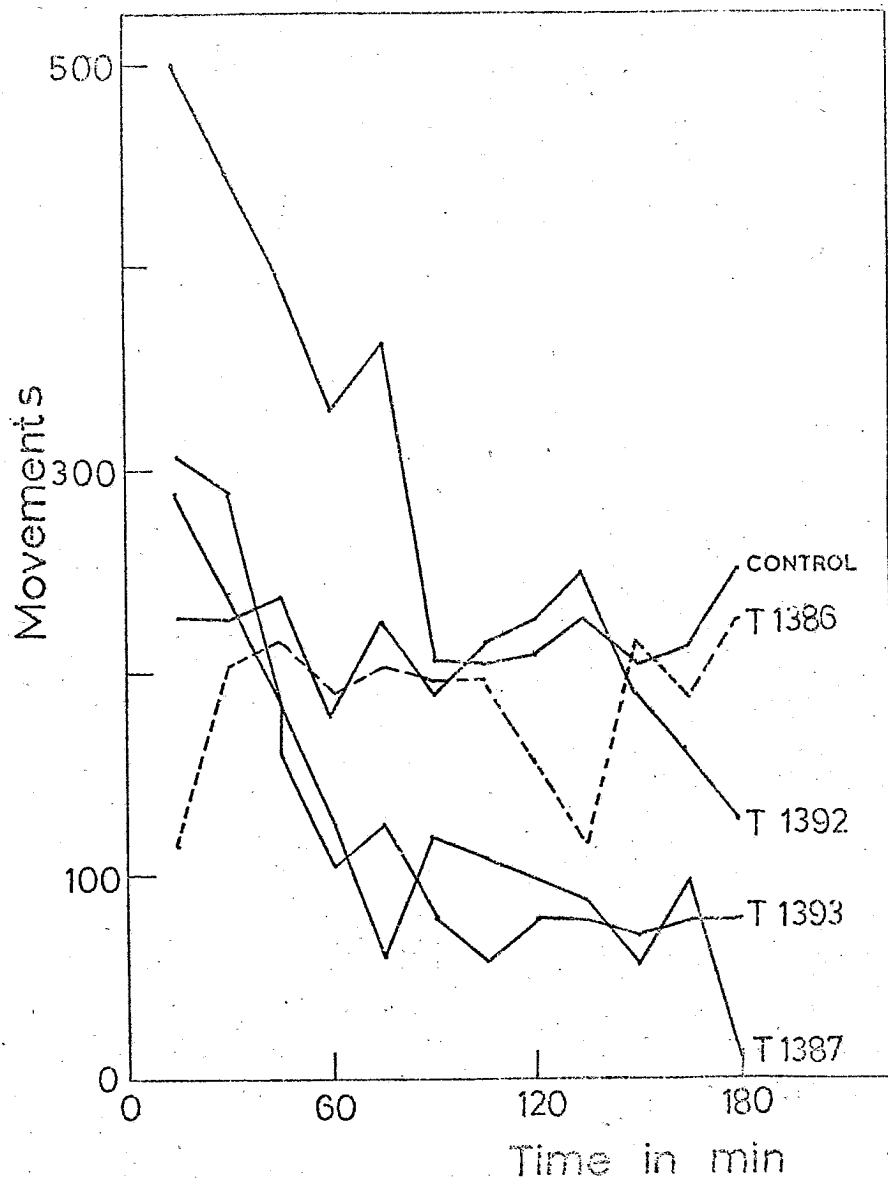
TABLE IV

Nr. Ref.	X	LD <sub>50</sub>
1391	CH <sub>3</sub> (CH <sub>2</sub> ) <sub>3</sub> NH	250 mgr/kg.
1387	(C <sub>2</sub> H <sub>5</sub> ) <sub>2</sub> N	300 »
1386	N-(CH <sub>2</sub> ) <sub>2</sub> -O (CH <sub>2</sub> ) <sub>2</sub>	550 »
1392	N-(CH <sub>2</sub> ) <sub>2</sub> - (CH <sub>2</sub> ) <sub>2</sub>	200 »
1393	(C <sub>2</sub> H <sub>5</sub> ) <sub>2</sub> N	300 »
1395	N-(CH <sub>2</sub> ) <sub>2</sub> -O-(CH <sub>2</sub> ) <sub>2</sub>	550 »
1394	N-(CH <sub>2</sub> ) <sub>4</sub> -CH <sub>2</sub>	350 »

The morpholino derivatives showed less toxicity than the other derivatives, which could not be related with the activity of these compounds.

The behavioural observations for all test compounds evoked alertness, slightly increased respiration rate, restlessness, vocalizations in larger doses (100 mgr/kg) «chewing» movements and grooming.

The motor activity test showed a diminution of the spontaneous activity (Fig.: II).



Where X =  $\text{CH}_2(\text{CH}_2)_2\text{NH}$ ,  $(\text{C}_2\text{H}_5)_2\text{N}$ ,  
 $\text{N}(\text{CH}_2)_2\text{O}(\text{CH}_2)_2$ ,  $\text{N}(\text{CH}_2)_4\text{CH}_2$ ,  $\text{N}(\text{CH}_2)_2(\text{CH}_2)_2$



Most of the substances tested evoked stereotypy of amphetamine type that is searching movements of the head<sup>(23)</sup>.

The body temperature between the control and treated group showed an increase of 10.5°C.

The effects of the compounds synthesized were recorded always in comparison with a control group and an other group which received amphetamine phosphate 10 mgr/kg. The facts obtained from these tests were that the behavioral observations made according to blind screening evoked an amphetamine like response, although less potent.

In motor activity test the investigators waited high activity because restlessness was already observed. Probably the chosen effective dose was high enough to cause diminution of motor activity, due probably to toxic manifestations. Our findings that the phenylethylamines synthesized exhibited an amphetamine like response could suggest a dopaminergic and a noradrenergic stimulation as produced by amphetamine. Horn<sup>(24)</sup> has shown that dopaminergic sites are less sensitive to structural changes than are noradrenergic sites. Thus particular structural changes to a molecule might substantially reduce the noradrenergic system effects and yet leave the effects on the dopaminergic system largely intact.

The finding of motor activity diminution which is in contrast with all the other amphetamine-like observations is probably due to a selective stimulation to one of the above monoamine systems, which determine a particular type of activity.

## Περίληψις

### *Σύνθεσις Ν-άλκυλαμινο-ακυλομεθοξυ-β-φαινυλαιθυλαμινῶν*

Εἰς τὴν παροῦσα ἐργασία περιγράφεται ἡ σύνθεσις Ν-άλκυλαμινο-ακυλομεθοξυ-β-φαινυλαιθυλαμινῶν.

Τὰ Ν-ὑποκατεστημένα αὐτὰ παράγωγα παρασκευάζονται ἐκ τῶν ἀντίστοιχων β-φαινυλαιθυλαμινῶν διὰ μετατροπῆς τῶν εἰς ἀκυλοχλωρίδια τῆ ἐπιδράσει χλωρακετυλοχλωριδίου καὶ ἐπὶ τῶν τελευταίων τούτων διαφόρων ἀμινῶν ἀλειφατικῶν ἢ ἑτεροκυκλικῶν.

Ἡ τοξικότης καὶ ἡ φαρμακολογικὴ δρᾶσις ἐπὶ τοῦ Κ.Ν.Σ. τῶν νεοσυνθεθεισῶν οὐσιῶν ἐμελετήθησαν ἐπὶ πειραματοζῴων.

## References

1. Ariens, E.J.: Adv. Drug, Res. **3**, 235 (1966).
2. Bloom, B., Gooldman, J.M.: Adv. Drug. Res. **3**, 121 (1966).
3. Ariens, E.J., Simonis, A.M.: Arch. Inter. Pharmacodyn, **127** 479 (1960).
4. Moed, H.D., Dijk, J. Nan.: Rec. Trav. Chim., **75**, 1215 (1956).
5. Moed, H.D., Dijk, J. Nan, Niewind, H.: Rec. trav. chim., **77**, 273-282 (1958).
6. Moed, H.D., Dijk, J. Nan, Niewind, H.: Rec. trav. chim. **74**, 919-936 (1955).
7. Baltzly, R., Mehta, N.: J. Med. Chem., **11**, 833-44 (1968).

8. Dellaby, R., Tsatsas G., Jendrot, M.C.: Bull. Soc. Chim., 231, (1960).
9. Buck, J.S.: Org. Synth. Coll. Vol., II, 620, (1947).
10. Dellaby, R., Tsatsas, G., Jendrot, M.C., Bull. Soc. Chim., 1830 (1956).
11. Tsatsas, G.: Bull. Soc. Chim., 884, (1949).
12. Erne, May, Ramirez, F.: Helv. Chim. Acta., **33**, 912 (1950).
13. Vogel, A.I.: Practical Organic Chemistry, Longmans 3d. ed., 374 (1956).
14. Dornon, H., Petsch, G.: Arch. Pharm., **285**, 323 (1952).
15. Tsatsas, G.: Ann. Pharm. Franç., **7**, 733 (1949).
16. Engelhard, H.: Ber, **92**, 1336, (1959).
17. Tsatsas, G.: Ann. Pharm. Franç. J., 740, (1949).
18. Cambell D.E.S., and RICHTER W.,: Acta Pharm. Toxicol. 25, 345, 1967.
19. Irwin S.: Gordon Res. Conf. on Medicinal Chemistry. 133, (1959).
20. Boissier J.R., Dremont C., Rotonis R., and Pagny I.: Arch. Intern. Pharmacodynamie, 24, 133. (1961).
21. Borsy J., Grangi E. and Caner J.: Arch. Intern. Med. 101, 562 (1958).
22. Randrap A., and Munkvad J.: Psychopharmacologia, II, <sup>300</sup>, <sup>(67)</sup>.
23. Turner R.A.: Screening Methods in Pharmacol. Academic Press, (1965).
24. Horn A.S.: Brit. J. of Pharmacol. **47**, 332 (1973).

## GLC-MS COMPUTER ANALYSIS OF THE ESSENTIAL OIL OF MASTIC GUM

V.P. PAPAGEORGIOU, A.N. SAGREDOS and R. MOSER

Laboratory of Organic Chemistry, College of Engineering

Department of Chemical Engineering Aristotle University of Thessaloniki Thessaloniki, GREECE

**Key Words Index:** *Pistacia lentiscus*, *Anacardiaceae*, mastic gum, essential oil, gas chromatography-mass spectral analysis.

### Abstract

By combination of gas-liquid chromatography and mass spectral computer analysis it was possible to isolate 31 constituents of the essential oil of mastic gum; 29 of these compounds could be identified. The main components are  $\alpha$ -pinene,  $\beta$ -pinene, myrcene and caryophyllene which make up more than 93% of the total oil. The results were compared with the previously published information.

### Introduction

The mastic gum is obtained by sticking the trunk of the tree *Pistacia lentiscus Chia* (or *Latifolia*). This tree is a special variety of *Pistacia lentiscus* (Fam. *Anacardiaceae*) and is cultivated in the Greek island of Chios for its flavour mastic gum. The chemical composition of mastic gum is: 1-3% essential oil, 4%  $\alpha$ - and  $\beta$ -mastichinic acid ( $C_{23}H_{36}O_4$ ), 0,5% mastichollic acid ( $C_{23}H_{36}O_4$ ), 20%  $\alpha$ -mastichonic acid ( $C_{32}H_{48}O_4$ ), 18%  $\beta$ -mastichonic acid ( $C_{32}H_{48}O_4$ ), 30%  $\alpha$ -mastichorezene ( $C_{35}H_{56}O_4$ ) and 20%  $\beta$ -mastichorezene ( $C_{35}H_{56}O_4$ ).

The major part of the production of mastic gum is used in the Middle East for flavouring alcoholic beverages. Small quantities are used for addition to medicines and cosmetics or a schewing gum.

### Results and Discussion

As for the chemical composition of mastic gum oil very few are known. In a recent paper Scrubis et al.<sup>1</sup> have examined the chemical composition of the essential oil of mastic gum. We also have examined the chemical composition of the above mentioned oil. It is the purpose of this paper to compare the published chemical composition of this essential oil with those obtained by the authors.

The gas chromatogram of mastic gum oil is showed in Figure 1. The results obtained from the analysis of mastic gum oil can be seen in Table I. In addition, the results obtained by Scrubis et al. are also presented in Table I, so that a comparison can be made between our analysis and the previously published data.

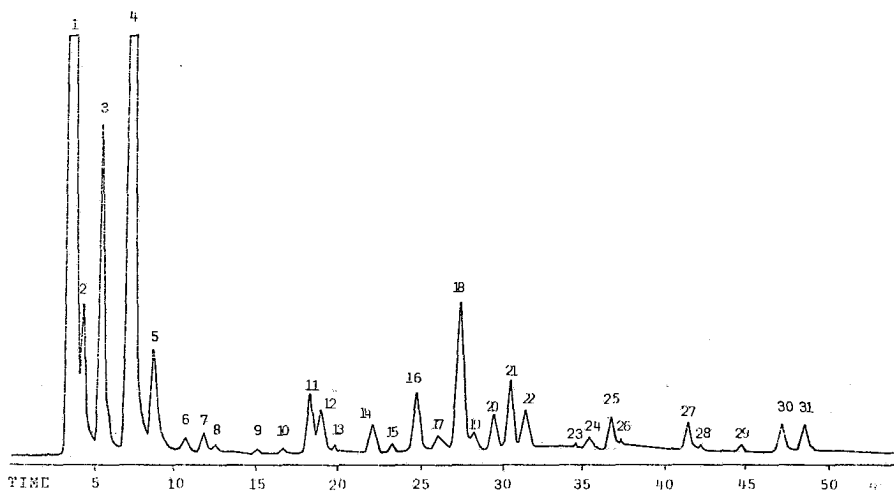


FIG. 1: Gas-chromatogram of the volatile oil of mastic gum.

Analysis and identification were carried out using a computerized gas chromatographic-mass spectrometric system. Identifications of the individual components were accomplished with the aid of various computer interpretative techniques, as well as by individual interpretation of some spectra<sup>2,3,4,5</sup>. The structures of the components of the essential oil are shown in Fig. 2.

The data obtained from the analysis of mastic gum oil were different to the previously published data as shown in Table I. Contrary to the previous results we found 12.27% of myrcene and 0.95% limonene. We did not, however, isolate and identify any  $\beta$ -thujone, linalyl acetate and thymol. In addition, we also confirmed the presence of camphene,  $\gamma$ -terpinene, p-cymene, terpinolene, 6-methyl-5-hepten-2-one, 2-nonanone, o-cresol-methyl ether, perillene dehydro-p-cymene,  $\alpha$ -copaene, bornyl acetate, caryophyllene, methyl-monyl ketone, myrtenal, *trans*-perillyl alcohol, *cis*-perillyl alcohol,  $\alpha$ -terpineol,  $\delta$ -cadinene, myrtenol, anethol, *trans*-carveol, methyl-eugenol, *cis*-methyl-isoeugenol, *trans*-methyl-isoeugenol.

### Experimental

50 g of ground mastic gum were distilled in a Clevenger's apparatus. The resulting oil was dried over anhydrous magnesium sulphate and was subjected

to a gas chromatography analysis in a Hewlett-Packard 5830 A instrument. A 3m × 3.18 mm ID glass column was used, packed with 3% of Carbowax 20M (Chromosorb W-AW-DMCS, 80-100 mesh). The injector temperature was 100°C, the flame ionization detector was heated to 300°C and the column temperature was programmed between 90-220°C at the rate of 3°C/min. Helium (99.999%) was the carrier gas flowing at 35 ml/min. A Hewlett-Packard 5989 A mass spectrometer (data system) connected to the gas chromatograph was used for the mass spectra (ionization voltage was 70 eV).

TABLE I. Comparative Chemical Composition of Mastic Gum Oil.

Peak No	R <sub>t</sub> (min)	Compound	Area Percentage*	
			1	2
1	3.7	α-Pinene	77.10	78.90
2	4.4	Camphene	1.04	n.d.
3	5.5	β-Pinene	2.46	2.50
4	7.3	Myrcene	12.27	0.89
5	8.7	Limonene	0.95	11.52
6	10.6	γ-Terpinene	0.08	n.d.
7	11.7	p-Cymene	0.13	n.d.
8	12.4	Terpinolene	0.05	n.d.
9	15.0	6-Methyl-5-hepten-2-one	0.01	n.d.
10	16.6	2-Nonanone	0.03	n.d.
11	18.2	o-Cresol-methyl-ether	0.44	n.d.
12	18.9	Perillen	0.34	n.d.
13	19.8	Dehydro-p-cymene	0.01	n.d.
14	22.1	Unidentified	0.19	n.d.
15	23.2	α-Copaene	0.01	n.d.
16	24.8	Linalool	0.48	1.29
17	26.0	Bornyl acetate	0.18	n.d.
18	27.4	Caryophyllene	1.47	n.d.
		Methyl-nonyl-ketone		
19	28.2	Myrtenal	0.13	n.d.
20	29.4	trans-Perillyl alcohol	0.29	n.d.
21	30.5	cis-Perillyl alcohol	0.55	n.d.
22	31.4	α-Terpineol	0.35	n.d.
23	34.4	δ-Cadinene	0.01	n.d.
24	35.3	Myrtenol	0.09	n.d.
25	36.6	Anethol	0.23	n.d.
26	37.0	trans-Carveol	0.04	n.d.
27	41.4	Unidentified	0.23	n.d.
28	42.0	Methyl-eugenol	0.02	n.d.
29	44.6	cis-Methyl-isoeugenol	0.04	n.d.
30	47.1	trans-Methyl-isoeugenol	0.21	n.d.
31	48.5	Unidentified	0.21	n.d.

\* 1 = author's results, 2 = Scrubis et al., n.d. = not detected.

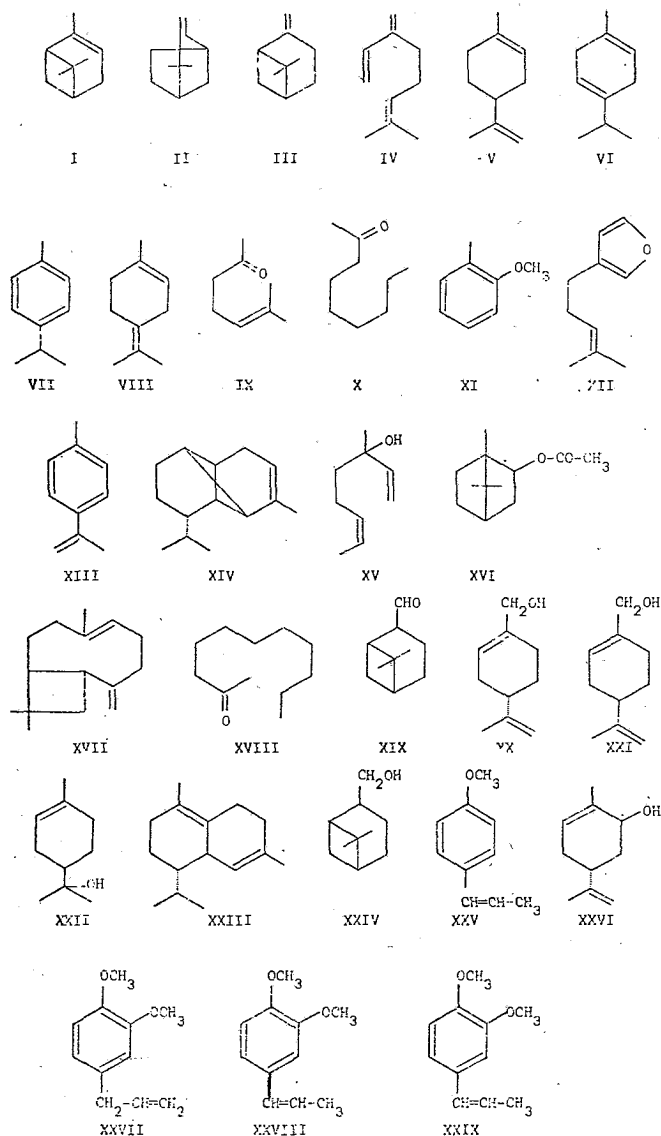


FIG. 2: Structures of the chemical compositions found in the mastic gum oil; (I) *α*-Pinene, (II) Camphene, (III) *β*-Pinene, (IV) Myrcene, (V) Limonene, (VI) *γ*-Terpinene, (VII) *p*-Cymene, (VIII) Terpinolene, (IX) 6-Methyl-5-hepten-2-one, (X) 2-Nonanone, (XI) *o*-Cresol-methyl-ether, (XII) Perillen, (XIII) Dehydro-*p*-cymene, (XIV) *α*-Copaene, (XV) Linalool, (XVI) Bornyl acetate, (XVII) Caryophyllene, (XVIII) Methyl-nonyl-ketone, (XIX) Myrtenal, (XX) *trans*-Perillyl alcohol, (XXI) *cis*-Perillyl alcohol, (XXII) *α*-Terpineol, (XXIII) *δ*-Cadinene, (XXIV) Myrtenol, (XXV) Anethol, (XXVI) *trans*-Carveol, (XXVII) Methyl-eugenol, (XXVIII) *cis*-Methyl-isoegenol, (XXIX) *trans*-Methyl-isoegenol.

### GLC-MS computer ανάλυση του αιθερίου έλαιου της μαστίχας

Με συνδυασμό GLC και MS computer ανάλυσεως κατορθώθηκαν να διακριθούν 31 συστατικά του αιθερίου έλαιου που προερχόταν από το ρητινώδες έκκριμα του δένδρου *Pistacia lentiscus Chia*. Από αυτά τα συστατικά 29 ταυτοποιήθηκαν πλήρως.

Είναι αξιοσημείωτο το γεγονός ότι 93% του αιθερίου έλαιου αποτελείται μόνο από ύδρογονάνθρακες και συγκεκριμένα από α-πινένιο, β-πινένιο, μυρκένιο και καρυφυλλένιο.

Τά αποτελέσματα της παρούσης μελέτης συγκρίνονται με τα αποτελέσματα προηγούμενης δημοσιεύσεως.

#### References

1. Scrubis, B., P. Markakis and M.J. Zabik: *Int. Flavours Food Addit.*, **6** (6), 349 (1975).
2. Von Sydow, E.: *Act. Chem. Scand.*, **17**, 2025 (1963).
3. Von Sydow, E.: *Act. Chem. Scand.*, **17**, 2504 (1963).
4. Von Sydow, E.: *Act. Chem. Scand.* **18**, 1099 (1964).
5. Stenhagen, E., S. Abrahamsson and F.W. McLafferty (eds.), *Archives of Mass Spectral Data*, Vol I, p. 389-579, New York, 1970, Interscience Publishers.